UNCLASSIFIED

AD 295 828

Reproduced
by the

ARMED SERVICES TECHNICAL INFORMATION AGENCY
ARLINGTON HALL STATION
ARLINGTON 12, VIRGINIA

UNCLASSIFIED
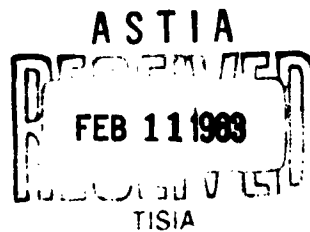
295 828

AERODYNAMIC AND RADIATION HEATING DURING FLIGHT

By

I. I. Drakin

295828

UNEDITED ROUGH DRAFT TRANSLATION

AERODYNAMIC AND RADIATION HEATING DURING FLIGHT

BY: I. I. Drakin

English Pages: 126

S/5621

AERODINAMICHESKIY I LUCHISTYY NAGREV V POLETE

FTD-TT-62-697/1+2

TABLE OF CONTENTS

FOREWORD

In connection with the widespread use of supersonic flying craft, close attention has been given to problems associated with aerodynamic and radiant heating in flight. Of particular importance is the heat shielding of the crew, of the structure and equipment, the selection of structural materials, and the determination of the thermal stresses in the structure. To solve these problems. it is necessary first to determine the temperature of the exterior shielding. This is the purpose of this work.

In considering aerodynamic heat transfer, we took into consideration the entire range of velocities and altitudes possible during flight in the atmosphere. However, not all the problems dealt with in this connection were given equal attention. This is explained by the limited attention devoted to certain questions in the scientific literature and by the fact that the work is intended, for the most part, for educational purposes.

In examining the problems of radiation heat transfer, primary attention is given to emission, since it is of great significance from the standpoint of thermal balance in aerodynamic as well as in radiant heating.

In connection with the increasingly wide use of shielding materials with low thermal conductivity, and also in connection with the use of thick shielding in the case of intensive heating, the present work presents a method for determining the temperatures

- 1 -

of thin as well as thick shielding. In addition the criterion for thin shielding is presented, as is a method for determining the thickness of the required insulation.

The present work is intended for preliminary tentative calculations; consequently, in the majority of cases we present approximation methods of calculation in order to obtain a quick result. In connection with the fact that we are pirmarily concerned with educational purposes, we consider only the simplest design elements (plate, shape, delta wing, cone, region of the critical point of the forward blunt end of the body).

Although this work takes into consideration a wide range of velocities, it should be borne in mind that the accuracy of the calculations with respect to heat transfer will decrease as the Mach numbers increase, since such factors as dissociation, recombination, and the development of the thickness of the boundary layer can be calculated only with a relatively low degree of accuracy. The radiation of the air behind the shock wave at high Mach numbers may lead to greater heat transfer than in the case of aerodynamic heat transfer and establishes the applicability limit of the above methods for the determination of the temperature at the critical point. The radiation of the air behind the shock wave is given only qualitative consideration.

In this work it has not been our intention to examine methods of heat shielding and consequently certain problems of heat transfer closely related to measures of heat protection have not been dealt with. Heat transfer in the case of porous cooling and sublimation is related to these questions. We have also not considered heat transfer through multilayered shielding.

To better explain the complex methods of thermal calculations,

- 2 -

this book presents numerical examples for which the initial data were arbitrarily adopted.

- 3 -

SYMBOLS

A — constant; accomodation coefficient;

$\underline{a}$ — coefficient of thermal diffusivity, in m^2/sec; speed of sound, in m/sec; constant;

$\underline{c}$ — specific heat capacity, in $kcal/kg \cdot deg$;

c_p — specific heat capacity of gas at constant pressure, in $kcal/kg \cdot deg$;

c_f — local coefficient of aerodynamic friction;

E — energy per unit time in $kg\text{-}m/sec$; total radiant energy per unit surface, per unit time, in $kg/sec \cdot m$;

F — area, in m^2;

G — weight, in kg;

$\underline{g}$ — acceleration of gravity, in m/sec^2;

H — flight altitude in m; ratio of displacement thicknesses and momentum losses for an incompressible fluid;

M_∞ — Mach number of an undisturbed flow;

M_δ — local Mach number;

Pr — Prandtl number;

p_∞ — pressure in undisturbed flow, in kg/m^2;

$\bar{p}_k$ — relative pressure at the surface, referred to the impact pressure of undisturbed flow;

$\bar{p}_\delta$ — relative pressure at the surface, referred to local impact pressure;

$\underline{q}$ — specific heat flow, in $kcal/m^2 sec$;

q_a — specific heat flow, developing as a result of aerodynamic heating, in $kcal/m^2 sec$;

q_0 — specific heat flow, developing as a result of aerodynamic heating at the critical point, in $kcal/m^2 sec$;

- 4 -

q_1 — specific heat flow of radiant energy absorbed by a body, in kcal/m²sec;

q_{iz} — specific heat flow radiated by a body, in kcal/m²sec;

q_{nag} — specific heat flow involved in the heating of a body, in kcal/m²sec;

q_t — flow of heat removed as a result of the heat conduction beyond the boundary of the body under consideration, referred to 1 m² of the outer surface of a body, in kcal/m²sec;

q_{pog} — specific heat flow absorbed by a body, in kcal/m²sec;

q_{okh} — specific heat flow of cooling, in kcal/m²sec;

R — radius of surface curvature, in m;

Re — Reynolds number;

Re_δ — local Reynolds number;

Re_{kr} — critical Reynolds number;

Re^* — Reynolds number corresponding to the determining temperature;

r — temperature recovery factor;

S — specific heat flow of solar radiation, in kcal/m²sec;

St — Stanton number;

s — proportionality factor for the Stanton number;

T — absolute temperature, in °K;

T_∞ — temperature of an undisturbed flow, in °K;

T_r — temperature of the adiabatic wall, in °K;

T_δ — temperature of the air at the outer limit of the boundary layer (local temperature), in °K;

T_k — temperature of the inner structure, in °K;

T_{ob} — temperature of the shielding, in °K;

T_{st} — temperature of the outer surface of the shielding, in °K;

T_{vn} — temperature of the inner surface of the shielding, in °K;

T^* — determining temperature, in °K;

u_{st} — rate of recombination at the wall, in cm/sec;

V — velocity, in m/sec;

V_δ — local velocity at the limit of the boundary layer, in m/sec;

V_∞ — undisturbed flow velocity, in m/sec;

V_{kos} — first cosmic velocity (circular velocity), in m/sec;

$\underline{x}$ — distance from the leading edge or the nose, in m;

$\bar{x}$ — relative coordinate from the nose or the leading edge;

$\underline{y}$ — coordinate normal to the surface, in m;

$\underline{z}$ — coordinate along the surface, perpendicular to the flow, in m;

α — heat-transfer coefficient, in $kcal/m^2 sec \cdot deg$;

α_0 — heat-transfer coefficient at the critical point of the blunt nose, in $kcal/m^2 sec \cdot deg$;

α_1 — heat-transfer coefficient referred to increment in heat content, in $kg/m^2 sec$;

α_{ek} — equivalent coefficient of heat transfer, in $kcal/m^2 sec \cdot deg$;

β — coefficient of the integral absorption of radiant energy; the Biot criterion of similarity;

γ — bulk weight, in kg/m^3;

δ — thickness of the boundary layer, in m;

δ_{ob} — thickness of the shielding, in m;

δ^* — thickness of the displacement of the boundary layer, in m;

δ^{**} — thickness of momentum loss of the boundary layer, in m;

ε — coefficient of integral radiation from a smooth surface;

ε_λ — coefficient of monochromatic radiation of wavelength λ;

ε_p — relative temperature difference along the thickness of the shielding;

θ — relative temperature;

ϑ_k — half-angle of conic flare, in radians;

κ — adiabatic exponent;

λ — coefficient of thermal conductivity, in $kcal/m \cdot sec \cdot deg$; wavelength;

λ_m — wavelength of maximum intensity, in μ;

μ — coefficient of viscosity, in $kg \cdot sec/m^2$;

μ^* — coefficient of viscosity in the case of the determining temperature, in kg·sec/m²;

ν — coefficient of kinematic viscosity, in m²/sec;

ν^* — coefficient of kinematic viscosity in the case of the determining temperature, in m²/sec;

ξ — similarity parameter for conic flows; relative coordinate;

ρ_δ — air density of the outer limit of the boundary layer, in kg·sec²/m;

ρ_∞ — air density in undisturbed flow, in kg·sec²/m⁴;

ρ^* — air density in the case of the determining temperature, in kg·sec²/m⁴;

σ — Stefan-Boltzmann constant, in kcal/m²sec·deg⁴;

τ — time, in seconds;

φ — Fourier criterion; the angle between the normal to the surface of the body and the vertical, in radians; the angle between the direction of flow and the tangent to the surface of the wing, in radians;

χ — coefficient characterizing the distribution of velocities near the critical point; wing sweepback angle, in radians;

ψ — angle between the direction of the solar rays and the normal to the surface, in degrees;

ω — exponent.

Chapter 1

HEAT TRANSFER IN AERODYNAMIC HEATING

§ 1.1. HEAT FLOWS DEVELOPING IN FLIGHT AT THE SURFACE OF A BODY

In the case of constant air flow about any type of body, the flow at its walls will have a velocity equal to zero. The kinetic energy of the flow in this instance is converted into heat and the air at the wall is heated.

In the case of complete conversion of the kinetic energy of the flow into thermal energy, the decelerated flow temperature would be

$$T_0 = T_i \left(1 + \frac{\varkappa - 1}{2} M_0^2 \right).$$

However, with the conversion of kinetic energy into thermal energy, a part of this energy is dissipated and the temperature of the air at the adiabatic wall, i.e., that part of the wall neither absorbing nor radiating heat, will be:

$$T_r = T_i \left(1 + r \frac{\varkappa - 1}{2} M_i^2 \right), \tag{1.1}$$

where $\underline{r}$ is the temperature recovery factor

$$r = \frac{T_r - T_i}{T_0 - T_i}. \tag{1.2}$$

The temperature T_r is called the recovery temperature or the temperature of the adiabatic wall, since the temperature of the latter will actually equal T_r.

The value of the recovery factor depends in the main on the structure of the boundary layer and on the physical properties of

- 8 -

the air which are determined by the Prandtl number

$$Pr = \frac{v}{a} = \frac{g\mu c_p}{\lambda},$$ (1.3)

where a is the coefficient of thermal diffusivity.

The engineering calculations may be assumed in approximate terms for the laminar boundary layer

$$r_\Lambda = (Pr^*)^{1/2},$$ (1.4)

for the turbulent boundary layer

$$r_T = (Pr^*)^{1/3},$$ (1.5)

where the Prandtl number should correspond to the determining temperature which may be determined from the formula given in the work of Eckert [35]:

$$T^* = T_\delta + 0.5 (T_{cr} - T_\delta) + 0.22 (T_r - T_\delta).$$ (1.6)

The introduction of the determining temperature produces great differences in the temperature of the air along the thickness of the boundary layer. It leads to a situation in which the physical properties of the air (viscosity, density, and thermal conductivity) along the thickness of the boundary layer are variable. In principle, it is possible to solve problems of heat transfer without the determining temperature by means of the corresponding integration of the equations of the boundary layer. However, for a compressible gas even in the case of a laminar boundary layer, it is necessary to carry out the unwieldy numerical integration of two second-order equations. A.D. Young [30] showed that the integration of the equations for a laminar boundary layer of a compressible gas may be substantially simplified, if the viscosity is represented in the following form:

$$\mu = AT^\omega.$$

In this case we will obtain results even in the form of formulas, although admittedly these are quite cumbersome. However, use of the

above formula for viscosity is possible only within a comparatively narrow temperature range in the boundary layer, since ω is not a constant. Actually, in the absolute temperature range from 300 to 500°K, ω = 0.72, while in the temperature range from 1000 to 2000°K, ω = 0.58.

In the presence of a turbulent boundary layer it is not possible to obtain simplified solutions, even of this type. In connection with the difficulty of solving boundary layer equations, the method of the determining temperature is fruitful. With this method we may use the results of the solution of boundary layer equations for an incompressible gas, assuming the physical properties of the air for the determining temperature.

The value of the determining temperature depends not only on the temperatures in Formula (1.6), but on the structure of the boundary layer and on the Mach number. For example, G. Young and E. Hansen proposed the following for the laminar boundary layer in the Mach-number region from 0 to 5 [35]

$$T^* = T_i + 0{,}58 \, (T_{cr} - T_i) + 0{,}19 \, (T_r - T_i),$$

while for Mach numbers from 5 to 10

$$T^* \quad 0{,}77 T_i + 0{,}58 T_{cr} + 0{,}237 T_i M^2.$$

E. Eckert showed that it is possible to give a general formula for the determining temperature (1.6) for the entire practical range of Mach numbers. Eckert's verification of this formula for a laminar boundary layer by means of the results based on an exact calculation without the determining temperature and obtained in a computer by Young and Hansen indicated that in the range of Mach numbers from 0.2 to 22 Formula (1.6) leads to an error not exceeding 3% in the determination of the frictional resistance, and consequently, in the determination of heat transfer; moreover, in the majority of cases

- 10 -

(in 38 of 50) the error was less than 1% [35].

E. Eckert [35] in analyzing the investigations and experimental data produced by other authors comes to the conclusion that Formula (1.6) may also be used in the case of a turbulent boundary layer. P. Monaghan [48] came to the same conclusion. Monaghan found on the basis of theoretical investigations and an analysis of the experimental data obtained with Mach numbers up to M = 8 that the determining temperature for a turbulent boundary layer may be the same as that taken for a laminar boundary layer.

K. Erike [37] shows that the determining-temperature method may be applied not only to laminar and turbulent boundary layers, but also to dissociated gas. It is true that he notes that the application of the determining-temperature method is most convenient for preliminary aerothermodynamic calculations. A more exact solution could be obtained with the aid of computers.

As can be seen from Formula (1.6), the determining temperature may be calculated when the recovery temperature T_r and the temperature of the wall T_{st} are known, but these temperatures are unknown. Consequently, the aerodynamic heating in the case of steady-state thermal processes should be calculated by the method of successive approximations, initially determining the Prandtl number approximately. In the case of nonsteady-state thermal process, as is shown in § 4.1, the calculation may be carried out without successive approximations.

The dependences of the Prandtl number on the temperature according to N.B. Vargaftik [25] and according to E. Van Dreist [5] are given in Fig. 1.1. It is apparent from this figure that in the temperature range of from 0 to 1400°C, the Prandtl number changes within a relatively narrow range from 0.68 to 0.72. Taking the mean value

- 11 -

0.70, in accordance with Formulas (1.4) and (1.5), we obtain for the calculation of the first approximation

$$r_\mathrm{a} = 0{,}83; \quad r_t = 0{,}89.$$

The specific flow of heat to the wall from the air heated in the boundary layer will be expressed according to the formula of Newton

$$q_\mathrm{a} = \alpha\,(T_r - T_{c_i}),$$ (1.7)

where α is the heat-transfer coefficient.

The values of the specific flows of heat will be determined in $kcal/m^2sec$. Consequently, the units of the heat-transfer coefficient will be expressed in $kcal/m^2sec \cdot deg$.

In addition to the indicated gas-kinetic heat flow which heats the body, the outside surface of the body may be subject in flight to the influence of radiant energy emitted by the body, the earth, the moon, comets, and by the galaxy; only flows of heat coming from the sun and the earth are of practical significance in flights about the earth. The remaining heat flows are significant only in flights in the vicinity of corresponding planets or in galactic flights.
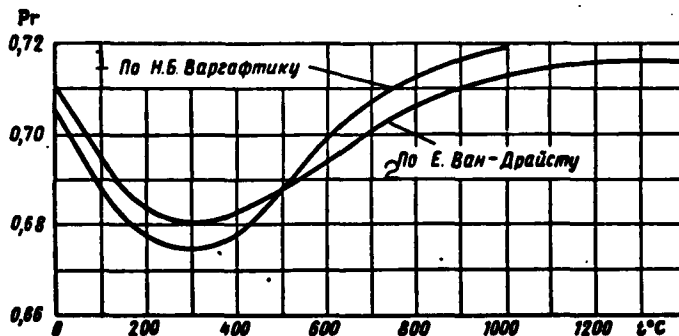
Fig. 1.1. Dependence of the Prandtl number on the temperature for air. 1) According to N.B. Vargaftik; 2) According to E. Van Dreist.

The specific heat flow of direct solar radiation absorbed by the irradiated surface

- 12 -

$$q_c = \beta S \cos \psi, \qquad (1.8)$$

where S is the specific heat flow of solar radiation, normal to the surface; ψ is the angle between the direction of the solar rays and the normal to the surface of the body; β is the absorption coefficient which depends on the material of the surface, its structure, and temperature.

The specific heat flow of solar radiation without taking into consideration the absorption and scattering of its atmosphere in an earth orbit (see [34]) is S = 0.332 kcal/m^{2}sec. At altitudes below 40 km, S will be less than the indicated value and will depend on the altitude and zenith distance of the sun, and also on the meteorological conditions. At the surface when the sun is at its zenith, S decreases by approximately 2 1/2.

The specific heat flow reflected from the surface of the earth and from the clouds of solar rays is several times less than the specific heat flow of direct solar radiation. At an altitude of 500 km of the earth-sun line, in approximate terms

$$q_{or} = 0,016\,(1+2\cos\varphi)\,\beta. \qquad (1.9)$$

The specific heat flow of the earth's radiation will be even less: at a height of 500 km it is approximately

$$q_3 = 0,007\,(1+2\cos\varphi)\,\beta. \qquad (1.10)$$

The heat flow of the reflected solar rays of the earth's radiation decreases with altitude. At altitudes of several thousand kilometers they may be disregarded.

The total specific heat flow absorbed by the body in flight will be

$$q_{nr} = q_{\pi} + q_{\pi}, \qquad (1.11)$$

where

$$q_{\pi} \quad q_c + q_3 + q_{or}. \qquad (1.12)$$

- 13 -

The heat being absorbed by the body will influence the radia-
tion; it will heat the body and will be drawn beyond the limits of
the section under consideration as a result of heat conduction.
The over-all heat balance when there is no cooling will be:

$$q_{нор} = q_{из} + q_{нар} + q_т. \qquad (1.13)$$

The specific radiation-heat flow

$$q_{из} = \varepsilon \sigma T_{ст}^4, \qquad (1.14)$$

where σ is the Stefan-Boltzmann constant and is equal to

$$\sigma = 13,6 \cdot 10^{-12} \text{ cal/m}^2 \text{sec} \cdot \text{deg}^4;$$

ε is the radiation coefficient which depends on the material of the
surface, its structure and temperature. Information on the numerical
values of ε is given in Chapter 2.

The specific heat flows involved in the heating of the body
and withdrawn through the boundaries on the side depend on the tem-
perature gradient and the thickness of the shielding at the surface
of the body $(\partial T/\partial y)_{st}$ and on the thermal conductivity λ:

$$q_{нар} + q_т = -\lambda \left(\frac{\partial T}{\partial y} \right)_{ст}. \qquad (1.15)$$

where y is the coordinate directed from the surface to the flow.

The thermal conductivity is seldom measured in kcal/m·hr·deg,
however, the introduction of the hours as the unit of time does
does not correspond to the technical system of units and may be
justified only in the case of constructions in which the thermal
processes last for hours and days. In the case of flying craft sub-
ject to substantial aerodynamic heating, the length of the limiting
thermal processes is usually measured in seconds and minutes. Conse-
quently, the coefficient of thermal conductivity in the given work
will be measured in kcal/m·sec·deg.

The temperature gradient at the surface of the body $(\partial T/\partial y)_{st}$

in the general case should be determined by the Fourier equation [9]

$$c\gamma \frac{\partial T}{\partial \tau} = \frac{\partial}{\partial x}\left(\lambda \frac{\partial T}{\partial x}\right) + \frac{\partial}{\partial y}\left(\lambda \frac{\partial T}{\partial y}\right) + \frac{\partial}{\partial z}\left(\lambda \frac{\partial T}{\partial z}\right),$$ (1.16)

where $\underline{c}$ is the specific heat capacity of the shielding material; γ is its bulk weight.

The specific heat flow involved in the heating of the shielding

$$q_{oar} = \int_0^{\delta_{oar}} c\gamma \frac{\partial T}{\partial \tau} \, dy,$$

should also be found in the general case with Eq. (1.16).

When there is a temperature gradient $\partial T/\partial x$ or $\partial T/\partial z$, there will arise in the shielding heat flows perpendicular to the heat flows described above. They will be proportional to $\lambda(\partial T/\partial x)$ or $\lambda(\partial T/\partial z)$ and should also be determined in the general case with Eq. (1.16).

§ 1.2. HEAT-TRANSFER COEFFICIENT WITH FLOW ABOUT A FLAT PLATE AT ZERO ANGLE OF ATTACK

Determination of the heat-transfer coefficient at supersonic speeds is a rather complex problem and at the present time we have comparatively exact solutions only for a flat plate at zero angle of attack, and that without taking into consideration the pressure produced along the plate by a boundary layer whose thickness is increasing. Problems with respect to determination of heat transfer in the case of more complex flows can usually be reduced to those of heat transfer for flat plates, making one or another assumptions.

The heat-transfer coefficient may be expressed in terms of the dimensionless Stanton St number. The Stanton number is the similarity criterion for heat transfer with forced motion. Here

$$\alpha = St \, \gamma_\delta V_\delta c_p \, \iota.$$ (1.17)

Frequently, in addition to the Stanton number, we also use the dimensionless Nusselt number which is equal to

- 15 -

$$Nu = \frac{\alpha x}{\lambda},$$ (1.18)

moreover, the Nusselt number is related to the Stanton number in the following way:

$$Nu = St \, Re \, Pr,$$ (1.19)

where Re is the Reynolds number

$$Re = \frac{Vx}{\nu}.$$ (1.20)

The Stanton number is proportional to the local coefficient of friction

$$St = s c_f,$$ (1.21)

moverover, the proportionality coefficient $\underline{s}$ is a dimensionless quantity. At low velocities and small temperature differences in the boundary layer, $\underline{s}$ in the laminar boundary as well as in the turbulent boundary layer is equal to (see [35])

$$s = \frac{1}{2} Pr^{-2/3}.$$ (1.22)

To calculate the compressibility of the flow in the case of laminar boundary layers, the Prandtl number in Formula (1.22) should be calculated for the determining temperature [35], i.e.,

$$s_л \approx \frac{1}{2} (Pr^*)^{-2/3}.$$ (1.23)

In the case of a turbulent boundary layer, the use of Formula (1.23) is less well founded; however, until other methods are developed we may assume [35]

$$s_т \approx \frac{1}{2} (Pr^*)^{-2/3}.$$ (1.24)

It should be noted that as a result of the fact that the Prandtl number varies within a very narrow range, the range of the possible changes in the coefficient $\underline{s}$ will also be narrow. Adopting as the Prandtl number the new value Pr = 0.7, we will obtain:

$$s \approx 0,64.$$

- 16 -

This value may be used for the first-approximation calculation. If the coefficient s̲ is known, the calculation of the Stanton number is reduced to the determination of the local coefficient of friction. For incompressible flow in the case of a laminar boundary layer, the local coefficient of friction may be expressed ([35], [33], p. 119) in the following way:

$$c_f = \frac{0,664}{\sqrt{Re}}.$$ (1.25)

In the case of a turbulent boundary layer, we may use the following formula up to Re = 10^7 (see [48], [33], p. 425):

$$c_f = \frac{0,0592}{(Re)^{0,2}}.$$ (1.26)

The formula is in good agreement with experiments for values $10^6 \leq Re \leq 10^9$ (see [35], [33], p. 433)

$$c_f = \frac{0,37}{(\lg Re)^{2,584}}.$$ (1.27)

The above formulas may also be used in the case of compressible flow, if the Reynolds number is calculated from the determining temperature, using Formula (1.6). Here the coefficient c_f is referred to the physical parameters of the air for the determining temperature, i.e., to ρ^* and μ^*. The Stanton number in Formula (1.17) is referred to $c_{p\delta}$; for compressible flow it is necessary to calculate c_p or the determining temperature. If we consider the above, the friction coefficient referred to the physical properties of the air at the limit of the boundary layer, will be:

$$c_{f\,c\kappa} = c_f^* \frac{\rho^*}{\rho_\lambda},$$ (1.28)

while the Stanton number

$$St = s^* c_{f\,\kappa}^* c_p^* / c_\lambda c_{p\,\lambda}.$$

Substituting this expression in Formula (1.17), we obtain for the local heat-transfer coefficient:

- 17 -

$$\alpha = gs^{*}c_{f}^{*}c_{p}^{*}V_{\delta}. \tag{1.29}$$

If we take into consideration Formulas (1.23), (1.24), (1.25), (1.26), and (1.27), we will find the over-all heat-transfer coefficient; here the heat-transfer coefficient will be:

for the laminar boundary layer

$$\alpha_{\lambda} = 3{,}26\,(\text{Re}^{*})^{-1/2}\,(\text{Pr}^{*})^{-2/3}\,\rho^{*}c_{p}^{*}V_{\delta}, \tag{1.30}$$

for the turbulent boundary layer and $\text{Re} \leq 10^{7}$

$$\alpha_{t} = 0{,}29\,(\text{Re}^{*})^{-0.2}\,(\text{Pr}^{*})^{-2/3}\,\rho^{*}c_{p}^{*}V_{\delta}, \tag{1.31}$$

for the turbulent boundary and $10^{6} \leq \text{Re} \leq 10^{9}$

$$\alpha_{t} = 1{,}81\,(\lg \text{Re}^{*})^{-2.584}\,(\text{Pr}^{*})^{-2/3}\,\rho^{*}c_{p}^{*}V_{\delta}. \tag{1.32}$$

The value of the density for the determining temperature may be determined from the characteristic equation, taking into consideration the fact that the pressure in the boundary layer does not change:

$$\rho^{*}/\rho_{\delta} = T_{\delta}/T^{*}. \tag{1.33}$$

The Prandtl number in these formulas may be determined from the graph given in Fig. 1.1. To determine the Reynolds number, it is necessary to know the relation of the viscosity to the temperature. For this we may use the formula (see [48])

$$\mu = 1{,}49 \cdot 10^{-7}\,\frac{T^{3/2}}{T+110} \quad \text{kg sec/m}^{2}. \tag{1.34}$$

This formula is thoroughly validated by experiments in the temperature range of 100 to 2000°K. The coefficient of kinematic viscosity in the Reynolds number

$$\nu = \mu/\rho. \tag{1.35}$$

The specific heat capacity of the air may be determined from the graph given in Fig. 1.2 This graph is constructed from the data of N.V. Vargaftik [25] and E. Eckert [35].

For flying craft with cosmic and near-cosmic velocities the thermal regime may be of the essence at altitudes where due to the

great rarefaction of the air, boundary layer theory is not applicable.

This is the region of free-molecular flow; it is characterized

by the fact that the mean molecular free path (before collision) be-

comes greater than the dimensions of the body. In such flow, there

is no boundary layer. The relation of the mean molecular free path

to the linear dimension of the body is called the Knudsen number.

The region of the free-molecular flow is characterized by the Knudsen

number (see [50])

$$Kn = \sqrt{\frac{\varkappa}{2} \varkappa \frac{M}{Re}} > 10.$$

(1.36)
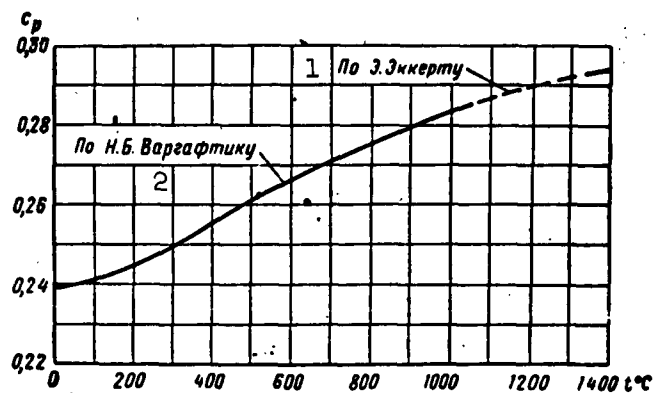
Fig. 1.2. Dependence of the specific
heat capacity of the air on the tem-
perature. 1) According to E. Eckert;
2) According to N.V. Vargaftik.

The heat transfer of the free-molecular flow depends on the

relative amount of energy transmitted by the molecules to the air

against which they collide. This relative energy is called the accom-

odation coefficient, the value of which is influenced to a certain

extent by the material and the structure of the surface. The accom-

odation coefficient values are close to unity; Table 1.1 gives the

value of the accomodation factor for certain materials [39]. A good

agreement between the theoretical heat transfer and the experimental

heat transfer is obtained if we assume A = 0.9 [23].

- 19 -

TABLE 1.1

Accomodation Coefficients for Certain Materials

Материал 1	Коэффи- циент акко- модации A 2	Материал	Коэффи- циент акко- модации A
Алюминий машинной бработки 3	0,95÷0,97	Литая сталь машинной обработки 6	0,87÷0,88
Алюминий травленый 4	0,89÷0,97	7 Литая сталь травленая	0,69÷0,96
Алюминий полирован- ый 5	0,87÷0,95	Литая сталь полиро- ванная 8	0,87÷0,93

1) Material; 2) accomodation coefficient A; 3) machine-worked aluminum; 4) etched aluminum; 5) polished aluminum; 6) machine-worked lithium steel; 7) etched lithium steel; 8) polished lithium steel.

The heat transfer of the free-molecular flow may also be determined from Formulas (1.1) and (1.7); we must, however, take into consideration the fact that the temperature recovery factor in free-molecular flow increases and becomes greater than unity. Theoretically, in the case of free-molecular flow past a flat plate, the recovery factor equals (see [23])

$$r_{cm} = 7/6 = 1,17.$$

Experiments confirm the theoretical value of the recovery factor for the region $4 \geq Kn \sqrt{Re} \geq 1$. For $Kn \sqrt{Re} > 4$, the experimental values are higher than the theoretical values and reach $r_{sm} = 1.4$ (see [23]).

The heat-transfer coefficient may be determined from Formula (1.17), while the Stanton number for free-molecular flow past a flat plate at zero angle of attack will be (see [23]):

$$St_{cm} = 0{,}242 A/\zeta, \tag{1.37}$$

where A is the accomodation coefficient, while ζ is the ratio of the velocity of light to the most probable molecular velocity. The value of ζ may be expressed in terms of the Mach number (see [23]):

$$\zeta = M \sqrt{\frac{1}{2} \varkappa}. \tag{1.38}$$

Substituting Formulas (1.137) and (1.38) in Formula (1.17), we obtain:

$$\alpha_{cm} = 0.342 a\gamma c_p A / \sqrt{\varkappa}.$$

(1.39)

It is apparent from this formula that the velocity of the flight has no influence on the heat-transfer coefficient in free-molecular flow while if we take into consideration the small changes in a, $\varkappa$, c_p, and A, the density of the air is the basic factor determining the heat-transfer coefficient.

In free-molecular flow there will be no shock wave; however, due to the collisions of the molecules with the surface these molecules may be dissociated and ionized. Due to the great length of the molecular free path in free-molecular flow, at great hypersonic velocities an extensive ionization zone developes in front of the moving body.

For the range of Knudsen numbers [50]

$$0.01 < Kn < 0.1$$

the flow will have a boundary layer; however, the velocity at the surface will not equal zero. This is This is called slippage flow. The sudden increase in the velocity in the boundary layer with slippage also produces a sudden increase in the temperature. The theoretical determination of heat transfer in the case of flow with slippage is quite complex and extremely unreliable [50]. A comparison of experimental data on heat transfer with data calculated on the basis of the theory of constant flow (continuum) with a laminar boundary layer indicates that the heat transfer in the case of flow with slippage is somewhat lower than the heat transfer obtained from formulas for continuum flow [50].

§ 1.3. THE HEAT-TRANSFER COEFFICIENT IN THE CASE OF FLOW PAST A PLATE, A WING PROFILE, AND A BODY OF REVOLUTION

At small angles of attack for a flat plate, the heat transfer can be determined from formulas corresponding to the plate with a zero angle of attack, taking into consideration the local values of the velocity, the density, and the temperature of the air at the limit of the boundary layer. It is the lower surface that is of greatest significance from the standpoint of heat shielding, since the highest temperatures are attained on this surface.
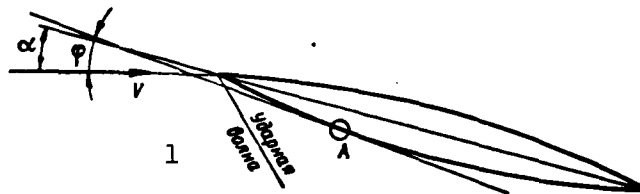
Fig. 1.3. Diagram of flow about the nose of the profile. 1) Shock wave.

In the case of flow about the lower surface of a plate with a positive angle of incidence, an oblique compression wave develops on the leading edge. Let us consider the more general case of a wing profile, when the tangent to the profile at the investigated point A forms the angle φ with the direction of the flow on the lower surface (see Fig. 1.3). In this case the local pressure p_δ at point A on the surface of the wing may be represented according to Buzeman in the following way (see [29]:

$$\bar{p}_a = \frac{p_b - p_\infty}{\frac{1}{2} \rho_\infty V_\infty^2} = c_1 \varphi + c_2 \varphi^2 + c_3 \varphi^3 + \ldots \qquad (1.40)$$

We are frequently restricted to two terms of this expansion. This is entirely permissible, if the Mach numbers are not substantially greater than 5-6. At great hypersonic velocities the neglecting of the third term may produce a substantial error. As an example,

Fig. 1.4 gives the error as a function of M_∞ when $\varphi = 5^\circ$. As can be seen from the curve, when $M_\infty > 20$, the error may be greater than 20%. Consequently we introduce the values of the factors for a trinomial expansion.

If we assume that the adiabatic exponent for air is 1.4, for the coefficients c_1, c_2, and c_3 we obtain the following expression, if φ is determined in radians (see [29]):

$$c_1 = 2(M_\infty^2 - 1)^{-1/2}; \tag{1.41}$$

$$c_2 = \frac{1}{2}[(M_\infty^2 - 2)^2 + 1.4M_\infty^4](M_\infty^2 - 1)^{-2}; \tag{1.42}$$

$$c_3 = (0.36M_\infty^8 - 1.493M_\infty^6 + 3.6M_\infty^4 - 2M_\infty^2 + 1.33)(M_\infty^2 - 1)^{-3.5}. \tag{1.43}$$

Here the coefficient c_3 reflects the influence of the shock wave. When the flow expands (when there is no shock wave), the values of the coefficients c_1 and c_2 will remain the same, while coefficient c_3 is somewhat changed and can be expressed in the following way:

$$c_3' = (0.4M_\infty^8 - 1.813M_\infty^6 + 4M_\infty^4 - 2M_\infty^2 + 1.33)(M_\infty^2 - 1)^{-3.5}. \tag{1.44}$$

In the case of flow expansion, φ is negative. If the flow expansion precedes the shock wave, as for example in the case of flow about the rear section of the profile, the coefficient c_3' is also calculated from Formula (1.44), but a term expressing the influence of the shock wave is added to the expansion:

$$c_3' \varphi_1^3,$$

where φ_1 is the angle of inclination of the surface in the forward section in front of the shock wave, and

$$c_3' = c_3 - c_3' = -(0.04M_\infty^8 - 0.32M_\infty^6 + 0.4M_\infty^4)(M_\infty^2 - 1)^{-3.5}. \tag{1.45}$$

Figure 1.5 presents a graph for the determination of the coefficients c_1, c_2, c_3, and c_3' as functions of the M_∞ number in undisturbed flow.

Having determined the pressure on the lower surface of the plate or on the nose of the wing profile by means of Formula (1.40), we can determine the air density at this same surface with the Hugoniot equation (see [29]):

$$\frac{\rho_b}{\rho_\infty} = 1 + 5\frac{p_b/p_\infty - 1}{p_b/p_\infty + 6}. \qquad\qquad (1.46)$$
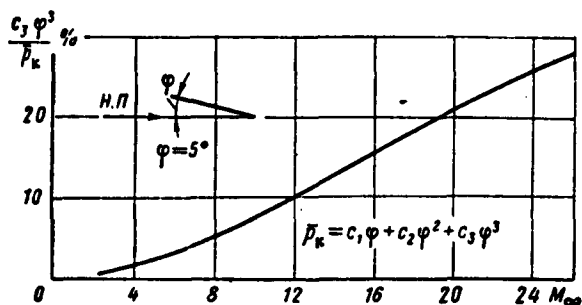
Fig 1.4. Relative error if we neglect the third term of the expansion in series of the relative pressure values.
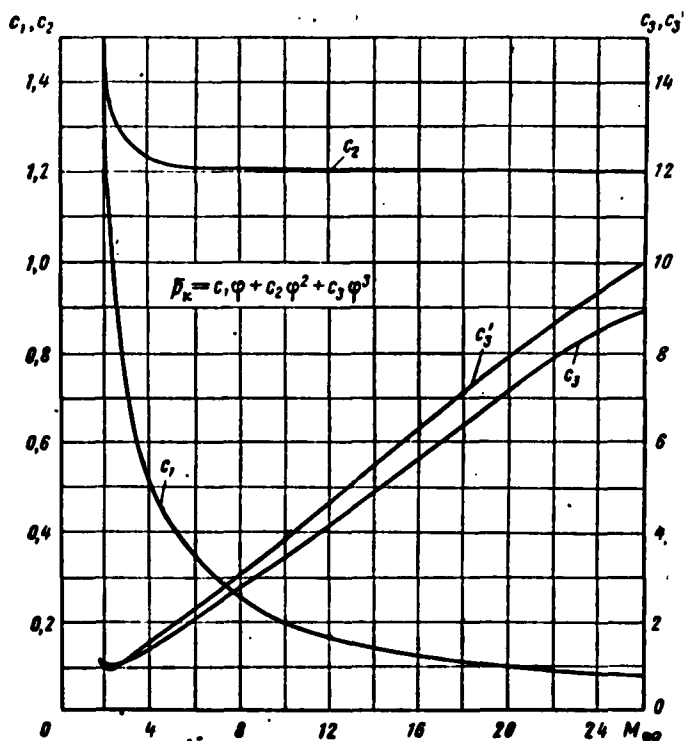
Fig. 1.5. Coefficients of the expansion in series of relative pressure as a function of M_∞.

If there is no shock wave (for example, for the upper surface

- 24 -

of a plate or, in certain cases for the profile). the density must be determined from the equation of the adiabatic curve:

$$p_\delta/p_\infty = (p_\delta/p_\infty)^{1/\kappa} = (p_\delta/p_\infty)^{0.715}. \tag{1.47}$$

If the flow expands behind the shock wave, we initially determine the density behind the shock wave from Formula (1.46), and then by means of the equation of the adiabatic curve we determine the density at the surface being investigated.

The air temperature at the limit of the boundary layer will be found from the characteristic equation:

$$T_\delta/T_\infty = (p_\delta/p_\infty)(\rho_\infty/\rho_\delta). \tag{1.48}$$

Making use of the fact that the flow-retardation temperature does not change even in the presence of compression waves, we obtain:

$$T_\infty\left(1 + \frac{\kappa-1}{2}M_\infty^2\right) = T_\delta\left(1 + \frac{\kappa-1}{2}M_\delta^2\right).$$

Taking into consideration that $\kappa = 1.4$, we find:

$$M_\delta^2 = 5\left[(T_\infty/T_\delta)(1 + 0.2M_\infty^2) - 1\right]. \tag{1.49}$$

Formula (1.40) and the values of the coefficients in this formula correspond to a wing of infinite span. However, this formula can also be used in the determination of the pressure on a straight wing of finite span for that part located outside the Mach end cones.

At the ends of the wing the pressure drops linearly along the span; moreover, at the very end, the excess pressure equals zero. Hence, it is not difficult to determine the pressure at any point inside the Mach end cones.

In the case of aerodynamic heating the case in which the leading edge of the delta wing becomes "supersonic" is of particular interest; in this case the excess pressure is greater than on a wing with a "subsonic" leading edge.

- 25 -

For a very thin wing (a plate), the excess pressure on the section lying outside of the Mach cone emanating from the peak of the triangle forming the wing will be (see [26], [27]):

$$\bar{p}_{\kappa\Delta} = \frac{2\alpha}{\sqrt{M_\infty^2 - 1 - \mathrm{tg}^2\chi}},$$

where χ is the sweepback angle of the leading edge; for the section of the wing lying inside the Mach cone, the pressure will be less and expressed as:

$$\bar{p}_{\kappa\Delta} = \frac{2\alpha}{\sqrt{M_\infty^2 - 1 - \mathrm{tg}^2\chi}}\left[1 - \frac{2}{\pi}\arcsin\frac{\mathrm{tg}\,\chi}{\sqrt{M^2-1}}\sqrt{\frac{1-(M_\infty^2-1)(z/x)^2}{1-(\mathrm{tg}^2\chi)(z/x^2)}}\right],$$

where x is the coordinate along the flow, while z is the coordinate perpendicular to the plane of symmetry (the origin of the coordinates is at the apex of the triangle).

For a wing of infinite span, with a very thin profile (a plate), the excess pressure according to the linearized theory is

$$\bar{p}_{\kappa\infty} = \frac{2\alpha}{\sqrt{M_\infty^2 - 1}}.$$

The greatest heat flows are developed on a delta wing in the section lying outside of the Mach cone. The pressure on this section of the wing may be determined from the formula

$$\bar{p}_{\kappa\Delta} = \frac{\sqrt{M_\infty^2 - 1}}{\sqrt{M_\infty^2 - 1 - \mathrm{tg}^2\chi}}\,\bar{p}_{\kappa\infty},$$

while calculating the value of $\bar{p}_{k\infty}$ from Formula (1.40).

It should be noted that as the Mach number increases, the correction factor approaches unity.

Thus, when M = 5 and χ = 60°, this factor equals 1.07, while when M = 10, it equals 1.015. The latter formula may also be used for the determination of the pressure on a sweptback wing, i.e., on that section of it which lies outside the central Mach cone.

The formulas presented here together with the formulas given

in § 1.2 enable us to find the heat-transfer coefficient on a flat plate as well as on a thin wing, if the angles of incidence are relatively small.

In § 3.1 we give an example of the determination of the heat-transfer coefficient on the profile of a wing.

It should be noted that the presence of pressure and temperature gradients on the surface (for example, on a curvilinear profile) increases the error in the determination of the heat-transfer coefficient; moreover, this error increases as the Mach number increases.

The heat transfer on a cylindrical surface with an axis parallel to the flow may be determined from the formulas for a flat plate, if the thickness of the boundary layer is substantially less than the curvature radius of the surface. The applicability criterion for the theory of a flat plate for a cylindrical surface may be expressed in the following inequalities:

for a laminar boundary layer $x/R < 0.02 \ Re^{1/2}$;　　(1.50);

for a turbulent boundary layer $x/R < 0.3 \ Re^{1/5}$,　　(1.51).

The heat-transfer formulas for a flat plate may also be used for a cone; however, the local values of M_δ, ρ_δ, and T_δ should correspond to the flow past the cone and the conical nature of the flow should be taken into consideration.

Because of the conical surface not all of the gas streams at the surface have identical lengths of contact with the surface. The streams beginning at the point of the nose have the greatest lengths of contact with the surface. Other streams are shorter, since they approach the surface at some distance from the point of the nose. Thus, while determining the heat transfer or the frictional coefficient at a given point of the cone, it should be borne in mind that the mean length at which particles of gas in the boundary layer

are subject to the influence of viscosity forces will be less than the length of the generatrix.

Consequently, in using the heat-transfer formulas for a flat plate in the determination of the heat transfer on a cone, we should find the Reynolds number from the given length x_{pr} which depends on the length of the generatrix $\underline{x}$ and the structure of the boundary layer. In the case of laminar boundary layers $x_{pr}/x = 1/3$; in the case of turbulent boundary layers $x_{pr}/x = 1/2$ (see [5], [30]).

To determine the parameters of the flow at the surface of the cone, let us introduce the similarity parameter for conical flows

$$\xi = \vartheta_k M_\infty, \tag{1.52}$$

where ϑ_k is in radians.

Using the denotations of Fig. 1.6, according to N.F. Krasnov ([10], p. 258), we will have:

$$\bar{p}_k = 2.09 (1 + 0.143/\xi^{7/3}) \vartheta_k^2, \tag{1.53}$$

where

$$\bar{p}_k = \frac{p_k - p_\infty}{\frac{1}{2} \rho_\infty V_\infty^2}. \tag{1.54}$$
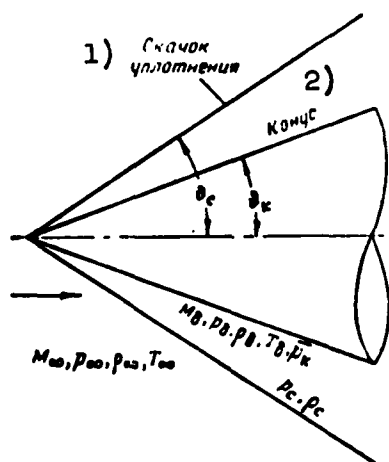
Fig. 1.6. Diagram of the symbols of the parameters of the flow about the cone. 1) Compression wave; 2) cone.

To determine the remaining local parameters of the flow at the limit of the boundary layer, it is necessary to take into consideration the nonisotropic change in the flow with the transition through the compression wave; these changes depend on the angle of inclination ϑ_s of the surface of the compression wave and M_∞. The angle of inclination of the compression wave according to N.F. Krasnov ([10], p. 249), is deter-

- 28 -

mined from the following formula

$$\vartheta_c/\vartheta_\kappa = 1{,}093 + 0{,}06\,(7-\xi)/\xi^{1/4}. \tag{1.55}$$

Formula (1.53) and (1.55) are approximations of the exact solution and may be used with a sufficiently high accuracy for $0.5 < \xi < \infty$, $M_\infty > 2.5$, and $\vartheta_k < 30°$.

If we know the angle of inclination for the compression wave, we can determine the relative pressure behind the discontinuity ([10], p. 37):

$$p_c/p_\infty = \frac{1}{6}\,(7M_\infty^2\sin^2\vartheta_c - 1). \tag{1.56}$$

The density of the air behind the compression wave is found from the Hugoniot equation

$$\frac{\rho_c}{\rho_\infty} = 1 + 5\,\frac{p_c/p_\infty - 1}{p_c/p_\infty + 6}. \tag{1.57}$$

The transition to the density of the air at the surface of the cone can be accomplished by means of the equation of the adiabatic curve:

$$\rho_\delta/\rho_c = (p_\delta/p_c)^{1/\kappa} = [(p_\delta/p_\infty)(p_\infty/p_c)]^{0,715}. \tag{1.58}$$

The quantity p_δ/p_∞ in this equation can be determined from Formula (1.54), using elementary transformations of this value; here we will obtain:

$$p_\delta/p_\infty = 1 + \frac{1}{2}\,\kappa M_\infty^2\bar{p}_\kappa = 1 + 0{,}7M_\infty^2\bar{p}_\kappa. \tag{1.59}$$

The temperature T_δ at the limit of the boundary layer of the cone and the local M_δ number can be determined from Formulas (1.48) and (1.49), respectively.

In the case of a pointed body of revolution with a curvilinear generatrix, the flow parameters at the point may be determined from the formulas for a cone having an angle ϑ_{k0} (see Fig. 1.7). At other points on the nose surface, the flow parameters can also be found
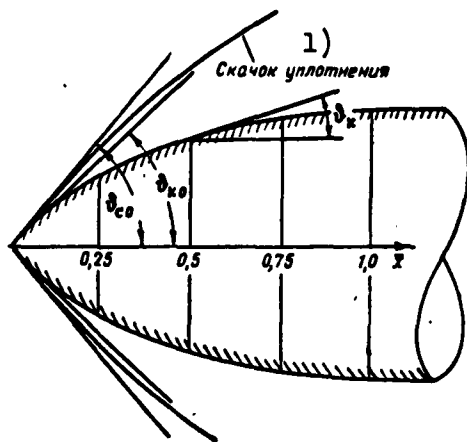
Fig. 1.7. Diagram of denotations for the geometric characteristics of a pointed body of revolution. 1) Compression wave.

approximately from the formulas for a cone with an angle ϑ_k which is equal to the angle of inclination of the nose surface at the given point (see Fig 1.7).

§ 1.4. HEAT-TRANSFER COEFFICIENTS IN THE CASE OF FLOW ABOUT FRONTAL AREAS

The forward noses of bodies and the leading edges of the lifting surfaces are related to the frontal surfaces. Heat transfer in the case of flow about frontal surfaces may be determined from the formulas for a plate, if we take into consideration the local characteristics of the flow.

With flow about rounded noses or leading edges, the blunt section of the nose in the region of the critical point is streamlined by subsonic flow (Fig. 1.8). On the basis of experiments [5] it was determined that the velocity of the flow along the meridional cross section is proportional to the relative distance from the critical point:

$$V_\iota = \chi V_\infty x/R. \qquad (1.60)$$

The geometric values of $\underline{x}$ and R are given in Fig. 1.8. The value of the coefficient χ depends on the shape of the frontal surface and the flight Mach number. In the case of incompressible flow ($M_\infty = 0$), $\chi = 1.5$ for a spherical nose, and for a cylindrical leading edge $\chi = 2$; when M_∞ increases, the value of χ decreases and may be determined for a spherical nose from the formula of M. Romig [20]:

$$\chi = 0{,}8M_\infty^{-0{,}232}. \qquad (1.61)$$

This formula is used for $M_\infty > 1$.

Because of the large negative pressure gradient and the low Reynolds numbers, the boundary layer must be laminar in the region of the critical frontal-surface point. The Reynolds number for the determining temperature, if we take into account Formula (1.60), will be

$$Re^* = xV_\delta/\nu^* = \chi V_\infty x^2/\nu^* R.$$

Substituting this value of the Reynolds number into Formula (1.30), and also substituting the value of V_δ from Formula (1.60), we will obtain the expression for the heat-transfer coefficient in the region of the critical point of the nose:

$$\alpha_0 = A\chi^{1/2}V_\infty^{1/2}R^{-1/2}(\mu^*\rho^*)^{1/2}(Pr^*)^{-2/3}c_p^*. \qquad (1.62)$$

Here the constant A is a function of nose shape. Using the corresponding numerical values given by E. Van Driest [5], we may assume the following:

for a spherical nose .... A = 7.5

for a circular cylindrical nose .... A = 5.6

The determining temperature at the critical point may be determined from the formulas for the deceleration temperature and from Formula (1.6); taking into consideration the fact that in the case under consideration $T_\delta = T_0$, where

$$T_0 = T_\infty\left(1 + \frac{\varkappa-1}{2}M_\infty^2\right),$$

we get:

$$T^* = T_0 - 0.5\,(T_0 - T_{ст}) - 0.22\,(1-r)\,(T_0 - T_\infty).$$

To determine the air density at the body surface from the determining temperature, we first determine the pressure behind the compression wave in the region of the critical point. From this pressure, we find the density of the air behind the compression wave and then from the adiabatic equation and the characteristic equation

- 31 -

we make the transition to the density of the air in the case of the determining temperature.

For a spherical or straight cylindrical nose, the pressure behind the compression wave may be found from Formula (1.56), if we assume that $\vartheta_s = 90°$. The density ρ_s behind the compression wave is determined from the Hugoniot equation (1.57). The transition from this density to the density ρ_δ at the surface can be made by means of the adiabatic equation (1.58). The sought value of the air density for the determining temperature may be found from the characteristic equation:

$$p^* /p_c = (\rho_\delta/\rho_c)\,(p^*/p_\delta) = (\rho_\delta/\rho_c)\,(T_0/T^*).$$

In determining the heat transfer on the leading edge of the wing, it should be borne in mind that the sweepback of the wing decreases heat transfer. In approximate terms, this decrease in the heat transfer may be determined from Fig. 1.9 (see [24]). In selecting the sweepback, it should be borne in mind that a very large sweepback (greater than 70°) decreases the critical Reynolds number.
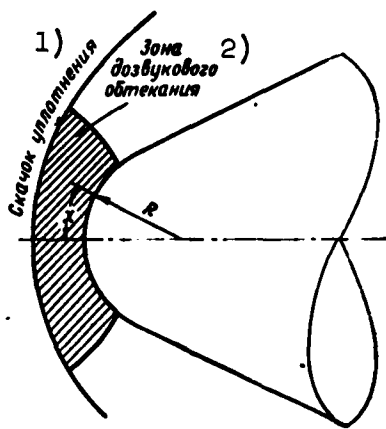
Fig. 1.8. Diagram of flow about a round nose. 1) Compression wave; 2) zone of subsonic flow.
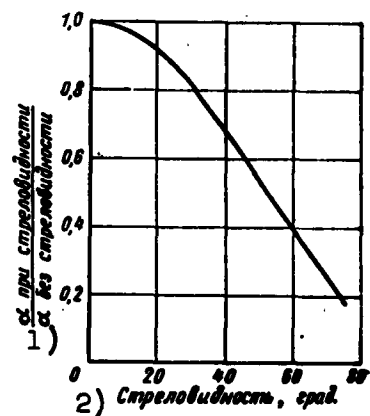
Fig. 1.9. Influence of the sweepback of the wing on the heat transfer at the critical point of the leading edge. 1) (α with sweepback)/ /(α without sweepback); 2) sweepback, deg.

If a rounded nose is streamlined by a laminar boundary layer, the heat transfer at the critical point will be at its maximum. However, if the boundary layer at the nose becomes turbulent, the maximum heat transfer will be in the vicinity of the point with the local number $M_\delta = 1$ [21].

§ 1.5. FACTORS INFLUENCING THE TRANSITION FROM A LAMINAR BOUNDARY LAYER TO A TURBULENT BOUNDARY LAYER

The structure of the flow in the boundary layer may be laminar or turbulent. In the case of a laminar boundary layer, the frictional resistance is substantially less than in the case of a turbulent boundary layer. The decrease in the friction of the laminar boundary layer decreases the heat transfer, and consequently, the temperature of the surface also.

As an example Fig. 1.10 gives steady-state temperatures of the wing surface in the case of laminar and turbulent boundary layers when $M_\infty = 5$. It is apparent from the graph that in the case of the laminar boundary layer, the temperature of the surface is 200 to 235° lower than in the case of a turbulent boundary layer. At higher values of M_∞, the temperature drop across the surface in the case of a laminar boundary layer will be even greater.

Thermal shielding of the structure is one of the most effective methods of ensuring a laminar structure for the boundary layer. The laminarization of the boundary layer also decreases the frictional resistance and, by the same token, decreases the weight of the engine.

If there are no factors producing turbulence in the nose section of a streamlined body, the nose section will generally be streamlined by a laminar boundary layer. The transition from a laminar boundary layer to a turbulent boundary layer at subsonic flight velocities depends on the Reynolds number, and on a flat plate with a

zero angle of incidence, this transition generally takes place at $Re_{kr} = 5 \cdot 10^5$ [33].

At supersonic flight velocities, as experiment shows, the boundary layer becomes turbulent at higher Reynolds numbers.
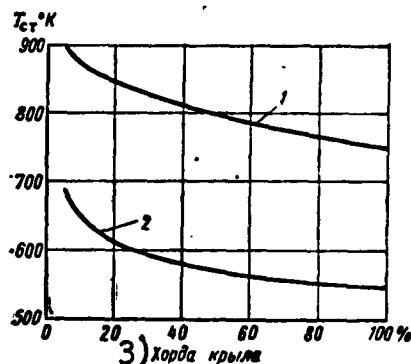
Fig 1.10. Temperature of a wing surface, with aerodynamic heating. 1) Turbulent boundary layer; 2) laminar boundary layer; 3) wing chord; M = 5, H = 30 km, $\alpha = 10°$, $\varepsilon = 0.8$, $\bar{c} = 0.03$.

The cause of turbulence in a boundary layer is the instability of the laminar boundary layer at high Reynolds numbers. In connection with this, the random velocity pulsations in the boundary layer are not attenuated but are developed and cause the turbulence of the boundary layer. Time is required to develop the turbulence and the disturbances, and consequently, the Reynolds number for the initial turbulence is greater than the Reynolds number for the initial steady-state motion.

The source of the disturbing pulses is usually the turbulence of the exterior flow, roughness, undulation, and other disruptions of smooth flow about the surface. By decreasing the disturbing pulses, we increase the time required for the development of the turbulence, and consequently, increase the critical Reynolds number for the transition from a laminar to a turbulent boundary layer. For example, by decreasing the turbulence of the flow through the use of damping grids we succeeded in obtaining a critical Reynolds number of $Re_{kr} = 3 \cdot 10^6$ in addition to the usual value $5 \cdot 10^5$ [33] on a flat plate at subsonic velocities.

Although it might have been assumed that the viscosity forces in the boundary layer would be a stabilizing factor, in reality they

reduce the stability of the laminar motion. In this a basic role
is played by the nature of the change in the velocity through the
thickness of the boundary layer; in the final analysis it is the
nature of this change which is determined by the viscosity forces.

If the wall cools the boundary layer, for example, by means of
its heat capacity or radiation, the density of the air at the wall
is increased and, by the same token, the kinetic energy referred to
the volume is increased. This increases the stability of the boundary
layer.

Figure 1.11 illustrates the nature of the change in the tempera-
ture and the density of the air through the thickness of the boundary
layer. Curves MN'P' and AB'C' correspond to the adiabatic wall,
while curves MNP and ABC correspond to the wall which is cooling
the boundary layer. In the section BC, the density is increased and
this increases the stability of the boundary layer.
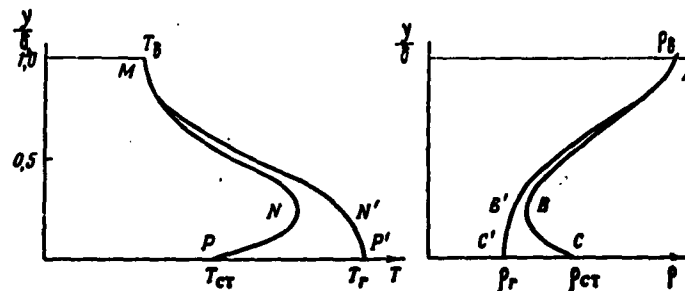
Fig. 1.11. Temperature distribution and air den-
sity through the thickness of the boundary layer.

With supersonic velocities and real walls there is always heat
transfer from the boundary layer, although this is the result of the
radiation of the wall. Consequently, the critical Reynolds numbers
at supersonic velocities are substantially greater than the critical
Reynolds numbers of the subsonic section.

L. Lees [47] showed theoretically that by cooling a wall stream-

lined by flow, we can completely stabilize the boundary layer of the supersonic flow, i.e., the critical Reynolds numbers may be made higher than those used in practice. In these cases the practical criterion of stability will not be the Reynolds number, but the relative wall temperature T_{st}/T_δ or T_{st}/T_r.

E. Van Dreist calculated the required relative temperatures of the wall for total stabilization of the boundary layer at various Mach numbers [52].

Figure 1.12 shows a graph of the stability limits according to E. Van Dreist: the regions within the curves B, C, and D correspond to the laminar boundary layer [5]. The ratio of the ordinates of the curves B, C, and D tothe ordinate of the curve A characterizes the degree of required cooling for total stabilization of the boundary layer.
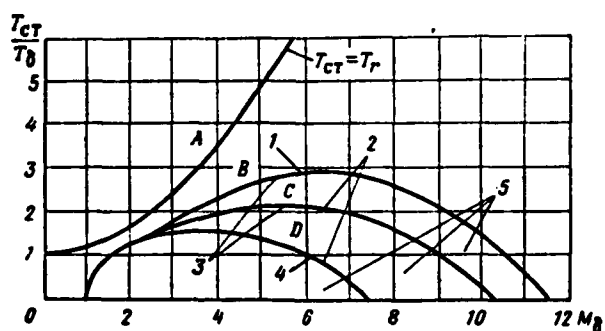
Fig. 1.12. Limits of the total stabilization of the boundary layer according to E. Van Dreist. 1) Cone; 2) plate; 3) in flight; 4) in a tube; 5) laminar boundary layer.

The region above the stability curves do not necessarily correspond to the turbulent boundary layer. For these regions the transition from the laminar boundary layer to a turbulent boundary layer will be determined by the Reynolds number.

Notwithstanding the great number of theoretical investigations of boundary-layer stability, the mechanism of the transition of a

laminar boundary layer into a turbulent boundary layer has not been completely discovered as yet. As a result, the determination of the critical Reynolds numbers by theoretical means is not yet possible.

Re·10^{-6}

Турбулентность в %
4) скорости потока
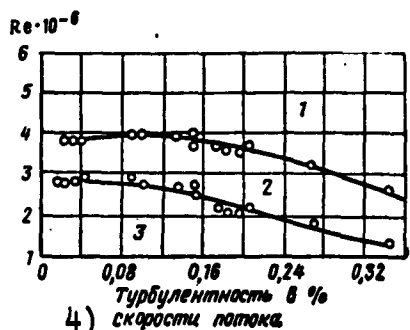
Fig. 1.13. The influence of flow turbulence on the critical Reynolds number of a flat plate at subsonic velocities. 1) Turbulent region; 2) transition region; 3) laminar region; 4) turbulence in % of flow velocity.

The experimental data have not been adequately systematized; moreover, there is a great divergence in the result of various experiments. This is explained by the various conditions under which experiments have been conducted and, in particular, by the fact that the flow turbulence, the roughness of the models, and the pressure gradient are not considered in many of the experiments.

The extent of turbulence can be seen from the experiments on the determination of the critical Reynolds numbers on a plate when $M < 1$ [12]. In these experiments the flow turbulence was changed and the formation of a temperature gradient was excluded. The results of these experiments are given in Fig. 1.13, whence it is apparent that depending on the magnitude of the turbulence, the critical Reynolds number may change within a wide range. We should also note the fact that with a turbulence of 0.08%, $Re_{kr} = 3 \cdot 10^6$ is almost reached; this is six times greater than the critical Reynolds number ordinarily assumed for a plate in a subsonic region.

We should also devote some attention to the experiments carried out in order to determine the critical Reynolds numbers on the cone, said experiments carried out by E. Van Dreist in a wind tunnel [53]. The cone being tested was cooled from within by means of liquid and gaseous nitrogen; in this manner it was possible to determine the critical

Reynolds numbers for various degrees of cooling. The test results are presented in Fig. 1.14. Curves A, B, and C correspond to the limits of total stability (see Fig. 1.12). Curves A', B', and C', passed through the experimental points, represent the limits above which the boundary layer becomes turbulent.
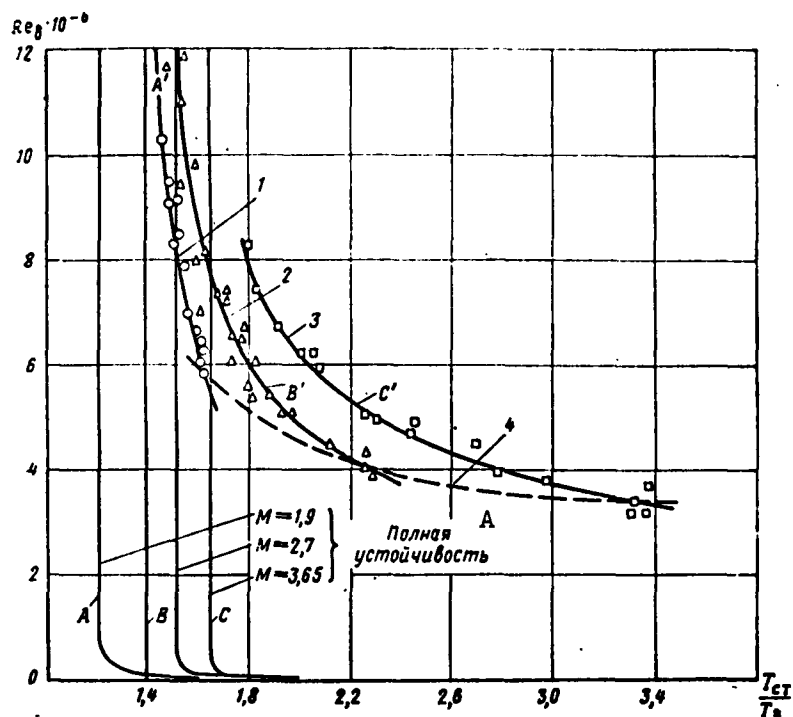
Fig. 1.14. Limits of stability for the boundary, in accordance with experiments carried out on a cone be cooled in a wind tunnel. 1) $M_\delta = 2.9$; $Re_\delta/meter \approx 2.13 \cdot 10^7$; 2) $M_\delta = 2.7$; $Re_\delta/meter \approx 2.4 \cdot 10^7$; 3) $M_\delta = 3.65$; $Re_\delta/meter \approx 1.97 \cdot 10^7$; 4) insulated walls; A) total stability.

We should note the fact that the Reynolds numbers for the experimental points shown in Fig. 1.14 correspond to the end of the transition (buffer) zone between the laminar boundary layer and the turbulent layer. In accordance with measurements of wall temperatures in the described experiment, the difference in Reynolds numbers between the beginning and the end of this transition amounts approximately to $2 \cdot 10^6$.

For a comparison against other experiments, curves A', B', and C'

have been constructed again in Fig. 1.15, where M_δ has been selected

as the argument, and the degree of wall cooling — characterized by the

ratio T_{st}/T_r — has been chosen as the paramenter. For an adiabatic wall

$T_{st}/T_r = 1$; in the case of wall cooling, $T_{st}/T_r < 1$. The cooling of the

surface increases the critical Reynolds numbers, particularly for $M_\delta < 3$.
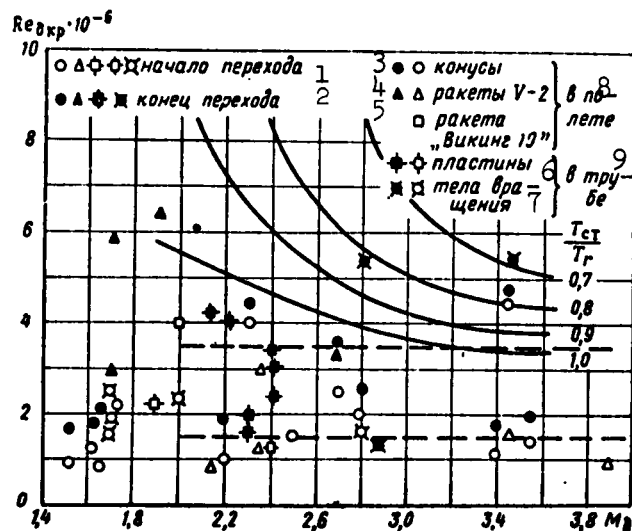
Fig. 1.15. Critical Reynolds numbers for
the transition from the laminar to the
turbulent boundary layer, according to
experiments carried out both in a wind
tunnel and in flight. 1) Beginning of
transition; 2) end of transition;
3) cones; 4) V-2 rocket; 5) Viking 10
rocket; 6) plate; 7) solids of revolu-
tions; 8) in flight; 9) in wind tunnel.

In Fig. 1.15 the experimental points obtained during flight tests

of cones and rockets have been plotted, as have the experimental points

obtained in tests of plates and solids of revolution in wind tunnels [44],

[22]. The values of the critical Reynolds numbers, obtained in these ex-

periments, show significant scattering, but on the average (for the end

of the transition) are close to the critical Reynolds numbers obtained

by E. Van Dreist (see the curve for $T_{st}/T_r = 1$).

The factors responsible for this divergence between various

- 39 -

experiments cannot be ascertained with a sufficient degree of accuracy; however, it should be pointed out that the magnitude of the critical Reynolds number determined during the experiment can, in addition to the factors indicated above, be affected by the method employed to determine the beginning and the end of the transition from the laminar to the turbulent boundary layer. As was pointed out above, the turbulence of the stream has a significant effect on the critical Reynolds numbers. In the experiments used for the preparation of Fig. 1.15, the turbulence of the air varied, and is completely unknown for a number of cases.

For $M_\delta > 2$ in the case of $T_{st}/T_r \approx 1$, it can be assumed, on the average, that the beginning of the transition occurs at $Re_\delta = 1.5 \cdot 10^6$, and that the end of the transition takes place at $Re_\delta = 3.5 \cdot 10^6$. The last value corresponds to the Van Dreist curve for $M > 3.0$. The difference between the above-indicated Reynolds numbers corresponds to the difference obtained in Van Dreist's experiments [53].

Note should be taken of the fact that the critical Reynolds numbers for plates and solids of revolution, according to the cited experiments, show no pronounced divergence and can therefore, in approximate terms, be assumed to be identical.

Very few experimental data with respect to the critical Reynolds numbers are presented in the literature for the case of $M > 4$. The following experiments might be cited. In the GALCIT (USA) [Guggenheim Aironautical Laboratory, California Institute of Technology] wind tunnel. it was found that in the case of $M = 5.8$ the laminar boundary layer on a plate is preserved to Reynolds numbers of $5.5 \cdot 10^6$. In this case, the laminar boundary layer was extremely stable [8]. In flight tests (No. 27) of the V-2 rocket it was found that at $M_\delta = 4.2$ the beginning of the transition from the laminar to the turbulent boundary layer takes place at $Re_\delta = 2.5 \cdot 10^6$ [44].

M. Bertman found in experiments with cylindrical bodies in a wind tunnel at $M = 6.9$ that the critical Reynolds number may range from $1.2 \cdot 10^6$ to $4.5 \cdot 10^6$, depending on the thickness of the leading edge; in this case, with an increase in the thickness of the leading edge the critical Reynolds number increases. The above-mentioned critical Reynolds number of $4.5 \cdot 10^6$ corresponds to the Reynolds number calculated on the basis of the leading-edge thickness and is equal to $3 \cdot 10^4$ [38].

The above— enumerated experiments at $M > 4$ demonstrate that with great $M(ach)$ numbers, the critical Reynolds numbers do not diminish and lie approximately within the same range as in the case of $M < 4$; therefore, for $M > 4$ the same critical Reynolds numbers can be employed as in the case of $M < 4$.

In the case of surface cooling, i.e., for $T_{st}/T_r < 1$, the critical Reynolds numbers Re_δ will increase as a result of the reduction in viscosity and the increase in density at the surface of the wall. In approx imate terms, it may be assumed that the critical Reynolds numbers are inversely proportional to T_{st}/T_r. This is completely confirmed by the Van Dreist experiments for the case of $M > 3.5$, said experiment shown in Fig. 1.15. For $M < 3.5$ the effect of cooling will be more pronounced, but the cooling itself, caused by thermal radiation, will not be great.

In the case of great $M(ach)$ numbers, the quantity T_{st}/T_r can be substantially reduced and in this connection we can anticipate a pronounced increase in the critical Reynolds number. However, in actual fact, with the cooling of the boundary layer the displacement thickness of the boundary layer diminishes and at a certain cooling ratio the reduced displacement thickness may become close to the height of the roughness protuberances. In this case, any further cooling of the boundary layer will not only fail to increase the critical Reynolds number

but will actually cause it to drop, since the roughness is one of the significant factors resulting in the instability of the boundary layer, particularly if the roughness exceeds the displacement thickness. This phenomenon may be referred to as the reversal of the cooling effect.

The presence of a pressure gradient along the flow has a pronounced effect on the critical Reynolds number: in the case of a positive pressure gradient, the critical Reynolds numbers diminish, whereas in the case of a negative pressure gradient, they increase. With a negative pressure gradient the following pressure is exerted on an elementary portion of air having a volume dxdydz

$$-\frac{dp_1}{dx}\,dx\,dy\,dz,$$

which accelerates the motion of this portion of air. The decelerating force of friction, acting on this same portion of air, will be:

$$\frac{\partial}{\partial y}\left(\mu\,\frac{\partial V}{\partial y}\right)dx\,dy\,dz.$$
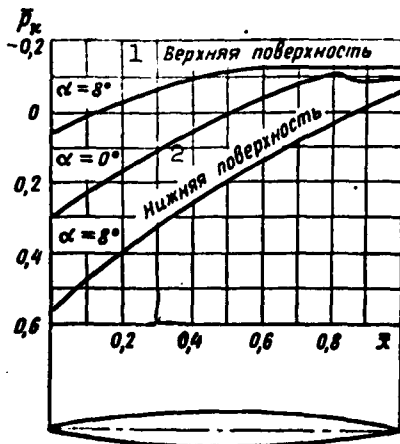
Fig. 1.16. Distribution of pressure over the lenticular profile of a wing. $M = 2.13$; $\bar{c} = 1.1$; $Re = 6.4 \cdot 10^5$; 1) Upper surface; 2) lower surface.

The negative pressure gradient counteracts the decelerating effect of the viscosity forces, as a result of which the stability of the boundary layer is increased.

In the case of supersonic velocities, significant negative pressure gradients are formed on certain types of wing profiles and nose-parts of airframes, and these gradients enhance the stability of the boundary layer. Figure 1.16 shows, as an example, the pressure distribution over the lenticular profile of a wing at $M = 2.13$ [31]. We can see from the cited graph that with small angles of attack the negative

gradient covers almost the entire cord of the profile.

The influence that the pressure gradient exerts on the critical Reynolds number can be determined in approximate terms on the basis of the kinetic-energy balance of the boundary layer. To simplify the derivation of the corresponding relationships, we will assume that the velocity of the flow and the pressure gradient along the surface are constant, which is close to the truth for thin profiles in the case of small angles of attack, as well as in the case of elongated nose sections.

We choose the displacement thickness δ^* as the parameter which characterizes the thickness of the boundary layer in the case of a pressure gradient. The energy introduced into the boundary layer per unit time as a result of the pressure difference along the flow will be

$$E_p = -V_1 \frac{dp}{dx} \int_0^x \delta_{cx}^{\cdot} \, dx.$$

For a compressible fluid, the displacement thickness is equal to (see [48])

$$\delta_{cx}^{\cdot} = \int_0^{\infty} \left(1 - \frac{\rho_y V_y}{\rho_1 V_1} \right) dy.$$

On a flat plate, for the laminar boundary layer, in an incompressible fluid (see [33])

$$\delta^* = 1{,}72 \frac{x}{\sqrt{Re_1}} .$$

(1.63)

In a compressible fluid, the displacement thickness can be found by introducing into Formula (1.63) the ratio of the shape parameters and the densities:

$$\delta_{cx}^{\cdot} = 1{,}72 \frac{H_{cx}}{H} \frac{\rho^*}{\rho_1} \frac{x}{\sqrt{Re^*}} .$$

(1.64)

Here ρ^* and Re^* are calculated for a definite temperature.

The shape parameter

$$H = \frac{\delta^*}{\delta^{**}} ,$$

(1.65)

- 43 -

where δ^{**} is the thickness of momentum loss. For the laminar boundary layer in an incompressible fluid (see [33],[48])

$$H = 2{,}59,$$

and in a compressible fluid (see [48])

$$\frac{H_{cж}}{H} = 1 + 1{,}2\left(\frac{T_{ст}}{T_{\iota}} - 1\right) + 0{,}4\left(\frac{T_r}{T_{\iota}} - 1\right). \qquad (1.66)$$

Expression (1.64) was derived on the basis of Formulas (1.25) and (1.28) and the following relationship (see [48])

$$\frac{H_{cж}}{H} = \left(\frac{\delta^{*}_{cж}}{\delta^{*}}\right)\left(\frac{c_f}{c_{f\,cж}}\right).$$

Substituting the value of $\delta^{*}{}_{szh}$ into the expression for E_p in accordance with Formula (1.64) and assuming the quantity (H_{szh}/H) $(\rho^{*}\mu^{*})^{1/2}$ to be constant along the wall, we will obtain:

$$E_p = -1{,}72\frac{dp}{dx}\frac{H_{cж}}{H}\frac{1}{\rho_{\iota}}(\rho^{*}\mu^{*})^{1/2}V_{\iota}^{1/2}\int_{0}^{x} x^{1/2}dx = -\frac{2}{3}V_{\iota}\delta_{cж}\frac{dp}{dx}x.$$

The energy of the viscosity forces absorbed by the boundary layer per unit time will be

$$E_{\mu} = \int_{0}^{x}\frac{1}{2}c_{f\,cж}\rho_{\iota}V_{\iota}^{3}dx.$$

Taking into consideration the value of $c_{f\,szh}$ in accordance with Formulas (1.25) and (1.28), we will obtain:

$$E_{\mu} = 0{,}332\,(\rho^{*}\mu^{*})^{1/2}\,V_{\iota}^{1/2}\int_{0}^{x} x^{-1/2}dx = \rho_{\iota}V_{\iota}^{3}c_{f\,cж}x.$$

The energy lost in the boundary layer will be:

$$E_{\mu} - E_p = \rho_{\iota}V_{\iota}^{3}c_{f\,cж}x\left(\frac{1 + \frac{1}{3}\delta^{*}_{cж}\frac{dp}{dx}}{\frac{1}{2}c_{f\,cж}\rho_{\iota}V_{\iota}^{2}}\right).$$

According to Formulas (1.25),(1.28), and (1.64), we will find:

$$\frac{\delta^{*}_{cж}}{c_{f\,cж}} = H_{cж}x.$$

Let us make the following denotation:

$$\bar{p}_i = \frac{p}{\frac{1}{2}\rho_i V_i^2},$$

(1.67)

so that

$$E_\mu - E_p = c_{fcx} x \left(1 + \frac{1}{3} H_{cx} \frac{d\bar{p}_i}{dx} x\right) \rho_i V_i^3.$$

(1.68)

Let $(Re_{kr})_0$ be the critical Reynolds number for the given flow parameters at the wall, without any effect due to the pressure gradient, and let $(Re_{kr})_p$ be the critical Reynolds number, with the pressure gradient having been taken into consideration. The value of $(Re_{kr})_p$ will be set equal to that Reynolds number at which the energy losses in the boundary layer will be equal to the energy losses in the boundary layer for which the effect of the pressure gradient has not been taken into consideration. Denoting the quantities which correspond to the flow with a pressure gradient with the subscript "p," and the quantities corresponding to a flow for which the effect of the pressure gradient has not been taken into consideration with the subscript "0" we will have the following for the critical numbers:

$$(E_\mu)_p - E_p = (E_\mu)_0.$$

Let us substitute the value of E from Formula (1.68) into the last expression:

$$(c_{fcx}x)_p \left(1 + \frac{1}{3} H_{cx} \frac{d\bar{p}_i}{dx} x_p\right) = (c_{fcx}x)_0.$$

Since the quantity $c_{f\ szh}$ is inversely proportional to $x^{1/2}$,

$$\frac{x_p}{x_0} = \left(1 + \frac{1}{3} H_{cx} \frac{d\bar{p}_i}{dx} x_p\right)^{-2}.$$

(1.69)

From this expression we can find the sought value of x_p and the ratio x_p/x_0, which correspond to the critical Reynolds numbers, with

$$\frac{(Re_{xp})_p}{(Re_{xp})_0} \approx \frac{x_p}{x_0}.$$

(1.70)

In order to simplify the determination of x_p, a graph constructed in accordance with Formula (1.69) is presented in Fig. 1.17.
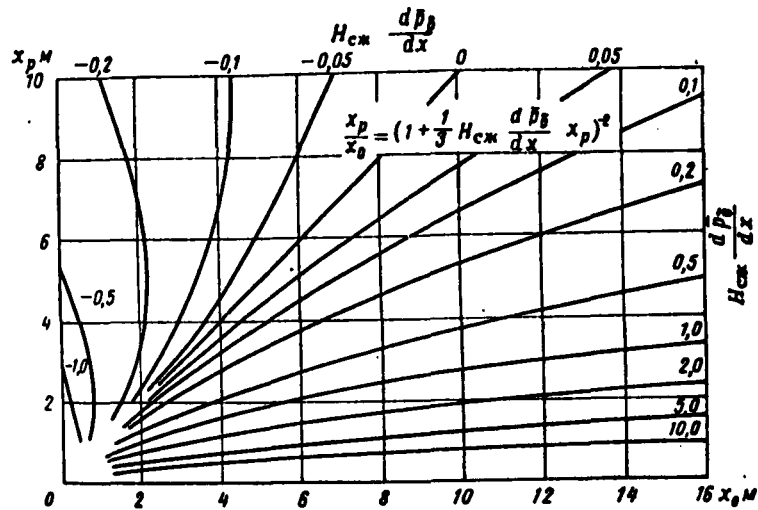
Fig. 1.17. Graph for the determination of the critical length x_p in the presence of a pressure gradient as a function of the critical length x_0 for a flow without a pressure gradient.

For an experimental verification of Formula (1.69) we will present it in a different form for the $M < 1$ case. Let us introduce the Pohlhausen parameter

$$\lambda = -\frac{dp}{dx}\frac{v^2}{\mu V_1}.$$

The thickness of the boundary layer at whose boundary the velocity differs from the streamline velocity by 0.1% (see [33], page 118), will be equal to

$$\delta = \frac{6x}{\sqrt{Re}},$$

and consequently

$$\lambda = -18\frac{d\bar{p}_1}{dx}x.$$

Taking into consideration that for the case $M < 1$ the value of $H = 2.59$, Formulas (1.69) and (1.70) can be presented in the following form:

$$\frac{(Re_{xp})_p}{(Re_{xp})_0} = (1 - 0.048\lambda)^2. \tag{1.71}$$

Figure 1.18 shows a comparison of Formula (1.71) and the experimental data derived in a subsonic wind tunnel [12].
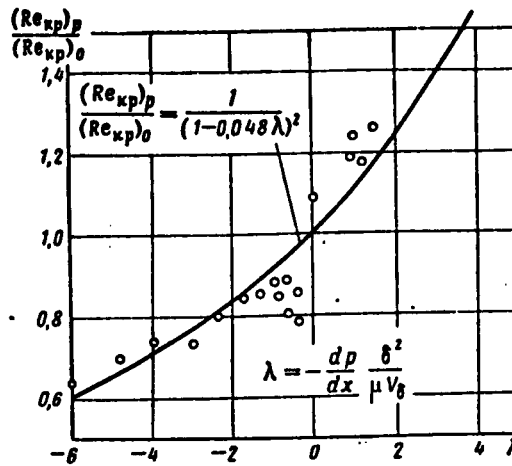
Fig. 1.18. Comparison of theo-
retical and experimental values
of relative critical Reynolds
number in the presence of a pres-
sure gradient.

§1.6. FEATURES OF HEAT TRANSFER IN THE CASE OF HYPERSONIC VELOCITIES

In the case of hypersonic velocities (M > 5) certain mechanical,

physical, and physicochemical phenomena develop at the surface of the

body past which the flow is moving, and these phenomena change the

physical parameters of the air and may either be endothermic or exo-

thermic reactions.

The dissociation, recombination, and ionization of the air can be

included among such phenomena. Moreover, as a result of the increase

in the displacement thickness of the boundary layer in the case of hyper-

sonic velocities, the increasing pressure of the flow at the surface

of the body begins, in this case, to exert a pronounced effect on heat

transfer.

The above-mentioned phenomena are of great significance for heat

transfer in the case of M > 10.

In the case of air dissociation produced by high air temperature,

molecules of oxygen O_2 and nitrogen N_2 decompose into atoms, and in

this case a substantial quantity of heat is absorbed. For example, at

- 47 -

M = 20, the temperature of an ideal gas not subject to dissociation must be 17,500°C in back of a normal shock wave, and for the case of a real gas, taking into consideration the absorption of energy for dissociation, at an altitude of 50 km the temperature will be only 6500° K. For oxygen, total dissociation sets in at 6,000°K, and for nitrogen, at 10,000°K [7].
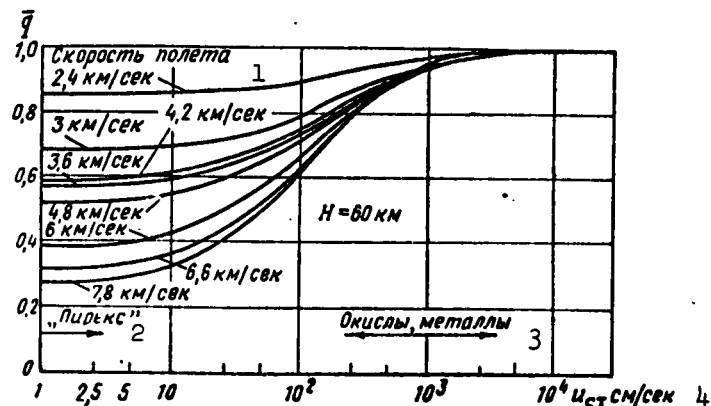
Fig. 1.19. Relative gas-kinetic specific heat flow as a function of the rate of air recombination. 1) Flight velocity, 2.4km/sec; 2) "Pyrex"; 3) oxides, metals; 4) u_{st}cm/sec.

Since the wall-surface temperature in the case of hypersonic velocities will always be lower than the air temperature behind the shock wave, an inverse process — the recombination of the atomic gases — may take place at the wall. In this case, thermal energy will be liberated. Below, we present some data on the effect that dissociation has on heat transfer at the critical point of a blunt body.

The quantity of heat liberated in the case of recombination is a function of the rate of recombination which, in turn, is determined by the concentration of atoms at the surface and the catalytic properties

of the wall. Figure 1.19 shows the theoretical relationship between the relative specific heat flow to the wall ($\bar{q} = q_u/q_{u = \infty}$) and the rate of recombination u_{st} at the wall [8]; the radius of nose curvature in this case is assumed to be 0.5m and the wall temperature is taken as 700°K.

It follows from the cited graph that with recombination rates in excess of 10^3 cm/sec, the effect of recombination on heat transfer becomes close to the maximum and is a weak function of any further increase in the rate. In the case of an infinite recombination rate, heat transfer will be almost the same as in the case in which there is no dissociation [28], i.e., the recombination almost completely offsets the effect of dissociation.

Conversely, at rates of recombination below 10 cm/sec, its effect is insignificant and heat transfer as a result of dissociation may diminish substantially as, for example, with a flight velocity of 7.8 km/se this drop will be greater than by a factor of three.

The rates of natural recombination (without catalysts) are quite low. If atoms impinge on the wall, the rate of recombination may increase manyfold. In this case, the wall acts as a catalyst.

The catalytic properties of the wall are a function of the material of which the wall is made. Metals yield higher rates of recombination, whereas for nonmetallic walls the rates of recombination are substantially lower. Figure 1.20 [8] shows the rates of recombination for oxygen and nitrogen at walls made of various materials; these rates were derived experimentally. There is little data on rates of recombination and therefore the graph shows curves as well as individual points (circles) and approximate areas (large circles with chemical denotations of elements.

A comparison of the curves shown in Figs. 1.19 and 1.20 shows clearly that a metallic wall will receive only slightly less heat than

at which recombination takes place at an infinately great rate. It should be borne in mind that with an increase in temperature the rate of the catalytic reactions also increases; this can also be seen from Fig. 1.20. Therefore, in first approximation, dissociation need not be taken into consideration in the case of a metallic surface.
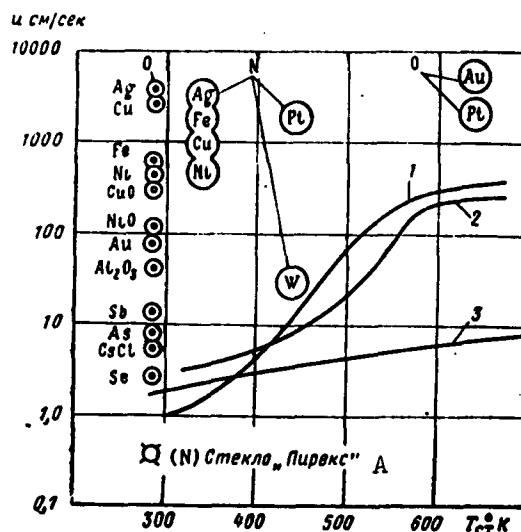
Fig. 1.20. Catalytic properties of various materials in recombination of air atoms at the wall. 1) KCl; 2) LiCl; 3) "Pyrex" glass; A) "Pyrex" glass.

In the case of a wall made of a glass-based material, the reduction in the transfer of heat may be significant, since the rates of recombination in this case will not be great.

Chlorides, oxides of metals, and certain other nonmetallic materials will yield intermediate heat-transfer values. It should be pointed out that since with an increase in wall temperature the rate of recombination increases, a comparatively slight drop in heat transfer with respect to the transfer of heat in the case of an infinite recombination rate may be permitted for the group of materials under consideration.

In the case of flow past plane and cylindrical surfaces, the

- 50 -

phenomena of dissociation and recombination take place under somewhat different conditions than in the case of flow past the area close to the critical point. The theoretical investigations of heat transfer in the case of a laminar boundary layer show that the effect of dissociation on heat transfer in this case is not too great [19].

Given high temperatures, characteristic in the case of hypersonic-velocity flow past bodies, the atoms and molecules of the air, in addition to dissociation, will also be subject to ionization. Given the air temperatures that prevail about a body flying through the atmosphere at hypersonic velocities, the degree of ionization will not be great. For example, with M = 20 approximately 1% of the air will become ionized (see [3]). This degree of ionization has little effect on heat transfer.

Although for M < 25 the effect of ionization on heat transfer is insignificant, it may be important in the case of radio communications [21].

In determining heat transfer, it is necessary to know the temperature difference $T_r - T_{st}$ [see Formula (1.7)]. On the other hand, the specific heat of the air is included in Formula (1.29) in order to determine the heat-transfer coefficient. The product of these two parameters must characterize the change in gas energy as the gas is cooled from a temperature of T_r to the temperature T_{st}.

In the case of hypersonic velocities, it frequently becomes necessary to deal with an extremely great temperature difference $T_r - T_{st}$ in which range the specific heat of the air may undergo pronounced change. Therefore, instead of the following product

$$(T_r - T_{ct}) c_p^*$$

it is more effective to introduce the enthalpy

$$i = \int_0^T c_p \, dT \qquad (1.72)$$

- 51 -

and to express the specific flow of heat during aerodynamic heating in the following form:

$$q_\bullet = \alpha_i (I_r - I_{cr}),$$

(1.73)

where

$$\alpha_i = gs^* c_{p}^{\bullet} V_\bullet.$$

(1.74)

The value of the heat-transfer coefficient α_1 may be determined by means of Formulas (1.30), (1.31), (1.32), (1.39), and (1.62), if the quantity c_p^* in this formula is removed.

The enthalpy value for various temperatures can be found from Fig. 1.21 (see [48]).

Formula (1.62) was derived for the determination of heat transfer at the critical point of a rounded nose. In the case of great hypersonic velocities, a structurally simpler formula may be employed; this formula was derived on the basis of experiments carried out in a wind tunnel (see [41]):

$$q_0 = 2,63 \cdot 10^4 \left(\frac{p_\infty}{p_0}\right)^{\prime/\prime} \left(\frac{V_\infty}{V_{koc}}\right)^{3,15} R^{-\prime/\prime} \frac{i_0 - i_{cr}}{i_0 - i_{300}},$$

(1.75)

where V_{kos} is the first cosmic velocity at the ground equal to $V_{kos} = 7.$ km/sec.
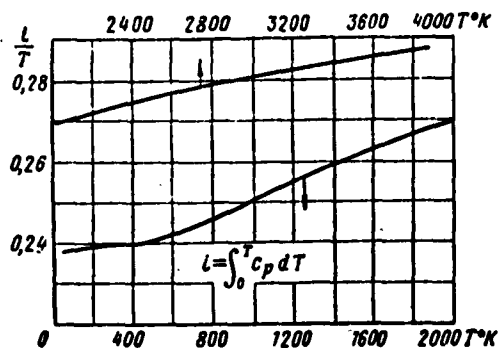
Fig. 1.21. Enthalpy of air, referred to temperature, as a function of air temperature.

Since in the derivation of Formula (1.75) we have taken into consideration the experiments that were carried out at hypersonic velocities all the way to cosmic velocities, the effect of the dissociation and recombination of the air has, therefore, been accounted for in this formula. The experiments which served as the basis for this formula were carried out with glass "pyrex" models, and this material exhibits weak catalytic properties (see Fig. 1.20). However, the transfer of hea

- 52 -

in these experiments was measured by means of calorimeters which consist of platinum plates placed into the stream (see [49]). We can see from Fig. 1.20 that platinum exhibits high catalytic properties ($u_{st} >$ 10^3 cm/sec), and therefore Formula (1.75) yields the transfer of heat for the surfaces that exhibit the greatest recombination rates.

The enthalpy value i_0 at the critical point may also be derived on the basis of the fact that all of the kinetic energy in the decelerated flow is converted into thermal energy. Then

$$i_0 = i_\infty + \frac{\frac{1}{2} V_\infty^2}{427g} = i_\infty + 1,2 \cdot 10^{-4} V_\infty^2, \qquad (1.76)$$

where i_∞ is the enthalpy of the air in an undisturbed flow; this value of the enthalpy, as well as i_{st} and i_{300} can be found from Fig. 1.21.

Because of the existence of the boundary layer, the main stream is deflected from the wall by approximately the displacement thickness (see[48]). With great hypersonic velocities, the displacement thickness of the boundary layer shows a pronounced increase, and this results in an increase for the angle of inclination of the limit of the displacement thickness, and consequently it leads to an increase of pressure in the stream and at the wall. The increased pressure results in increased air density which, in turn, produces an increased heat-transfer coefficient.

The increase in pressure produced by the boundary layer can be determined by assuming the boundary layer, having a thickness δ^*_{szh}, to have solidified. In this case, a flat plate will be similar to a profile exhibiting maximum thickness at the trailing edge.

The local angle of inclination for the limit of the boundary layer, corresponding to the displacement thickness, will be

$$\Delta \varphi = \frac{d \delta^*_{cx}}{dx}. \qquad (1.77)$$

This angle is added to the local geometric angle for the flow; in

the case of a cone, the half-angle of the cone flare increases by the angle $\Delta\varphi$.

The value of the derivative in Formula (1.77) is easily determined for a plate with a laminar boundary layer by Formula (1.64):

$$\frac{d\delta_{cx}^*}{dx} = \frac{1}{2}\,\delta^*/x. \qquad (1.78)$$

Hence we can see that with an increase in the displacement thickness there is an increase in the local angles of stream inclination.

Having determined the value of $\Delta\varphi$, the formulas presented in §1.3 can be used to find the heat-transfer coefficient, making provision for consideration of the pressure produced by the boundary layer. As a result of the increase in pressure, the air parameters for the boundary layer change, and this produces a change in the displacement thickness. Therefore, in order to increase accuracy, second-approximation calculations can be carried out. However, in the case of $M_\infty < 15$ and $R_e > 10^5$, one approximation is sufficient.

The influence exerted by the boundary layer on pressure is a strong function of the Reynolds number. Figure 1.22 shows the graph for pressure at the surface of a flat plate in the case of two Reynolds numbers with respect to M_∞ numbers. We can see from the graph that for $Re_\infty > 10^6$ the effect of the boundary layer on pressure is not great.

The boundary layer exerts a significant effect on the pressure in the case of low Reynolds numbers. Therefore, it is particularly important to take into consideration this effect in the case of flights at great altitudes, as well as in the determination of heat transfer in the area of the leading wing edge or close to the pointed nose of a cone.

The boundary layer is generally turbulent for $Re_\infty > 10^6$, and therefore its effect on pressure is not great.

Since the effect exerted by the boundary layer diminishes with the increase in the Reynolds number (Fig. 1.22) a negative pressure gradient

can be observed along the surface. This will enhance a rise in the critical Reynolds number.

The heating of the air behind the shock wave increases the intensity of air radiation. At near-cosmic velocities, the intensity of radiation from the air behind the normal shock wave is so great that it can sometimes produce a radiant energy flux that impinges on the forward surface and is of the same order of magnitude as the heat flows which occur as a result of aerodynamic heating.
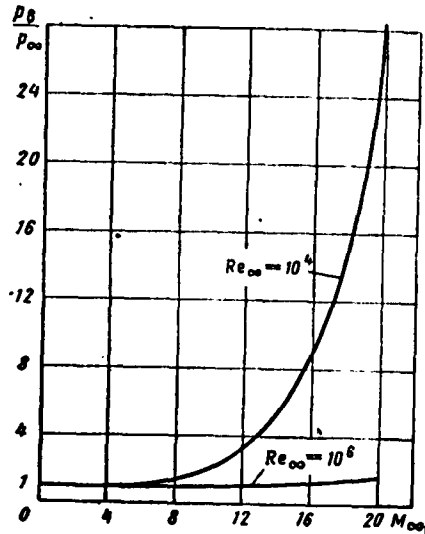
Fig. 1.22. Relative pressure at surface of plate at $\alpha = 0$, said pressure arising as a result of the boundary layer.

The importance of this radiant-energy flux in the over-all transfer of heat resulting from the increase in flight velocity exhibits an extremely rapid rise. Indeed, if the specific convection heat flow q_a at the critical point of a blunt-nose body is approximately proportional to

$$q_a \sim \rho_\infty^{1/2} R^{-1/2} V^3,$$

the heat flow q_1 of radiant energy emitted by the air behind the shock wave is approximatly proportional to (see [16])

$$q_a \sim \rho_\infty^{1/2} R V^{10}.$$

We can also see from the last relationship that the radiant heating being examined here will increase with a drop in altitude, and this will take place more intensly than aerodynamic heating. It is also characteristic that with an increase in the radius of nose curvature the aerodynamic heating is reduced and radiant heating increases.

The gases included in the composition of the air do not radiate in an identical manner, and so the importance of the radiation from the various components of the air changes with temperature and density. For

example, at a temperature of 8,000° K, i.e., characteristic of the air behind the shock wave, in the case of near-cosmic velocities a great role is played in the total radiation by nitrogen monoxide NO which is formed at high temperatures in the air, and molecular nitrogen N_2 is also extremely important. At a temperature of 12,000° K, characteristic of velocities close to the second cosmic velocity, molecular nitrogen and nitrogen monoxide dissociate and the primary emitters are the atoms and ions of nitrogen and oxygen.

The thickness of the emission layer which, in first approximation, can be assumed to be equal to the distance between the shock wave and the critical point, exerts great influence on the intensity of air radiation. The distance between the shock wave and the critical point, in turn, is a function of a number of factors including the radius of nose curvature, the density of the air, and the degree of dissociation.

In connection with the great number of factors which affect the radiation of the air behind the shock wave, a purely theoretical determination of the emissivity of the air behind the shock wave is extremely complex and none too reliable. For this reason, experimentation plays a more important role. At the present time, these experiments are being carried out in wind tunnels.

It was found in the experiments that were carried out that given a nose radius of 0.3 m, and M = 20 and at altitudes of the order of 30 km, radiative heat transfer will amount approximately to 10% of the tota heat flow to the critical point (see [13]). A similar result was obtaine by R. Meyerott [16] in his theoretical determination of radiation for a nose having a radius of curvature of 0.6 m at V = 7.5 km/sec for an altitude of 37 km.

However, at greater flight velocities the heat flow due to the rad iation of the air may exceed the convection heat flow. For example, in

accordance with calculations carried out by K. Gezli and D. D. Messon during a vertical ascent into the atmosphere at a velocity of 10.7 km/sec of a sphere having a radius of 0.46 m, at altitudes between 30 and 40 km the heat flow due to radiation was greater approximately by a factor of two than the convection heat flow (see [16]).

A rough estimate of the heat produced by the radiation of the air behind the shock wave and absorbed at the critical point of a blunt-nosed body can be obtained in accordance with the following formula:

$$q_s \approx 1,6 \cdot 10^6 \left(\frac{\rho_\infty}{\rho_0}\right)^{1/2} \left(\frac{V_\infty}{V_{кос}}\right)^{10} R.$$

(1.79)

This formula was derived on the basis of an evaluation of calculation values from the approximate functional relationship presented above. This formula can be employed for the determination of the limits of applicability for Formulas (1.62), (1.73), and (1.75). If the value is of the same order of magnitude as q_0 according to the cited formula, where if the value is greater, then it is evident that it is impossible to determine heating by means of the aerodynamic heating formulas alone.

Chapter 2

RADIATIVE AND ABSORPTIVE PROPERTIES OF BODIES

§2.1. THE BASIC LAWS OF RADIATION AND THE ABSORPTION OF RADIANT ENERGY

The significance of radiation in the general thermal balance depends on the surface temperature and the magnitude of the exterior heat flows. With aerodynamic heating in flight at velocities of $M < 3$, the significance of surface radiation is comparatively slight; however, it should be considered. In the case of a flight in which $M > 5$, radiation may be considerable; here, radiation may be the most effective means for reducing surface temperature.

For instance, in the example of aerodynamic heating discussed in §3.1 where $M = 5$ at an altitude of 30 km, the temperature of the surface at a distance corresponding to 10% of the wing chord, in the absence of radiation, would equal 860°C, while as a result of radiation it is reduced to 380°C, i.e., by 480°C. When flight velocity increases, the radiation required to reduce surface temperature is increased.

The heat of radiation in the case of a steady-state thermal regime has the greatest influence on the surface temperature, whereas in the case of aerodynamic heating

$$q_{rad} = q_a.$$

In the case of a nonsteady-state regime of aerodynamic heating, the influence of radiation decreases, since,

$$q_{rad} = q_a - q_{mar}.$$

For space vehicles, radiation is the only practical method of dissipating the heat of radiant solar and planetary energy absorbed by

the surface of the craft. Using the radiation, we may also dissipate the heat given off by the electronic equipment.

Also of great significance for space craft is the reflective capacity of the wall, since the amount of the absorbed radiant energy from the sun and planets depends on the magnitude of this reflective capacity.

The radiation of an absolutely black body obeys Planck's law;

$$E_\lambda = \frac{c_1 \lambda^{-5}}{(e^{c_2/\lambda T} - 1)},$$ (2.1)

where E_λ is the intensity of the monochromatic radiation; λ is the wavelength of the radiation; T is the absolute temperature of the radiating body.

If the letter E denotes the total energy radiated per unit body surface per unit time, then

$$E_\lambda = \frac{dE}{d\lambda}.$$ (2.2)

The constants c_1 and c_2 in Eq. (2.1) are equal to (see [4]):

$c_1 = 8.85 \cdot 10^{-10}$ kcal $\cdot$ m^2/sec; $c_2 = 1.44 \cdot 10^{-2}$ m $\cdot$ deg.

The integration of Eq. (2.2) simultaneously with Eq. (2.1) enables us to find the radiation energy of an absolutely black body; the radiant energy is

$$E = \frac{\pi^4 c_1 T^4}{15 c_2^4} = \sigma T^4,$$ (2.3)

where σ is the Stefan-Boltzmann constant, equal to

$$\sigma = 13 \cdot 6 \cdot 10^{-12} \text{ kcal/m}^2 \cdot \text{sec} \cdot \text{deg.}^4$$

Real bodies are not entirely subject to Eq. (2.3). The magnitude of their radiation is less than the radiation of an absolutely black body, so that for a real body

$$E = q_{1z} = \varepsilon \sigma T^4$$

where ε is the emissivity or blackness coefficient and $\varepsilon < 1$.

- 59 -

The radiant energy falling on the surface of the body is completely absorbed only in the case of an absolutely black body. Real bodies either reflect or admit a part of the incident energy, or they go through both processes simultaneously. The relation between the absorption and radiation capacities is established by the Kirchhoff law.

If ε_λ is the emissivity for a given spectral wave, and β_λ is the absorption coefficient for the same wave, equal to a portion of the absorbed energy, then in accordance with the Kirchhoff law, at a given surface temperature

$$\beta_\lambda = \varepsilon_\lambda.$$

The coefficients of intergral radiation and absorption at a given surface temperature do not equal one another and depend on the spectral composition of the radiated and absorbed energy. The value of these coefficients may be defined as the mean integrals, using Eq. (2.3);

$$\varepsilon = \frac{\int\limits_0^\infty \varepsilon_{\lambda 1} E_{\lambda 1}\, d\lambda}{\int\limits_0^\infty E_{\lambda 1}\, d\lambda} = \int\limits_0^\infty \varepsilon_{\lambda 1} E_{\lambda 1} \frac{d\lambda}{\sigma T_1^4}; \qquad (2.4)$$

$$\beta = \frac{\int\limits_0^\infty \beta_{\lambda 1} E_{\lambda 2}\, d\lambda}{\int\limits_0^\infty E_{\lambda 2}\, d\lambda} = \int\limits_0^\infty \varepsilon_{\lambda 1} E_{\lambda 2} \frac{d\lambda}{\sigma T_2^4}. \qquad (2.5)$$

Here, the subscript "1" is used to designate the magnitudes of the body being investigated, for a surface temperature T_1, while the subscript "2" is used to denote the magnitudes of the source of radiant energy absorbed by the body at temperature T_2. The values of $E_{\lambda 1}$ and $E_{\lambda 2}$ may be determined from Formula (2.1).

The intensity of the monochromatic radiation E_λ has a maximum for each temperature. As an example, Fig. 2.1 gives the curves of the values of $E_\lambda/(E_\lambda)_{max}$ for 6000°K (temperature of sun) and 1000°K; these curves were constructed according to Formula (2.1). It is apparent from the

graph that when the temperature of the surface increases, the maximum measurement intensity is shifted to the shorter waves and becomes more pronounced.
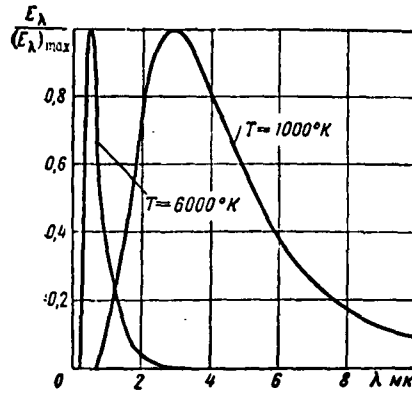
Fig. 2.1. Relative intensity of the radiation of an absolutely black body as a function of the length of the radiation wave and the temperature of the body.
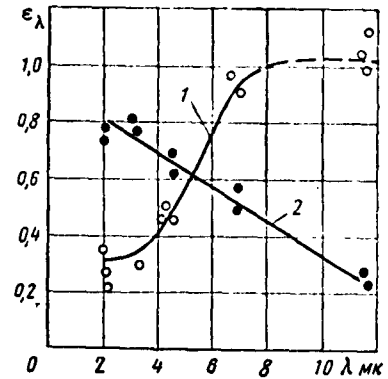
Fig. 2.2. Coefficients of monochromatic radiation as a function of the wave-length for nickel alloy and ceramics. 1) ceramic A-417/235, T = 760 to 1000°C; 2) nickel alloy, T = 760° to 800°C.

The ratio between the surface temperature of an absolutely black body and the wavelength λ_m at maximum radiation intensity is determined by Wien's law which may be obtained from Eq. (2.1) by differentiating. According to this law

$$\lambda_m = \frac{2898}{T},$$

(2.6)

where λ_m is measured in microns. Wien's law enables us to estimate the wavelength in the region in the region in which the radiation intensity is greatest.

Solids can be classified on the basis of their radiant and absorption properties as conductors of electric current, insulators, and semiconductors. Metals are associated with the conductors, while ceramic material such as plastics, lacquers, paints, etc., are associated with insulators.

Conductors and insulators radiate and absorb radiant energy in

- 61 -

various ways. Conductors exhibit low emissivity at normal temperatures, while insulators exhibit high emissivity. Conductors and insulators vary in the spectral composition of radiant energy: in the case of conductors radiative capacity is most important in the shortwave region, while in the case of insulators radiative is most important in the longwave region. As an illustration of this, Fig. 2.2 gives the coefficients of monochromatic radiation for metal and ceramics as function of wavelength; these coefficients were obtained by experiment [40].

§2.2 EMISSIVITIES FOR VARIOUS BODIES AND SURFACE CONDITIONS

The temperature of the surface can have a considerable influence on the radiative capacity of a body. Metals, as was indicated in §2.1, have low emissivity in the case of long waves. However, when the wavelength decreases, the emissivity of metals increases. If we take into consideration the fact that according to Wien's law the wavelength of maximum-intensity radiation decreases with an increase in the surface temperature, the integral radiative capacity of metals should increase with temperature. This is confirmed by experiments.

Figure 2.3 (see [40]) gives the curves of the integral emissivity for heat-resistant alloys (lower curves). As can be seen, at temperatures higher than 600°C, the increase in emissivity can be considerable.

The integral-radiation coefficients for some metals are given in Table 2.1; this table also gives the temperature ranges of the experiment and the corresponding ranges of the change in emissivity.

It is also apparent from Table 2.1 that as the temperature increases, emissivity increases.

Emissivity for metals depends on their electric conductivity. The best conductors have lower emissivity. We can see from Table 2.1 that good conductors of electricity, such as aluminum, gold, copper, and silver, have low emissivity.

- 62 -
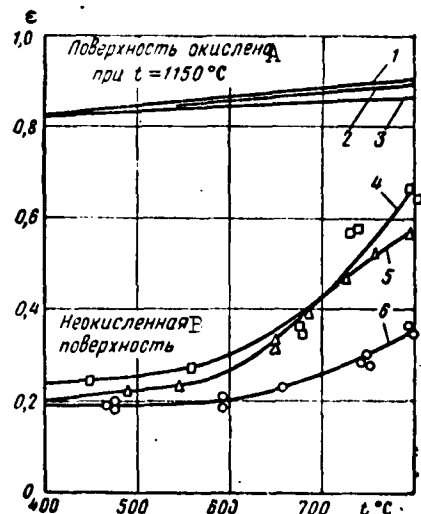
Fig. 2.3. The influence of the surface temperature on the coefficient of integral radiation from heat-resistant metals. 1) stainless steel; 2) nickel-cobalt alloy; 5) stainless steel; 6) nichrome; A) oxidized surface with t = 1150 C; B) unoxidized surface.

It is possible to coat a metal with lacquers or paints which are poor conductors of electricity and heat.

In this case, the emissivity increases sharply and approaches unity.

Table 2.2 gives the emissivity for certain paint coatings.

It should be noted that although certain paint coatings are white, their radiative capacity is close to unity. This is explained by the fact that their good reflective capacity (and consequently, poor radiative capacity) is manifested only in comparatively short wavelengths corresponding to the range of visible radiation. These coatings radiate infrared rays well. This same phenomenon may also be found in the case of certain other dielectrics. For example, at 20°C, the emissivity of chalk is 0.81 [9], for gypsum, it is 0.90 [17], and for glazed

- 63 -

TABLE 2.1.

Integral Emissivity for Some Metals (see [17])

1 Наименование	t° C	ε
2 3 Алюминий полированный	$225 \div 575$	$0,039 \div 0,057$
3 Железо полированное	$425 \div 1020$	$0,144 \div 0,377$
4 5 Железо литое необработанное	$925 \div 1115$	$0,87 \div 0,95$
Стальное литье полированное	$770 \div 1040$	$0,52 \div 0,56$
6 Сталь листовая шлифованная	$940 \div 1100$	$0,55 \div 0,61$
7 Нержавеющая сталь [40]	$480 \div 800$	$0,22 \div 0,575$
8 Никель чистый, полированный	$225 \div 375$	$0,07 \div 0,087$
9 10 Хром	$100 \div 1000$	$0,08 \div 0,26$
10 Нихром [40]	$480 \div 800$	$0,19 \div 0,35$
11 Никель-кобальтовый сплав [40]	$450 \div 800$	$0,25 \div 0,65$
12 Цинк (99,1%), полированный	$225 \div 325$	$0,045 \div 0,053$
13 Оцинкованное листовое железо	28	0,228
14 Золото полированное	$225 \div 635$	$0,018 \div 0,035$
15 Медь полированная, электролитная	$80 \div 115$	$0,018 \div 0,023$
16 Серебро полированное, чистое	$225 \div 625$	$0,020 \div 0,032$
17 Платина полированная, чистая	$225 \div 625$	$0,054 \div 0,104$
18 Бронза шлифованная [43]	65	0,04
19 Бронза пористая [43]	$75 \div 175$	0,57
20 Молибден [11]	$600 \div 1000$	$0,08 \div 0,13$
21 Молибден [11]	$1500 \div 2200$	$0,19 \div 0,26$

1) Item; 2) polished aluminum; 3) polished iron; 4) crude cast iron; 5) polished steel casting; 6) sheet ground steel; 7) stainless steel [40]; 8) nickel, pure; 9) chrome; 10) nichrome [40]; 11) nickel-cobalt alloy [40]; 12) zinc (99.1%), polished; 13) zinc-plated sheet iron; 14) polished gold; 15) polished copper, electrolytic; 16) polished silver, pure; 17) polished platinum, pure; 18) ground bronze [43]; 19) porous bronze [43]; 20) molybdenum [11]; 21) molybdenum [11]

porcelain it is 0.92 [17].

The use of paint coatings is limited because they are stable only to comparatively low temperatures, e.g., heat-resistant enamel 101/19 and black asphalt lacquer are stable when subject to extensive heating to 250°C. Heat-resistant enamel with an aluminum coating is stable approximately to 400°C; however, aluminum paints have a low emissivity $\varepsilon = 0.35$ [17]. The addition of aluminum powder has a telling effect.

We can use the oxide films of certain metals as heat-resistant coatings which have high radiation capacity. For example, iron oxide

TABLE 2.2.

Emissivities for Certain Paint Coatings

Тип покрытия [1]	t° C	ε	Литератур- ный источ- ник [2]
[3] Лак белый	40÷95	0,80÷0,95	[17]
[4] Лак черный матовый	40÷95	0,96÷0,98	[17]
[5] Лак черный блестящий	25	0,87	[17]
[6] Бакелитовый лак	80	0,93	[36]
[7] Шеллак черный матовый	74÷145	0,91	[17]
[8] Масляные краски различных цветов	100	0,92÷0,96	[17]
[9] Эмалевая краска	20	0,85÷0,95	[36]
[10] Сажа ламповая (0,075 мм и больше)	40÷370	0,94	[17]
[11] Сажа с жидким стеклом	100÷185	0,96÷0,95	[17]
[12] Алюминиевая краска	150÷315	0,35	[17]

1) Type of coating 2) literature source; 3) white lacquer; 4) dull black lacquer; 5) bright black lacquer; 6) bakelite lacquer; 7) dull black shellac; 8) oil paints of various colors; 9) enamel pain; 10) lamp black (0.75 mm and more; 11) carbon black with liquid glass; 12) aluminum paint.

in the temperature range from 500 to 1200°C exhibits an emissivity which ranges from 0.85 to 0.95; the emisivity of nickel oxide in the temperature range from 650 to 1255°C ranges from 0.59 to 0.86 [17].

The use of metal oxide films to increase radiation capacity is advantageous in that they are easy to apply, while the cohesion strength with metal in the case of a thin layer is substantial. The simplest method of obtaining a film involves the preliminary heating of a metal and keeping it at a high temperature in air for several minutes.

Figure 2.4 shows the emissivity curves for stainless steel at various temperatures as functions of the oxidation temperature. The tested specimens were kept at the oxidation temperature for fifteen minutes. The graph given in Fig. 2.4 was constructed on the basis of experimental data given in work [40].

It is apparent from the graph that the oxidation of stainless

steel at 50°C for fifteen minutes increases the emissivity approximately to ε = 0.9. This is also true for a number of other alloys (see Fig. 2.3).
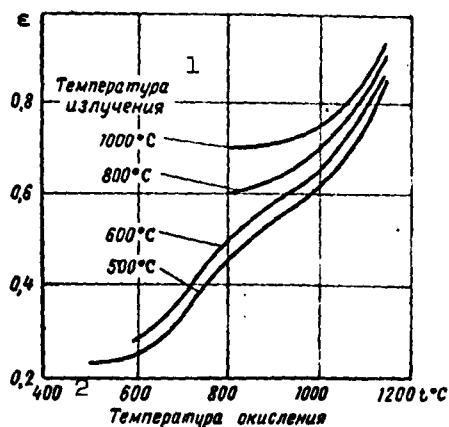
Fig. 2.4 The influence of the oxidation temperature on the emissivity of stainless steel. 1) Radiation temperature; 2) oxidation temperature.

While the oxide films are effective in the case of those metals indicated in Fig. 2.3, they are not as effective with others. For certain metals, even though the oxide film does increase the radiation, emissivity remains very far from unity. For example, in the case of an aluminum oxide film, obtained by means of soaking at 600°C, the emissivity is increased by a factor of approximately three, but the value of this coefficient is still small; for the temperature range from 200 to 600°C this value ranges from 0.11 to 0.19 [17].

Table 2.3 gives the emissivities for a number of metals with oxidized surfaces. For comparison, the emissivities of these same metals with nonoxidized surfaces are also given in this table.

The emissivity increases as the surface roughness increases. If the height of the roughness tubercles is several times greater than the radiation wavelength the emissivity ε_{sh} of the rough surface as a function of the emissivity ε of a smooth surface, may be expressed by the following formula;

$$\varepsilon_{sh} = \varepsilon [1 + 2,8(1 - \varepsilon)^2].$$

(2.7)

The structure of this formula is theoretically derived from Lambert's law, according to which the quantity of radiant energy at an angle ψ to the normal is proportional to $\cos \psi$.

TABLE 2.3.

The Effect of Oxidation of a Metal Surface on its Radiation Capacity

Наименование 1	t° C	ε	Литератур- ный источ- ник 2
3 Сталь литая полированная	770÷1040	0,52÷0,56	[17]
4 Сталь окисленная при 600° C	200÷600	0,80	[17]
5 Нержавеющая сталь	480÷800	0,22÷0,575	[40]
6 Нержавеющая сталь, окисленная при 800° C	450÷840	0,43÷0,63	[40]
7 Нержавеющая сталь, окисленная при 1000° C	480÷970	0,62÷0,73	[40]
8 Нержавеющая сталь, окисленная при 1150° C	480÷1150	0,85÷0,96	[40]
9 Никель полированный	225÷375	0,07÷0,087	• [17]
10 Никель, окисленный при 600° C	200÷600	0,37÷0,48	[17]
11 Нихром	480÷800	0,19÷0,35	[40]
12 Нихром, окисленный при 1150° C	480÷1150	0,75÷0,90	[40]
13 Никель-кобальтовый сплав	450÷800	0,25÷0,65	[40]
14 Никель-кобальтовый сплав, окисленный при 1150° C	450÷1150	0,85÷0,98	[40]
15 Алюминий полированный	225÷575	0,039÷0,057	[17]
16 Алюминий, окисленный при 600° C	200÷600	0,11÷0,19	[17]
17 Медь полированная	80÷115	0,018÷0,023	[17]
18 Медь, окисленная при 600° C	200÷600	0,57÷0,87	[17]
19 Латунь матовая	50÷350	0,22	[17]
20 Латунь, окисленная при 600° C	200÷600	0,61÷0,59	[17]
21 Цинк полированный	225÷325	0,045÷0,053	[17]
22 Цинк, окисленный при 400° C	400	0,11	[17]

1) Item; 2) literature source; 3) polished cast steel;
4) steel oxidized at 600°C; 5) stainless steel; 6) stainless steel
oxidized at 800°C; 7) stainless steel oxidized at 1000°C; 8) stainless
steel oxidized at 11502°C; 9) polished nickel; 10) nickel oxidized at
600°C; 11) nichrome; 12) nichrome oxidized at 1150°C; 13) nickel-
cobalt alloy; 14) nickel-cobalt alloy oxidized at 1150°C; 15) polished
aluminum; 16) aluminum oxidized at 600°C; 17) polished copper; 18)
copper oxidized at 600°C; 19) dull brass; 20) brass oxidized at 600°C;
21) polished zinc; 21) zinc oxidized at 400°C.

The coefficient 2.8 was determined on the basis of experiments.

Figure 2.5 gives the results of an experimental check of Formula (2.7).

The radiation capacity of porous bodies is substantially increased,
since each pore may be looked upon as an absolutely black body. For
example, porous bronze in the temperature range from 75 to 175° has an
emissivity of ε = 0.57, while ground bronze without pores at 65° has

an emissivity of $\varepsilon = 0.04$ [43].

At the present time, broad distribution has been given to laminated plates, which together with good structural properties possess superior heat-insulation properties. With respect to radiation capacity, they behave like all other dielectrics, i.e., they have high emissivity at temperatures lower than those which characterize their heat resistance.

Laminated plates are based on binding substances, generally resins and fillers. In laminated plates with high mechanical properties, we use fiberglas, glass fabric, asbestos fabric, cotton, or silk. Table 2.4 gives the emissivity of certain filler materials. We can determine the radiation of resin from the emissivity of bakelite lacquer, which is given in Table 2.2. As can be seen from Table 2.4 (and also Table 2.2), the emissivities of the materials forming the laminated plates are close to 0.9.
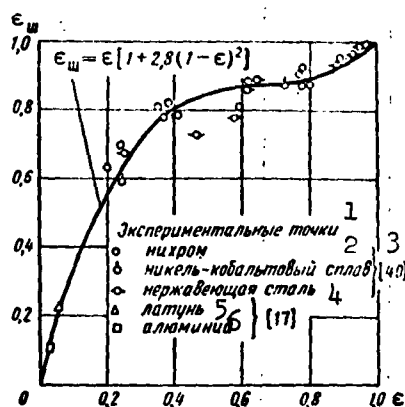
Fig. 2.5. The effect of roughness on the emissivity. 1) Experimental points; 2) nichrome; 3) nickel-cobalt alloy; 4) stainless steel; 5) brass; 6) aluminum.

TABLE 2.4.

Emissivities of Filler Materials for Laminated Plates, etc.

Наименование 1	t° C	ε	Литературный источник 2
3 Асбестовая бумага	40÷370	0,93÷0,95	[17]
4 Бумага тонкая, наклеенная на металлический-лист	95	0,89	[17]
5 Дерево	70	0,91	[36]
6 Стекло	20÷100	0,94÷0,91	[11]
7 Стекло	250÷1000	0,87÷0,72	[11]
8 Стекло	1100÷1500	0,70÷0,67	[11]
9 Уголь	100÷600	0,81÷0,79	[11]
10 Гипс	20	0,8÷0,9	[11]

1) Item; 2) literature source; 3) asbestos paper; 4) thin paper glued to a metal sheet; 5) wool; 6) glass; 7) glass; 8) glass; 9) carbon; 10) gypsum.

§2.3. ABSORPTION COEFFICIENTS FOR VARIOUS BODIES

In the case of flight at very high altitudes (higher than 150 km) and in the case of cosmic flights, a basic source of heat is the sun. In this case, as will be shown further in §3.3, the basic parameter in determining the temperature of the wall is the relation of the absorption coefficient to the radiation coefficient (emissivity), that is, β/ε [see Formulas (3.9), (3.10), and (3.11)]. Let us note that β corresponds to the solar radiation spectrum while ε corresponds to the spectrum of infrared rays at the temperature of the wall.

Because of the selective nature of the absorption capacity, the ratio β/ε will be located in a broad range of values. Figure 2.6 gives the coefficients β_λ of monochromatic absorption for certain polished metals depending on the length of absorbed radiant energy (see [15] p. 241). It is apparent from the graph that the absorption capacity of metals for the energy of solar rays with maximum intensity (the wavelength is 0.5 µ) increases greatly in comparison with the absorption capacity, and consequently with the radiation capacity (the Kirchhoff

law). For infrared rays corresponding to the possible temperature of the wall (the wavelength of a ray with maximum intensity is 6 to 8 μ).

In the case of metals with very good electric conductivity (silver, copper, gold) there is a sharp increase in the absorption coefficient, which begins at wavelengths of approximately 1 μ. For other metals, the absorption coefficient increases gradually as the wavelength decreases.
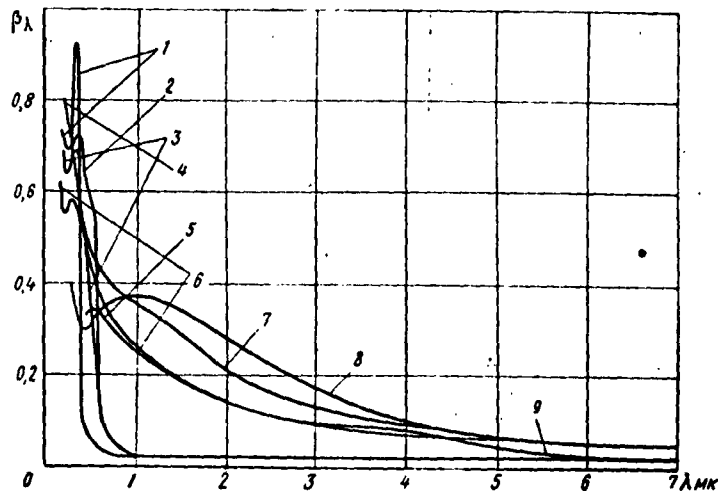
Fig. 2.6. Coefficients of monochromatic absorption of various metals. 1) silver; 2) gold; 3) copper; 4) steel; 5) aluminum; 6) nickel; 7) steel; 8) chrome; 9) nickel.

The integral absorption and radiation capacities are determined to a significant degree by coefficients corresponding to absorption and radiation at the wavelength λ_m of maximum intensity.

Table 2.5 gives values of the ratio $\beta_{\lambda 2}/\varepsilon_{\lambda 1}$, found from Fig. 2.6; In addition, $\beta_{\lambda 2}$ was determined at λ_m = 0.5 μ, while $\varepsilon_{\lambda 1}$ was determined at λ_m = 7 μ.

It is characteristic of metals that the ratio $\beta_{\lambda 2}/\varepsilon_{\lambda 1}$ is greater than one. Silver has the lowest value of $\beta_{\lambda 2}/\varepsilon_{\lambda 1}$ and gold has a higher value of $\beta_{\lambda 2}/\varepsilon_{\lambda 1}$; however, in the region of maximum absorption intensity (λ_m = 0.5 μ), the absorption coefficient for gold drops

- 70 -

sharply and consequently, the integral coefficient of absorption will
be lower than the value indicated in Table 2.5. The same applies to
copper. For example, for gold at $\lambda = 0.7\ \mu$, $\beta_{\lambda 2} = 0.06$ and, consequently,
$\beta_{\lambda 2}/\varepsilon_{\lambda 1} = 2.4$.

TABLE 2.5.
The Ratio of Absorption and Radiation Coefficients (Emissivity) for
Maximum-Intensity Wavelengths

Металл 1	2 $\beta_{\lambda 2}$ при $\lambda=0{,}5$ мк	2 $\varepsilon_{\lambda 1}$ при $\lambda=7$ мк	$\beta_{\lambda 2}{:}\varepsilon_{\lambda 1}$
Серебро	0,06	0,025	2,4
Хром	0,31	0,05	6,2
Алюминий	0,35	0,05	7,0
Сталь	0,48	0,05	9,6
Медь	0,38	0,025	15,2
Никель	0,40	0,025	16,0
Золото	0,60	0,025	24,0

1) Metal; 2) $\beta_{\lambda 2}$ at $\lambda = 0.5\mu$; 3) silver; 4) chrome; 5) aluminum; 6) steel; 7) copper; 8) nickel; 9) gold.

It should be borne in mind that a finely polished surface lowers
the value of the ratio β/ε in comparison with its value for ordinary
polishing. Actually, in the case of fine polishing, the average height
of roughness tubercles will be 0.1 to 0.5 μ, while in the case of or-
dinary polishing it will be 0.5 to 6 μ. During the transition from
ordinary polishing to fine-polishing, the radiation coefficient (emi-
ssivity) hardly changes, since in relation to the wavelength of the
radiation ($\sim 7\ \mu$), the surface in the case of both ordinary and fine
polishing will be smooth. As concerns the coefficient of absorption,
the surface with ordinary polishing with respect to the wavelength of
maximum absorption intensity ($\lambda_m = 0.5\ \mu$) will be rough, since the
height of the roughness tubercle will be several times greater than
the wavelength (1 to 12 times greater). Therefore, the absorption
coefficient in the case of fine polishing should be lower than in the

- 71 -

case of ordinary polishing, and consequently, the value of the ratio β/ε should be lower.

To shield against solar-ray heating we may use a dielectric surface coating which has high emissivity and a small solar-energy absorption coefficient.

In particular, it is possible to use a paint coating. Table 2.2 shows that the emissivity ε of paint coatings is on the average equal to 0.9, while the absorption coefficient of white paint for example ranges from 0.12 to 0.26. Consequently, the ratio β/ε will range from 0.13 to 0.3.

Certain materials have very low absorption coefficients when emissivity is of the order of 0.9. For example, gypsum has an absorption coefficient of 0.05 to 0.10, while magnesium oxide even has an absorption coefficient of 0.1 to 0.2.

Table 2.6 gives the absorption coefficient of certain materials at room temperature.

TABLE 2.6.
Coefficients of the Integral Absorption of Solar Energy of Certain Materials

1 Материал	β	Литературный 2. источник
3 Алюминий полированный	0,26	[17]
4 Алюминий матовый	0,38	[2]
5 Медь полированная	0,26	[17]
6 Железо полированное	0,45	[17]
7 Железо окисленное	0,74	[17]
8 Железо оцинкованное	0,66	[17]
9 Краска белая	0,12÷0,26	[17]
10 Краска черная	0,97÷0,99	[17]
11 Алюминиевая краска	0,35÷0,40	[2]
12 Белая фарфоровая эмаль	0,25÷0,35	[2]
13 Гипс	0,05÷0,10	[2]
14 Окись магния (матовая)	0,01÷0,02	[2]
15 Бумага белая	0,27	[17]
16 Бумага ватманская белая	0,15÷0,20	[2]

Key to Table 2.6. 1) Materials; 2) literature source; 3) polished aluminum; 4) dull aluminum; 5) polished copper; 6) polished iron; 7) oxidized iron; 8) iron; 9) white paint; 10) black paint; 11) aluminum paint; 12) white porcelain enamel; 13) gypsum; 14) magnesium oxide (dull); 15) white paper; 16) white Whatman paper.

Manu-
script   [List of Transliterated Symbols]
Page
No.

58        $q_{из} = q_{iz} = q_{izluchayemyy} = q_{radiated}$

58        $q_{a} = q_{a} = q_{aerodinamicheskyy} = q_{aerodynamic}$

58        $q_{наг} = q_{nag} = q_{nagrev} = q_{heating}$

66        $\varepsilon_{ш} = \varepsilon_{sh} = \varepsilon_{sherekhovatyy} = \varepsilon_{rough}$

Chapter 3

THE TEMPERATURE OF THE WALL DURING A STEADY-STATE THERMAL PROCESS

§3.1. THE TEMPERATURE OF THE WALL WITHOUT INTERNAL COOLING

The steady-state thermal process is characterized by a temperature which is constant with respect to time at any point of the flow and of the streamlined body. This process is of interest in the case of a long flight with constant velocity at constant altitude or in the case of space flights at sufficiently great distances from the earth or from another planet.

In the case of the steady-state thermal process, the equipment is not heated and consequently $q_{nag} = 0$. When there is no cooling of the inner surface, the thermal-balance equation (1.13), with consideration of Formula (1.11), will be:

$$q_{Har} = q_i + q_z - q_{H3} - q_r = 0. \tag{3.1}$$

Here the temperature of the wall will be constant with respect to its thickness. This is the temperature at which the heat flows approaching and leaving the plating reach a state of equilibrium. Consequently, this temperature is called the equilibrium temperature.

The heat loss q_t along the surface is produced by a temperature gradient along the surface; for a cylindrical surface with the length $\underline{1}$ from the generatrix perpendicular to the flow, the quantity of heat given off per second will be:

$$-\lambda \left(\frac{\partial T}{\partial x}\right)_z l\beta_{o\delta}.$$

where $\underline{x}$ is the distance from the investigated point.

The quantity of heat entering the same surface element will be:

$$-\lambda \left(\frac{\partial T}{\partial x}\right)_1 l \delta_{o6}.$$

Here "1" indicates the cross section through which the heat enters, while "2" indicates the cross section through which the heat exits. If the distance between cross sections is $\underline{dx}$, then

$$q_\tau = -\frac{\lambda\left[\left(\frac{\partial T}{\partial x}\right)_2 - \left(\frac{\partial T}{\partial x}\right)_1\right] l \delta_{o6}}{l\,dx} = -\lambda \frac{\partial^2 T}{\partial x^2} \delta_{o6}.$$

It is apparent from the formula obtained that the heat loss through the cross section of the plating will take place when the temperature gradient along the chord is not constant. Substantial losses may be observed in the vicinity of the pointed leading edge, at the nose of the cone, at the point at which the transition from a laminar to a turbulent boundary layer takes place, and at the places where the streamline profile is bent.

Since the heat-transfer coefficient and the recovery factor in q_a, and also the emissivity in q_{1z}, depend on the temperature of the wall, we can most conveniently determine the latter graphically. For this purpose, two or three values of T_{st} are given and we find q_{nag} from Formula (3.1); then we construct q_{nag} from T_{st}, and taking into consideration the fact that $q_{nag} = 0$, we find T_{st}.

The number of points for the determination of q_{nag} is taken depending on the available possibilities of obtaining the necessary accuracy for a preliminary evaluation of T_{st}. For example, if $T_r <$ < 500°K and there is no cooling, the temperature of the wall in the majority of the cases will be only somewhat less than the recovery temperature; consequently, we may give two values of T_{st} differing

- 75 -

from each other by 30 to 50°. If the preliminary estimation of T_{st} can be made only with an accuracy of several hundred degrees, we must calculate three, and possibly even four values of q_{nag}.

It should be noted that the wall radiates from two sides; however, the radiation of heat from whithin the structure in the case of a steady-state thermal process will be compensated by the absorption of the heat radiated by the structure or the opposite wall. Consequently, Formula (3.1) should take into consideration only one-sided radiation.

In order to make more clear the above method for determining the temperature of a streamlined surface in the case of a steady-state thermal process, we give below an example of the determination of the temperature of the lower wing surface.

The data derived are as follows: M_∞ = 5, H = 30 km, and α = 10°, the profile is lenticular, $\bar{c}$ = 0.03, chord length is 8 m, and surface emissivity is ε = 0.8. This calculation is for the lower surface.

We will determine the coefficients c_1, c_2, and c_3 from Fig. 1.5; for M_∞ = 5, they will be c_1 = 0.41, c_2 = 1.22, c_3 = 1.92. The angle of surface inclination for the profile at the leading edge in relation to the chord is ϑ_{k0} = $2\bar{c}$ = 0.06. The angle between the lower surface of the leading edge and the direction of the flow

$$\varphi = \alpha + \vartheta_{k0} = 0,175 + 0,06 = 0,235.$$

The pressure behind the compression wave is determined from Formula (1.40):

$$\bar{p}_\kappa = c_1 \varphi + c_2 \varphi^2 + c_3 \varphi^3 = 0,1885.$$

Hence, from Formula (1.59) we find:

$$p_\kappa / p_\infty = 1 + 0,7 M_\infty^2 \bar{p}_\kappa = 4,3.$$

- 76 -

Let us determine the relative density behind the compression wave from Formula (1.57):

$$\frac{\rho_c}{\rho_\infty} = 1 + 5 \frac{\frac{p_c}{p_\infty} - 1}{\frac{p_c}{p_\infty} + 6} = 2,6.$$

Table 3.1 gives the calculation formulas and the numerical calculations for the flow characteristics along the surface of the profile.

To determine the temperature of the surface, we calculate q_{nag} for two given temperatures and then graphically or analytically we find T_{st} (from the linear function between q_{nag} and T_{ot}) at which $q_{nag} = 0$. For a laminar boundary layer, we assume surface temperatures of 650 and 700°K while for a turbulent boundary layer we assume temperatures of 700 and 850° K.

To determine the temperature of the adiabatic wall, let us find the Prandtl number. From $r_1 = 0.83$ we determine the temperature of the adiabatic wall according to Formula (1.1) for a laminar boundary layer and for the average $M_\delta = 3.66$ and $T_\delta = 3.53$:

$$T_r = T_\delta (1 + 0,2 r_J M_\delta^2) = 1130° \text{ K};$$

then from Formula (1.6) where $T_{st} = 700°K$, we find the determining temperature:

$$T^* = T_\delta + 0,5 (T_{cr} - T_\delta) + 0,22 (T_r - T_\delta) = 697° \text{ K}.$$

From Fig. 1.1, let us find the Pr value for the obtained determining temperature (according to Van Dreist):

$$Pr^* = 0,684.$$

Similarly, for a turbulent boundary layer, from $r_t = 0.89$, for average $M_\delta = 3.87$ and $T_\delta = 325°K$ we will have:

$$T_r = 1190° \text{ K}, \quad T^* = 703° \text{ K} \quad \text{и} \quad Pr^* = 0,684.$$

At other wall temperatures, the Prandtl number changes very

little. With T_{st} = 650°K in the case of a laminar boundary layer,

Pr* = 0.683; when T_{st} = 850°K in the case of a turbulent boundary layer,

Pr* = 0.688. This change in the Prandtl number, in accordance with

Formulas (1.4) and (1.5), has very little influence on r_l and r_t. In

this connection, the found values of T_r are used as constants for fur-

ther calculations.

It should be borne in mind that since the braking temperature does

not change when the local flow characteristics change, the Prandtl

number may be taken as constant for all points of the surface; con-

sequently, we may assume that the temperatures of the adiabatic wall

calculated above are the same for all points on the surface. The values

of c_p* = 0.257 are also constant for all points on the surface (see

Fig. 1.2).

The specific radiation heat flow will depend only on the surface

temperature and consequently according to Formula (1.14) it will equal:

at a wall temperature of T_{st} = 650°K.........q_{lz} = 1.94 kcal/m^{2}sec

at a wall temperature of T_{st} = 700°K.........q_{lz} = 2.61　　"

at a wall temperature of T_{st} = 850°K.........q_{lz} = 5.68　　"

The heat flow of solar radiation will have no effect on the lower

surface; the heat flows from the earth will be insignificant (fraction-

al) in comparison with the heat flows from the aerodynamic heating

and radiation and they may therefore be neglected.

The beginning and the end of the transition of the laminar boun-

dary layer into a turbulent boundary layer are roughly determined at

first on the basis of a visual estimate of $T_{st}/T_r \approx 0.7$. Then, accord-

ing to the data given in §1.5, the critical Reynolds number for the

beginning of the transition

$$Re_i = \frac{1.5 \cdot 10^6}{(T_{cr}/T_r)} = 2.14 \cdot 10^6,$$

TABLE 3.1.

The Determination of Flow Characteristics on the Profile

Величина и формула[1]	№ формулы[2]	Численные значения[3]						
Величиной $\bar{x}$ задаемся[4]	—	0	0,05	0,10	0,20	0,50	0,75	1,00
$\vartheta_к = \vartheta_{к0}(1 - 2\bar{x})$	—	0,06	0,054	0,048	0,036	0	—0,03	—0,06
$\varphi = \vartheta_к + a$	—	0,225	0,229	0,223	0,211	0,175	0,145	0,115
$\bar{p}_к = c_1\varphi + c_2\varphi^2 + c_3\varphi^3$	(1.40)	0,1885	0,1807	0,1734	0,1586	0,1195	0,0900	0,0661
$p_б/p_\infty = 1 + 0,7M_\infty^2\bar{p}_к$	(1.59)	4,3	4,16	4,04	3,78	3,11	2,59	2,16
$p_б/p_c = [(p_б/p_\infty)(p_\infty/p_c)]^{0,715}$	(1.58)	1	0,980	0,957	0,911	0,795	0,694	0,611
$p_б/p_\infty = (p_б/p_c)(p_c/p_\infty)$	—	2,6	2,55	2,49	2,37	2,07	1,81	1,59
$T_б/T_\infty = (p_б/p_\infty)(p_\infty/p_б)$	(1.48)	1,65	1,63	1,62	1,595	1,50	1,43	1,36
$M_б^2 = 5[(T_\infty/T_б)(1 + 0,2M_\infty^2) - 1]$	(1.49)	13,2	13,4	13,5	13,7	15,0	16,0	1,90
$M_б$	—	3,64	3,66	3,67	3,70	3,87	4,00	4,12
$10^3 \times \rho_б = [\rho_\infty(p_б/p_\infty)] \times 10^3$	—	4,81	4,73	4,61	4,39	3,84	3,35	2,94
$T_б = T_\infty(T_б/T_\infty)$	—	357	353	351	346	325	310	294
$V_б = a_б M_б = 20M_б\sqrt{T_б}$	—	1375	1375	1375	1375	1395	1410	1410
$10^6 \times \mu_б = [1,49 \cdot 10^{-7}T_б^{3/2}/(T_б + 110)] \times 10^6$	(1.34)	—	2,14	2,12	2,10	2,01	1,94	1,83
$10^4 \times \nu_б = (\mu_б/\rho_б) \times 10^4$	—	—	4,53	4,60	4,78	5,24	5,79	6,24
$10^{-6} \times Re_б = (V_б x/\nu_б) \times 10^{-6}$	(1.20)	—	1,21	2,4	4,61	10,65	14,6	18,1

1) The value and formula; 2) number of formula; 3) numerical values; 4) the magnitude $\bar{x}$ is given.

the critical Reynolds number for the end of the transition

$$Re_б = \frac{3,5\cdot10^6}{T_{ст}/T_f} = 5\cdot10^6.$$

It is apparent from Table 3.1 that the beginning of the transition will take place at a distance approximately corresponding to 10% of the chord, while the end of the transition will take place at a distance corresponding to 20% of the chord.

The calculated values of q_{nag} are given Table 3.2. From the known values of q_{nag} = 0. If the temperatures of the wall, which are assumed in the determination of q_{nag}, are designated as T_1 and T_2, and the values of q_{nag} corresponding to these are designated as q_1 and q_2, then from the linear function between q_{nag} and T_{st} (for the interval

- 79 -

under consideration) we will have:

$$T_{cr} = T_1 + q_1 \frac{(T_2 - T_1)}{(q_1 - q_2)}.$$

The values of T_{st} determined from this formula are also given in Table 3.2.

In the determination of q_{nag} we take $q_t = 0$, since for most of the chord length the temperature gradient is almost constant. At the point of transition from a laminar boundary layer to a turbulent boundary layer (at a distance corresponding to 10 to 20% of the chord), the sign of the temperature gradient will change, as a result of which heat flows will develop along the plating; consequently, the breaks in the temperature curve should be rounded off.

On the basis of the temperatures obtained in Table 3.2, the critical Reynolds numbers can be made more exact.

For the beginning of the transition

$$\frac{T_{cr}}{T_r} = \frac{648}{1130} = 0,575;$$

for the end of the transition

$$\frac{T_{cr}}{T_r} = \frac{840}{1190} = 0,705.$$

Consequently, the critical Reynolds number for the beginning of the transition

$$Re_t = \frac{1,5 \cdot 10^6}{0,575} = 2,6 \cdot 10^6;$$

for the end of the transition

$$Re_t = \frac{3,5 \cdot 10^6}{0,705} = 4,96 \cdot 10^6.$$

According to Table 3.1, the points which are at distances corresponding to 11 and 21% of the chord correspond to these Reynolds numbers.

The temperature values found along the chord on the lower surface

of the wing profile are given in Fig. 3.1.

TABLE 3.2.
The Determination of the Surface Temperature of a Profile in a Steady-state Thermal Process

Величина и формула 1	№ формулы 2	Численные значения 3											
		ламинарный пограничный слой 5				турбулентный пограничный слой 4							
Величиной $\overline{x}$ задаемся 6	—	0,05		0,10		0,20		0,50		0,75		1,0	
Величиной $T_{ст}$ задаемся 7	—	650	700	650	700	700	850	700	850	700	850	700	850
$T^* = T_i + 0,5(T_{ст} - T_i) + 0,22(T_r - T_i)$	(1.6)	671	695	670	694	693	784	701	778	697	774	692	769
$10^3 \times \rho^* = (\rho_i T_i/T^*) \times 10^3$	(1.33)	2,49	2,40	2,42	2,34	2,19	1,94	1,78	1,605	1,49	1,345	1,25	1,123
$10^6 \times \mu^* = [1,49 \cdot 10^{-7}(T^*)^{1/2}/(T^*+110)] \times 10^6$	(1.34)	3,32	3,39	3,32	3,39	3,38	3,66	3,41	3,64	3,39	3,63	3,38	3,61
$10^3 \times \nu^* = (\mu^*/\rho^*) \times 10^3$	—	1,33	1,41	1,37	1,45	1,545	1,89	1,92	2,27	2,28	2,70	2,70	3,21
$10^{-6} \times Re^* = (V_i x/\nu^*) \times 10^{-6}$	(1.20)	0,413	0,390	0,804	0,758	1,425	1,163	2,91	2,46	3,70	3,13	4,18	3,52
$10^3 \times \alpha_л = [3,26(Re^*)^{-1/2}(Pr^*)^{-1/3}\rho^* c_p^* V_i] \times 10^3$	(1.30)	5,70	5,65	3,98	3,95	—	—	—	—	—	—	—	—
$10^3 \times \alpha_т = [0,29(Re^*)^{-0,2}(Pr^*)^{-1/3}\rho^* c_p^* V_i] \times 10^3$	(1.31)	—	—	—	—	16,8	15,5	12,0	11,2	9,7	9,1	7,9	7,4
$q_л = \alpha(T_r - T_{ст})$	(1.7)	2,74	2,43	1,91	1,70	8,24	5,26	5,89	3,81	4,76	3,09	3,87	2,52
$q_{шаг} = q_л - q_{из}$	(3.1)	0,80	−0,18	0,03	−0,91	5,62	−0,42	3,28	−1,87	2,15	−2,59	1,26	−3,11
$T_{ст} = T_1 + q_1(T_2 - T_1)/(q_1 - q_2)$	—	691		648		840		796		770		743	

1) Value and formula; 2) number of formula; 3) numerical values; 4) turbulent boundary layer; 5) laminar boundary layer; 6) the value of $\underline{x}$ is assumed; 7) the value of T_{st} is assumed.
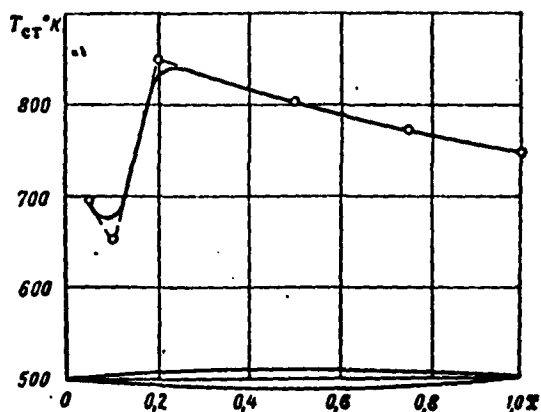
Fig. 3.1. Temperature distribution along the chord on the lower surface of the wing profile. M = 5; H = 30 km; α = 10°; ε = 0.8.

§3.2. THE TEMPERATURE OF THE WALL WHEN ITS INNER SURFACE IS COOLED

With a cooled wall and the coolant absorbing the specific q_{okh}, the heat-balance equation for small surface heat losses q_t will be

$$q_{\text{a}}+q_{\text{a}}-q_{\text{нз}}-q_{\text{ox}}=0. \qquad (3.2)$$

With a cooled outer surface, the wall temperature will be constant in width, and its determination will follow §3.1.

With an inner cooled wall surface (e.g., by circulating a liquid coolant) the wall temperature will vary in width. A temperature distribution diagram for the wall width is given in Fig. 3.2. For generality, Fig. 3.2 assumes that the wall consists of insulation and plating. Great aerodynamic heat flow cools the inner surface and increased surface radiation properties do not yield acceptable wall temperatures. Here, the radiant-energy heat flow q_{1} can be neglected, and Eq. (3.2) is simplified.

$$q_{\text{a}}-q_{\text{нз}}=q_{\text{ox}}. \qquad (3.3)$$

From this we can find the outer surface temperature T_{1z}. To determine the plating temperature we study the insulation's thermal conductivity.

With a steady-state thermal process, neither the insulation nor the plating are heated; consequently, the specific heat flow will pass through any surface parallel to the outer insulation surface

$$\lambda_{\text{нз}}\left(\frac{dT}{dy}\right)_{\text{нз}}=q_{\text{ox}},$$

specific heat flow will pass through any similar plating surface

$$\lambda_{\text{об}}\left(\frac{dT}{dy}\right)_{\text{об}}=q_{\text{ox}}.$$

If we assume that within the temperature difference across the width, thermal conductivity does not depend on temperature, we will have

$$\left(\frac{dT}{dy}\right)_{\text{нз}}=\frac{q_{\text{ox}}}{\lambda_{\text{нз}}}=\text{const} \quad \text{и} \quad \left(\frac{dT}{dy}\right)=\frac{q_{\text{ox}}}{\lambda_{\text{об}}}=\text{const}.$$

Consequently, the insulation and plating temperature will change linearly in width. The temperature differences across the insulation and plating will be

$$\Delta T_{\text{нз}}=\frac{q_{\text{ox}}\delta_{\text{нз}}}{\lambda_{\text{нз}}}; \qquad (3.4)$$

$$\Delta T_{\text{об}}=\frac{q_{\text{ox}}\delta_{\text{об}}}{\lambda_{\text{об}}}. \qquad (3.5)$$
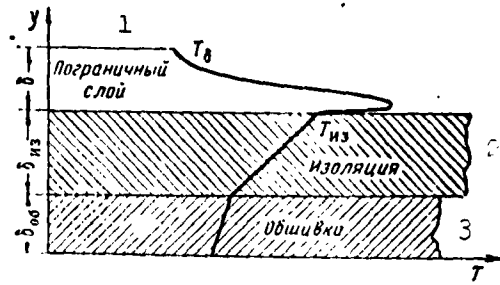
Fig. 3.2. Diagram of the temperature distribution along the width of the wall in a steady-state thermal process. 1) Boundary layer; 2) insulation; 3) plating

The temperature of the outer plating surface will be

$$T_{o6} = T_{u3} - \Delta T_{u6}. \qquad (3.6)$$

Similarly, using Formulas (3.5) and (3.6), we can determine the temperature of the inner plating surface.

§3.3. THE TEMPERATURE OF THE WALL DURING SOLAR HEATING

At altitudes higher than 150 km the aerodynamic heating becomes insignificant and may be neglected; the equation of heat balance in the case of a steady-state thermal process will take the following form:

$$q_{a} = q_{u3} + q_{r}. \qquad (3.7)$$

If we do not take into consideration the heat flows along the surface, i.e., assume that $q_t = 0$, then, expanding the value of q_{iz} from Formula (1.14), we obtain:

$$T_{cr} = \sqrt[4]{\frac{q_{a}}{e_0}} . \qquad (3.8)$$

For space craft several thousand kilometers away from the earth, the effect of terrestrial radiation and the solar rays reflected from the earth is insignificant in comparison with the effect of direct

- 83 -

solar rays, and consequently the specific heat flows q_z and q_{ot} can be neglected. In the case of lower altitudes, the effect of terrestrial radiation and solar rays reflected from the earth becomes greater; however, as can easily be seen from Formulas (1.9), (1.10), and (3.8), this effect is still quite small and these types of radiation will increase the temperature by less than 2%. Consequently, it is entirely permissible in a number of cases to neglect q_z and q_{ot}.

If we neglect q_z and q_{ot}, and take into consideration Formula (1.8), Formula (3.8) can be presented in the following form:

$$T_{cr} = \sqrt[4]{\left(\frac{\beta}{\epsilon}\right)\left(\frac{S}{\sigma}\right)\cos\psi}. \qquad (3.9)$$

Of particular interest is the temperature for $\psi = 0$, when the temperature is maximum; in this case, taking into consideration S and σ, we will have:

$$T_{max} = \sqrt[4]{\left(\frac{\beta}{\epsilon}\right)\left(\frac{S}{\sigma}\right)} = 395\sqrt[4]{\frac{\beta}{\epsilon}}. \qquad (3.10)$$

If the craft rotates rapidly about an axis perpendicular or almost perpendicular to the direction of the solar rays, and if the craft has a sufficiently thick plating with good heat conduction, the temperature of the plating may be identical over the entire surface. The same will be true when there is heat transfer through the inner wall. This average temperature may be found from the condition that the total flow of solar radiation falling on a hemisphere heats the entire surface of the sphere.

The total heat flow falling on the sphere and absorbed by it will be:

$$\pi R^2 S\beta,$$

- 84 -

The total radiation heat flow

$$4\pi R^2 s_0 T_{cp}^4,$$

where T_{sr} is the mean temperature of the entire surface.

From the equality of these heat flows we will find:

$$T_{cp} = \sqrt[4]{\frac{1}{4}\left(\frac{\beta}{\varepsilon}\right)\left(\frac{S}{s}\right)} = 280\sqrt[4]{\frac{\beta}{\varepsilon}}.$$

(3.11)

The value of β/ε in Formula (3.11) may be found from the material given in the §§ 2.2 and 2.3.

Manu-script Page No.	[List of Transliterated Symbols]
74	$q_{\text{наг}} = q_{\text{nag}} = q_{\text{nagrevaniye}} = q_{\text{heating}}$
74	$q_{\text{л}} = q_{\underline{l}} = q_{\text{luchistaya}} = q_{\text{radiant}}$
74	$q_{\text{из}} = q_{iz} = q_{\text{izluchayemyy}} = q_{\text{radiated}}$
74	$\underline{1}\delta_{\text{об}} = \underline{1}\delta_{\text{ob}} = \underline{1}\delta_{\text{obshivka}} = \underline{1}\delta_{\text{plating}}$
77	$T_{\text{ст}} = T_{\text{st}} = T_{\text{stenka}} = T_{\text{wall}}$
82	$q_{\text{ох}} = q_{\text{okh}} = q_{\text{okhlazhdeniye}} = q_{\text{cooling}}$
85	$T_{\text{cp}}^4 = T_{\text{sr}}^4 = T_{\text{srednyy}}^4 = T_{\text{average}}^4$

Chapter 4

THE HEATING OF A WALL DURING A NONSTEADY-STATE THERMAL PROCESS

§4.1. The Temperature of a Thin Wall

In the case of a nonsteady-state thermal process, the temperature at various parts of the body may change with time. Generally, to determine the temperature of a body at a given instant in the case of a nonsteady-state thermal process, we must solve simultaneously Eqs. (1.13), (1.15), and (1.16). However, this solution is possible only in certain specific cases in which a number of simplifying assumptions are made.

Taking into consideration the fact that generally the loss of heat along the surface produced by the temperature gradient is small in comparison with the heat which heats the body, we will in the future examine the one-dimensional problems for a flat plate, i.e., let us assume

$$\frac{\partial T}{\partial x} = 0 \quad \& \quad \frac{\partial T}{\partial z} = 0.$$

Let us also assume that the thermal-conductivity coefficient does not depend on the temperature and, consequently, is constant along the width of the plating. This is entirely permissible for metals and nonporous insulation materials (laminar plates, ceramics), if we take the mean value of thermal conductivity.

In the case of the assumptions made Eqs. (1.11), (1.13), (1.15), and (1.16) may be represented in the following way:

$$\lambda \left(\frac{\partial T}{\partial y}\right)_{cr} + \varepsilon \sigma T_{cr}^4 - \alpha (T_r - T_{ct}) - q_s = 0. \tag{4.1}$$

$$\frac{\partial T}{\partial t} = a \frac{\partial^2 T}{\partial y^2}, \tag{4.2}$$

where $\underline{a}$ is the coefficient of thermal diffusivity.

Structures with thin walls made of metals possessing good conductance are in wide use. In these cases the temperature difference across the width of the plating may be small and we can then assume that the plating is suddenly heated along the entire width. In §4.3 we presented a criterion characterizing the permissible constant temperture along the width of the plating, i.e., the criterion of thin shielding.

Assuming for a thin plating

$$T_{o6} \approx T_{cr},$$

let us find for the specific heat flow which heats the plating, the expression

$$q_{uar} = c\gamma\delta_{o6}\frac{dT_{o6}}{d\tau}.$$

In this case we can substitute the found expression for q_{nag} for the first term of Eq. (4.1): then

$$c\gamma\delta_{o6}\frac{dT_{o6}}{d\tau} + \varepsilon_{o6}\sigma T_{o6}^4 - \alpha (T_r - T_{o6}) - q_4 = 0. \tag{4.3}$$

Even though the plating radiates from two sides, in the case of the hollow unfilled casing formed by the plating (wing, nose of the body), as a result of the mutual heat transfer between the inner sections of the plating, the heat will not be able to escape through the inner surface. When there is a substantial temperature difference between the lower and upper surface, the internal radiation of the hotter plating section will be greater than the absorption. This may be taken into consideration by increasing the radiation coefficient (emissivity) determined on the basis of a first-approximation calculation.

In the presence of substantial heat-absorbing masses inside the casing, the total emissivity may be approximately determined from the

following formula

$$\epsilon_{06} = \epsilon \left\{ 1 + \epsilon_{\kappa} \left[1 - \left(\frac{T_{\kappa}}{T_{06}} \right)^4 \right] \right\},$$

where T_{κ} is the inside temperature of the structure. ϵ is the emissivity for one side of the plating; ϵ_{κ} is the emissivity of the inside of the structure.

Since α and T_r in the case of nonsteady-state heating are generally constant, Eq. (4.3) should be solved by numerical integration with finite temperature increments

$$\Delta T_{06} = \left[q_{\scriptscriptstyle\lambda} + \alpha (T_r - T_{06}) - \epsilon_{06} \sigma T_{06}^4 \right] \frac{\Delta \tau}{c \gamma \delta_{06}}. \tag{4.4}$$

It should be borne in mind that in the case of a nonsteady-state thermal process produced by aerodynamic heating, $q_{\scriptscriptstyle\underline{1}}$ generally can be neglected.

In order better to explain the method for determining the temperature of the plating, we examine below an example for the determination of the plating temperature of a cone with a flare angle of 20°, at $\alpha = 0$; the flight altitude is 15 km. The flight regime was as follows: the flight was initially stabilized at M = 1.5; then the velocity was uniformly accelerated for 20 seconds up to M = 4; this was followed by a velocity decrease corresponding to passive flight according to the law

$$\frac{1}{V} = \frac{1}{V_{\max}} + 10^{-6} \tau_{\scriptscriptstyle\mathrm{R}},$$

where τ_p is the passive-flight time.

Table 4.1 gives the calculation formulas and numerical calculation of the flow characteristics at the surface of the cone (beyond the limits of the boundary layer).

The temperature determination for an aluminum alloy plating with a thickness of 5 mm in a nonsteady-state flight regime is given in

- 88 -

Table 4.2. The same table gives the calculation formulas. The initial temperature of the plating (302°) was determined from the steady-state thermal process. The initial temperature in the given case is close to the temperature of the adiabatic wall. The temperature of the plating was determined for a point at a distance x = 0.1 m from the nose of the cone. The emissivity of the plating was taken as ε_{ob} = 0.8, the specific heat capacity was taken as c = 0.224, and the bulk weight was taken as γ = 2800.

TABLE 4.1.

Plating Temperature in the Case of Variable Flight Velocity

Величина и формула	№ фор-мулы	Время полета в сек.									
		0	5	10	15	20	25	30	40	50	60
$V_1 = 442 + 36.9\tau$; $V_2 = (0.85 \cdot 10^{-3} + 10^{-5}\tau)^{-1}$	—	442	626	810	995	1180	1110	1052	952	870	800
$M_\infty = 295V$	—	1.5	2.13	2.75	3.38	4.00	3.77	3.57	3.23	2.95	2.71
$t = \vartheta_x M_\infty$	(1.52)	0.262	0.372	0.481	0.591	0.700	0.659	0.624	0.565	0.516	0.474
$\bar{p}_x = 2.091(1 + 0.143/t^{7/6})t_x^2$	(1.53)	0.1320	0.1045	0.0912	0.0840	0.0796	0.0810	0.0825	0.0855	0.0887	0.0921
$\vartheta/\vartheta_x = 1.093 + 0.06(7 - t)t^{-7/6}$	(1.55)	4.113	2.843	2.265	1.940	1.738	1.803	1.871	2.003	2.142	2.300
$\sin\vartheta_c$	—	0.658	0.476	0.385	0.332	0.299	0.309	0.321	0.342	0.367	0.391
$p_c/p_\infty = \frac{1}{6}(7M_\infty^2 \sin^2\vartheta_c - 1)$	(1.56)	1.00	1.03	1.14	1.30	1.50	1.42	1.37	1.26	1.203	1.142
$p_c/p_\infty = 1 + 5(p_c/p_\infty - 1)/(p_c/p_\infty + 6)$	(1.57)	1.000	1.021	1.098	1.206	1.334	1.283	1.251	1.179	1.141	1.100
$p_b/p_\infty = 1 + 0.7M_\infty^2 \bar{p}_x$	(1.59)	1.206	1.332	1.481	1.672	1.890	1.807	1.737	1.624	1.540	1.473
$p_b/p_c = [(p_b/p_\infty)(p_\infty/p_c)]^{0.715}$	(1.58)	1.145	1.200	1.210	1.200	1.180	1.187	1.183	1.200	1.195	1.200
$p_b/p_\infty = (p_b/p_c)(p_c/p_\infty)$	—	1.145	1.225	1.328	1.445	1.573	1.522	1.482	1.415	1.365	1.320
$T_b/T_\infty = (p_b/p_\infty)/(n_b/p_\infty)$	—	1.052	1.090	1.118	1.158	1.200	1.185	1.170	1.150	1.130	1.115
$M_b^2 = 5[(T_\infty/T_b)(1 + 0.2M_\infty^2) - 1]$	(1.49)	1.9	3.75	6.25	9.20	12.50	11.25	10.20	8.40	7.10	6.10

1) Value and formula; 2) number of formula; 3) flight time in seconds.

The minimum Reynolds number Re_δ will be evident at the beginning of the flight when the velocity is lowest. In this case, on the basis of the data given in Table 4.1, we will have:

$$T_i = 216{,}5 \cdot 1{,}052 = 228; \quad a = 20\sqrt{T_i} = 302;$$
$$V_i = 302 \cdot 1{,}38 = 416 \ \text{m/sec}; \mu_i = 1{,}52 \cdot 10^{-7};$$
$$\rho_i = 1{,}145 \cdot 0{,}01974 = 0{,}0226;$$
$$\nu_i = 0{,}77 \cdot 10^{-5}; \quad Re_i = \frac{0{,}1 \cdot 416}{0{,}77 \cdot 10^{-5}} = 5{,}4 \cdot 10^6.$$

TABLE 4.2.

Determination of the Cone-plating Temperature

Величина и формула	№ формулы	Время полета в сек.										
		0	5	10	15	20	25	30	40	50	60	70
T_{06}	—	302	302	308,3	326	370	428	466	516	538,5	533	526
$T_i = T_\infty(T_i/T_\infty);\ T_\infty = 216{,}5$	—	228	236	242	250	260	257	254	249	245	242	—
$T_r = T_i(1+0{,}178M_i^2)$	(1.1)	305	394	510	658	836	770	716	621	553	505	—
$T^* = T_i + 0{,}5(T_{ст}-T_i) + 0{,}22(T_r-T_i)$	(1.6)	282	304	334	378	442	455	462	465	457	445	—
$(Pr^*)^{-1/3};\ Pr^*$ по фиг. 1.1	—	1,26	1,26	1,27	1,28	1,28	1,28	1,28	1,28	1,28	1,28	—
$10^7 \times \mu^* = [1{,}49 \cdot 10^{-7}(T^*)^{1/3}/(T^*+110)] \times 10^7$	(1.34)	1,80	1,91	2,04	2,24	2,51	2,56	2,58	2,60	2,57	2,48	—
$\rho^* = \rho_\infty(T_i/T^*)(\rho_i/\rho_\infty);\ \rho_\infty = 0{,}01974$	—	0,0182	0,0188	0,0190	0,0189	0,0183	0,0170	0,0161	0,0149	0,0144	0,0142	—
$10^6 \times \nu^* = (\mu^*/\rho^*) \times 10^6$	(1.35)	9,9	10,2	10,70	11,85	13,7	15,10	16,0	17,45	17,90	17,50	—
$V_i = 20M_i\sqrt{T_i}$	—	417	597	775	960	1140	1075	1015	915	835	768	—
$10^{-6} \times Re^* = (xV_i/\nu^*) \times 10^{-6}$	(1.20)	4,21	5,85	7,25	8,10	8,32	7,13	6,35	5,25	4,66	4,39	—
$(Re^*)^{-0{,}2}$	—	0,0475	0,0445	0,0425	0,0415	0,0413	0,0426	0,0435	0,0455	0,0461	0,0470	—
c_p^* по фиг. 1.2	—	0,240	0,240	0,240	0,241	0,244	0,244	0,244	0,244	0,244	0,244	—
$a = 0{,}29(Re^*)^{-0{,}2}(Pr^*)^{-1/3}\rho^*c_p^*V_i$	(1.31)	0,0323	0,0433	0,0552	0,0679	0,0780	0,0709	0,0642	0,0563	0,0502	0,0465	—
$q_a = a(T_r - T_{06})$	(1.7)	0,0975	4,03	11,13	27,5	36,3	24,2	16,05	5,92	1,025	−1,30	—
$q_{из} = \varepsilon_{06}\sigma T_{06}^4$	(1.14)	0,091	0,091	0,098	0,12	0,20	0,36	0,51	0,77	0,875	0,88	—
$\Delta T_{06} = (q_a - q_{из})\Delta\tau/c_т\gamma_{06}$	(4.4)	0	6,3	17,7	44	58	38	50	16,5	0,5	−7	—

1) Value and formula; 2) number of formula 3) flight time in seconds;
4) according to Fig. 1.2.
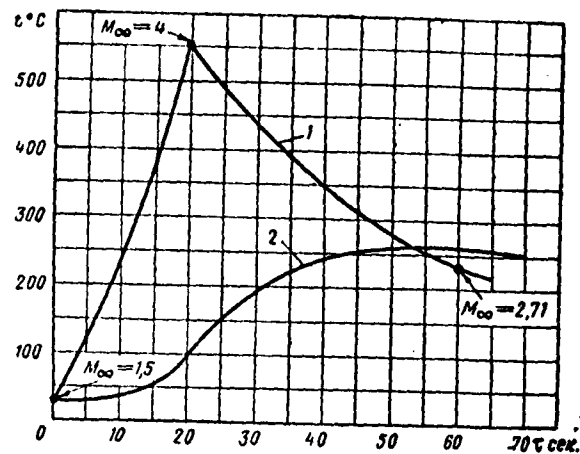
Fig. 4.1. Plating temperature in
the case of variable flight veloc-
ity. (plating made of aluminum
alloy, δ = 5 mm). 1) Temperature
of the adiabatic wall; 2) temper-
ature of the plating.

In the case of the obtained Reynolds number, the boundary layer
will be turbulent. Since, as the flight progresses, the Reynolds number
increases, it follows that the boundary layer will be turbulent for the
entire theoretical flight time.

The results of the calculation, given in Table 4.2, are repre-
sented graphically in Fig. 4.1. It is characteristic that the temper-
ature rise for the plating lags behind the temperature rise for the
adiabatic wall. This property is called thermal inertia and is deter-
mined by the heat capacity of the plating. The thermal inertia enables
us, during short-term heating, to use materials less heat resistant
than those which are required for extended heating.

In the case of flight at high altitudes, when the aerodynamic
heating is negligible or completely absent, Eq. (4.3) is simplified:

$$\frac{dT_{o\delta}}{d\tau} = \frac{\epsilon\sigma}{c\gamma\delta_{o\delta}}\left[\left(\frac{q_{\Lambda}}{\epsilon\sigma}\right) - \ ^{\bullet}T_{o\delta}^4\right].$$

(4.5)

If the magnitude of the absorbed radiant energy q_1 is constant
with respect to time, this equation is easy to integrate. Given the

- 91 -

variable q_1, Eq. (4.5) should be solved by numerical integration.

§4.2. TEMPERATURE DISTRIBUTION ALONG THE THICKNESS OF THE PLATING

When the thermal conductivity of the plating, or at least a major part of it, is small, the method for determining the temperature of the plating indicated in §4.1 may lead to very high errors. Actually, we do sometimes encounter conditions of aerodynamic heating in which the inner surface of the plating and the adjoining layers of materials cannot be heated substantially when, at the same time, the outer surface may already have a high temperature and may even be melting.

To explain the heat-shielding, heat-resistance, and strength properties of the plating it is necessary to know the temperature distribution along its thickness, while taking into consideration its thermal conductivity and heat capacity. To do this we solve the Fourier equation (4.2):

$$\frac{\partial T}{\partial \tau} = a \frac{\partial^2 T}{\partial y^2}.$$

The following boundary conditions are assumed:

1) there is no heat transfer on the inner wall: consequently, the temperature gradient on the inner wall should be zero:

$$\left(\frac{\partial T}{\partial y}\right)_{\text{вн}} = 0; \tag{4.6}$$

2) the heat transfer on the outer wall obeys Newton's law; the heat-transfer coefficient and recovery temperature are constant. In this case we will have:

$$\lambda \left(\frac{\partial T}{\partial y}\right)_{\text{ст}} = \alpha (T_r - T_{\text{ст}}). \tag{4.7}$$

This equation is a simplified version of Eq. (4.1) in which the radiated and absorbed radiant energy are assumed to be zero;

3) the initial surface temperature of the plating is, in general, constant along the thickness.

Fig. 4.2. Diagram of temperature distribution along the thickness of the boundary plating. 1) Boundary layer; 2) plating.

In the integration of the Fourier equation we will, for the most part, observe the method indicated by A. V. Lykov [14]. Let us introduce the dimensionless relative temperature

$$\theta = \frac{T_r - T}{T_r - T_0}, \tag{4.8}$$

where T is the temperature in any layer of the plating. Let us also introduce the relative coordinate

$$\xi = \frac{y}{\delta_{o\delta}}. \tag{4.9}$$

For symbol denotation see Fig. 4.2. The Fourier equation (4.2) for the relative temperature and relative coordinate will be:

$$\frac{\partial \theta}{\partial \tau} = \frac{a}{\delta_{o\delta}^2} \frac{\partial^2 \theta}{\partial \xi^2}. \tag{4.10}$$

Let us find the particular integral of this equation in the form

$$\theta = XZ,$$

where X is only a function of ψ, while Z is only a function of τ, i.e.,

$$X = X(\xi); \quad Z = Z(\tau).$$

- 93 -

Substituting the expression for β in Eq. (4.10), we get

$$\frac{dZ}{d\tau} : Z = \frac{a}{b_{06}^2} \frac{d^2X}{d\xi^2} : X.$$

Since the right and left sides of this equation are independent (they are functions of various independent arguments), evidently, each side should equal the constant B, i.e.,

$$\frac{dZ}{d\tau} : Z = B; \quad \frac{a}{b_{06}^2} \frac{d^2X}{d\xi^2} : X = B.$$

Let us integrate the first equation. Designating the value of Z as Z_0 for $\tau = 0$, we obtain

$$Z = Z_0 e^{B\tau}. \tag{4.11}$$

Let us designate

$$k^2 = -\frac{Bb_{06}^2}{a};$$

Then the second equation will be

$$\frac{d^2X}{d\xi^2} + k^2X = 0.$$

The integral of this equation

$$X = c_1 e^{k\xi i} + c_2 e^{-k\xi i}.$$

Condition (4.6) gives:

$$\left(\frac{dX}{d\xi}\right)_{\xi=0} = 0,$$

consequently,

$$c_1 = c_2.$$

Let us designate the value of X as X_1 for $\xi = 1$, then

$$X_1 = 2c_1 \frac{e^{ki} + e^{-ki}}{2} = 2c_1 \cos k,$$

whence

$$c_1 = \frac{1}{2} \frac{X_1}{\cos k},$$

consequently.

$$X = X_1 \frac{\cos (k\xi)}{\cos k}.$$

- 94 -

The value of θ may now be expressed in the following form

$$\theta = \left(\frac{X_1 Z_0}{\cos k}\right) e^{B\tau} \cos(k\xi) = \theta_{c\tau 0}\,\frac{\cos(k\xi)\,e^{B\tau}}{\cos k},$$

where it is denoted that

$$X_1 Z_0 = \theta_{c\tau 0}.$$

Here θ_{st0} is the relative temperature of the outer surface for $\tau = 0$.

Let us express the value of B in terms of $\underline{k}$; then

$$B\tau = -k^2\,\frac{a\tau}{\delta_{06}^2}.$$

The expression in this equation

$$\varphi = \frac{a\tau}{\delta_{06}^2} \qquad (4.12)$$

is the Fourier similarity criterion. This criterion is the fundamental quantity determining the temperature of a body in a nonsteady-state thermal process.

Expressing θ in terms of $\underline{k}$ and the Fourier criterion, for the particular integral of Eq. (4.10), we will obtain

$$\theta = \theta_{c\tau 0}\cos(k\xi)\,\frac{e^{-k^2\varphi}}{\cos k}. \qquad (4.13)$$

The value of $\underline{k}$ in Eq. (4.13) is determined from the boundary condition (4.7). Using Expressions (4.8) and (4.9), we represent this condition in the form

$$\left(\frac{\partial\theta}{\partial\xi}\right)_{c\tau} = -\beta\theta_{c\tau}, \qquad (4.14)$$

where

$$\theta_{c\tau} = \frac{T_f - T_{c\tau}}{T_f - T_0},$$

while β is the Biot number

$$\beta = \alpha\,\frac{\delta_{06}}{\lambda}. \qquad (4.15)$$

Differentiating (4.13) with respect to ξ:

$$\frac{\partial\theta}{\partial\xi} = -k\theta_{c\tau 0}\cdot\frac{\sin(k\xi)\,e^{-k^2\varphi}}{\cos k}.$$

Substituting this equation into Expression (4.14) and taking into consideration the fact that when $\xi = 1$, $\theta = \theta_{st}$, we will derive the following equation in which Eq. (4.13) will have been taken into consideration:

$$k \, tg \, k = \beta. \tag{4.16}$$

This equation is useful for determining $\underline{k}$. Since tan $\underline{k}$ is a periodic function with the period π, $\underline{k}$ will be a multivalued function. Equation (4.16) is transcendental and cannot be exactly solved analytically. We will deal with the practical determination of $\underline{k}$ below.

The total Eq. (4.10) integral can be a linear function of the particular integrals given by Eq. (4.13). If k_n is a value of $\underline{k}$, from Eq. (4.16), the total integral of Eq. (4.13) will be:

$$\theta = \sum_{n=-\infty}^{n=\infty} A_n \cos(k_n \xi) e^{-k_n^2 \tau}, \tag{4.17}$$

where the constants $\theta_{st0}/\cos k_n$ are included in the coefficients of the series A_n.

The values of A_n are determined from the initial conditions at $\tau = 0$. Let $\theta_0 = f(\xi)$ at the initial instant of time; then

$$\theta_0 = \sum_{n=-\infty}^{n=\infty} A_n \cos(k_n \xi) = f(\xi).$$

Let us multiply both sides of this equation by cos $(k_m \xi)d\xi$ and let us integrate the new equation obtained within the limits of change in ξ from 0 to 1:

$$\sum_{n=-\infty}^{n=\infty} A_n \int_0^1 \cos(k_n \xi) \cos(k_m \xi) \, d\xi = \int_0^1 f(\xi) \cos(k_m \xi) \, d\xi. \tag{4.18}$$

Replacing the derivative of the cosines by the sum of the cosines and integrating, we obtain:

$$I = \int_0^1 \cos(k_n \xi) \cos(k_m \xi) \, d\xi = \frac{1}{2} \int_0^1 [\cos(k_n - k_m) + \cos(k_n + k_m)] \, d\xi =$$

$$= \frac{1}{2} \left[\frac{\sin(k_n - k_m)}{k_n - k_m} + \frac{\sin(k_n + k_m)}{k_n + k_m} \right].$$

- 96 -

Taking into consideration the fact that

$$\lim_{k_m \to k_n} \left[\frac{\sin(k_n - k_m)}{k_n - k_m} \right] = 1,$$

where $k_m = \pm k_n$,

$$I = \frac{1}{2} \left(1 + \frac{1}{2k_n} \sin 2k_n \right).$$

Where $k_m \neq \pm k_n$, using Function (4.16), we will obtain:

$$I = \frac{1}{k_n^2 - k_m^2} (k_n \sin k_n \cos k_m - k_m \sin k_m \cos k_n) =$$

$$= \frac{\beta}{k_n^2 - k_m^2} (\cos k_n \cos k_m - \cos k_m \cos k_n) = 0.$$

Consequently, in the series of Expression (4.18), of all the terms only two remain, for which $k_n = k_m$ and $k_n = -k_m$; Expression (4.18) will, in this case, be written in the following way:

$$\frac{1}{2} A_n \left(1 + \frac{\sin 2k_n}{2k_n} \right) + \frac{1}{2} A_{-n} \left(1 + \frac{\sin 2k_n}{2k_n} \right) = \int_0^1 f(\xi) \cos(k_n \xi) \, d\xi.$$

Hence

$$A_n + A_{-n} = \frac{4 \sin k_n}{2k_n + \sin 2k_n} \frac{k_n}{\sin k_n} \int_0^1 f(\xi) \cos(k_n \xi) \, d\xi.$$

When $k_m = k_0$ only one term remains in the series of Expression (4.18):

$$\frac{1}{2} A_0 \left(1 + \frac{\sin 2k_0}{2k_0} \right) = \int_0^1 f(\xi) \cos(k_0 \xi) \, d\xi,$$

whence

$$A_0 = \frac{4 \sin k_0}{2k_0 + \sin 2k_0} \frac{k_0}{\sin k_0} \int_0^1 f(\xi) \cos(k_0 \xi) \, d\xi.$$

The total integral in (4.17) may now be represented in the following form $\theta = \sum_{n=0}^{n=\infty} \frac{4 \sin k_n}{2k_n + \sin 2k_n} \cos(k_n \xi) e^{-k_n^2 \varphi} \frac{k_n}{\sin k_n} \int_0^1 f(\xi) \cos(k_n \xi) \, d\xi.$

Here we take into consideration the fact that k_{-n} and that $\cos (k_n \xi)$ is the even function. This is the final expression for the relative temperature.

For the sake of convenience we will assign the subscript "1"

- 97 -

rather than "0" to the first term

$$B_n = \frac{4 \sin k_n}{2k_n + \sin 2k_n};$$

(4.20)

$$\zeta_n = \frac{k_n}{\sin k_n} \int_0^1 f(\xi) \cos (k_n \xi) \, d\xi.$$

(4.21)

then

$$\theta = \sum_{n=1}^{n=\infty} B_n \zeta_n \cos (k_n \xi) e^{-k_n^2 \varphi}.$$

(4.22)

The value of the coefficients B_n should be determined while taking into consideration Eq. (4.16) which determines the coefficients k_n. The first value of k_1 corresponds to the value of the angle in the first quarter of the circumference; the second value corresponds to the angle in the third quarter, etc. Thus the range of the values of k_n will be:

$$0 < k_1 < \frac{1}{2}\pi; \quad \pi < k_2 < \frac{3}{2}\pi; \quad 2\pi < k_3 < \frac{5}{2}\pi$$

The values of B_n corresponding to these values of k_n will agree with Formula (4.20):

$$1 < B_1 < 1.273; \quad 0 > B_2 > -0.425; \quad 0 < B_3 < 0.255.$$

The values of ζ_n are determined for the most part by the functions $f(\xi)$, and also by the values of the coefficients k_n. At constant temperature along the width of the plating at the beginning of heating, the functions $\theta = f(\xi) = 1$ and $\zeta_n = 1$. If the temperature in various layers of the plating is higher than the temperature of the outer surface at the beginning of heating, $f(\xi) < 1$ and, consequently, $\zeta_n < 1$.

Table 4.3 gives the values of the first three coefficients k_n, while Table 4.4 gives the values of the coefficients B_n obtained from the work of A. V. Lykov ([14], pp. 155 and 160).

Since $\xi = 1$ for the outside surface,

$$\theta_{cr} = \sum_{n=1}^{n=\infty} B_n \zeta_n \cos k_n e^{-k_n^2 \varphi}. \tag{4.23}$$

For the inside surface $\xi = 0$, $f(\xi) = 1$, and $\zeta_n = 1$; consequently,

$$\theta_{\text{вн}} = \sum_{n=1}^{n=\infty} B_n e^{-k_n^2 \varphi}. \tag{4.24}$$

In the majority of cases, for calculation of θ from Formulas (4.22) (4.23) and (4.24), it is entirely permissible to take three terms of the series, since the series for θ converges rapidly.

Formula (4.22) can be used to calculate the temperature distribution along the thickness of the plating and when α and T_r are variable. In this case the given heating or cooling times for the plating are subdivided into ranges such that within these ranges the change in α and T_r is comparatively small. Within these ranges it is assumed that α and T_r are constants and Formula (4.22) is used. Let us note that if T_r is variable, θ at the end of the preceding range does not equal the value of θ in the beginning of the subsequent range. This is explained by the step-wise nature of T_r.

Formula (4.22) did not take into consideration the radiation of the plating. It should be noted that in a nonsteady-state aerodynamic heating regime far from temperature equilibrium, the effect of the radiation heat on the temperature regime of the plating is not great. Consequently, in this case, the radiation heat may be calculated approximately by introducing the equivalent heat-transfer coefficient:

$$\alpha_{\text{эк}} = \alpha - q_{\text{из}}/(T_r - T_{cr}).$$

Since $q_{1z}/(T_r - T_{st})$ is variable, the calculation taking the radiation into consideration should be carried out in the same way as that of the variable heat-transfer coefficient, i.e., by dividing the

flight time into intervals.

At a wall temperature close to equilibrium, the radiation effect may be taken into consideration if we represent the specific heat flow involved in the heating of the plating in the form

$$q_{нат} = \alpha\,(T_r - T_{cт}) - \varepsilon\sigma T_{cт}^4 = \alpha_{эф}\,(T_{равн} - T_{cт}),$$

where $T_{равн}$ is the equilibrium temperature and determined from equation

$$\alpha\,(T_r - T_{равн}) - \varepsilon\sigma T_{равн}^4 = 0.$$

Calculating the latter formula from the preceding and factoring $T_{равн}^4 - T_{st}^4$, we get:

$$\alpha_{эф} = \alpha\left[1 + \left(\frac{T_r}{T_{равн}} - 1\right)\left(1 + \frac{T_{cт}}{T_{равн}}\right)\left(1 + \frac{T_{cт}^2}{T_{равн}^2}\right)\right].$$

For materials with low conductivity, for example, heat-insulation materials, after a short heating period, T_{st} gets very close to T_{ravn} and consequently in the latter expression we may assume $T_{st}/T_{ravn} \approx 1$, then

$$\alpha_{эф} \approx \alpha\left[1 + 4\left(\frac{T_r}{T_{равн}} - 1\right)\right].$$

We can sometimes be limited to one term of the series for θ. Actually, in this case when $\beta < 0.1$, the second term of the series will be less than 2% of the first, while the third will be less than 0.5% of the first. For $\phi > 0$, the relative values and the second and subsequent terms will be even lower.

For $\beta < 0.1$, we can assume in approximate terms

$$\operatorname{tg} k_1 \approx k_1,$$

then $k_1^2 = \beta$ and $k_1 = \beta$.

The error in the determination of k_1 under this assumption will be less than 1.6%. In this case

$$k_1^2\varphi=\beta\varphi=\frac{a\tau}{\delta_{o\delta}c\gamma}=\frac{\tau}{\tau_c},$$

TABLE 4.3.

Values of Coefficients k_n

$(k_n \tan k_n = \beta)$

β	0	0,001	0,002	0,004	0,006	0,008	0,01	0,02	0,04	0,06
k_1	0,0000	0,0316	0,0447	0,0632	0,0774	0,0893	0,0998	0,1410	0,1987	0,2425
k_2	3,1416	3,1419	3,1422	3,1429	3,1435	3,1441	3,1448	3,1479	3,1543	3,1606
k_3	6,2832	6,2833	6,2835	6,2838	6,2841	6,2845	6,2848	6,2864	6,2895	6,2927

β	0,08	0,1	0,2	0,3	0,4	0,5	0,6	0,7	0,8	0,9
k_1	0,2791	0,3111	0,4328	0,5218	0,5932	0,6533	0,7051	0,7506	0,7910	0,8274
k_2	3,1668	3,1731	3,2039	3,2341	3,2636	3,2923	3,3204	3,3477	3,3744	3,4003
k_3	6,2959	6,2991	6,3148	6,3305	6,3461	6,3616	6,3770	6,3923	6,4074	6,4224

β	1,0	1,5	2,0	3,0	4,0	5,0	6,0	7,0	8,0	9,0
k_1	0,8603	0,9882	1,0769	1,1925	1,2646	1,3138	1,3496	1,3766	1,3978	1,4149
k_2	3,4256	3,5422	3,6436	3,8088	3,9352	4,0336	4,1116	4,1746	4,2264	4,2694
k_3	6,4373	6,5097	6,5783	6,7040	6,8140	6,9096	6,9924	7,0640	7,1263	7,1806

β	10	15	20	30	40	50	60	80	100	∞
k_1	1,4289	1,4729	1,4961	1,5202	1,5325	1,5400	1,5451	1,5514	1,5552	1,5708
k_2	4,3058	4,4255	4,4915	4,5615	4,5979	4,6202	4,6353	1,6543	4,6658	4,7124
k_3	7,2281	7,3959	7,4954	7,6057	7,6647	7,7012	7,7259	7,7573	7,7764	7,8540

where we designate

$$\tau_c=\delta_{o\delta}c\gamma/a$$

$(\tau_s$ is the time constant of thermal inertia).

When β < 0.1, we may also simplify Expression (4.20) for B_1.

Assuming $k_1 \approx \sin k_1$, we obtain:

$$B_1=\frac{2}{1+\cos k_1}=\frac{2}{1+\cos\sqrt{\beta}}.$$

With the assumption made, θ may be represented in the form

$$\theta=\frac{2\cos(\sqrt{\beta}\xi)}{1+\cos\sqrt{\beta}}e^{-\tau/\tau_c}\zeta_1. \tag{4.25}$$

In the case of equilibrium temperature distribution along the thickness of the plating, when $\tau = 0$, $\zeta_1 = 1$, and consequently,

$$\theta=\frac{2\cos(\sqrt{\beta}\xi)}{1+\cos\sqrt{\beta}}e^{-\tau/\tau_c}, \tag{4.26}$$

where β is determined from Formula (4.15).

- 101 -

TABLE 4.4.

Values of Coefficients B_n

$$\left(B_n = \frac{4\sin k_n}{2k_n + \sin 2k_n}; \quad k_n \operatorname{tg} k_n = \beta\right)$$

β	0	0,001	0,002	0,004	0,006	0,008	0,01	0,02	0,04	0,06
B_1	1,0000	1,0002	1,0004	1,0008	1,0012	1,0015	1,0016	1,0030	1,0065	1,0099
B_2	0,0000	—0,0002	—0,0004	—0,0008	—0,0012	—0,0016	—0,0020	—0,0040	—0,0080	—0,0119
B_3	0,0000	0,0000	0,0001	0,0002	0,0003	0,0004	0,0005	0,0010	0,0020	0,0030

β	0,08	0,10	0,20	0,30	0,40	0,50	0,60	0,70	0,80	0,90
B_1	1,0130	1,0159	1,0312	1,0450	1,0581	1,0701	1,0813	1,0918	1,1016	1,1107
B_2	—0,0158	—0,0197	—0,0381	—0,0555	—0,0719	—0,0873	—0,1025	—0,1154	—0,1282	—0,1493
B_3	0,0040	0,0050	0,0100	0,0148	0,0196	0,0243	0,0289	0,0335	0,0379	0,0423

β	1,0	1,5	2,0	3,0	4,0	5,0	6,0	7,0	8,0	9,0
B_1	1,1192	1,1537	1,1784	1,2102	1,2287	1,2403	1,2478	1,2532	1,2569	1,2598
B_2	—0,1517	—0,2013	—0,2367	—0,2881	—0,3215	—0,3442	—0,3604	—0,3722	—0,3812	—0,3880
B_3	0,0466	0,0667	0,0848	0,1154	0,1396	0,1588	0,1740	0,1861	0,1959	0,2039

β	10	15	20	30	40	50	60	80	100	∞
B_1	1,2612	1,2677	1,2699	1,2717	1,2723	1,2727	1,2728	1,2730	1,2731	1,2732
B_2	—0,3934	—0,4084	—0,4147	—0,4198	—0,4217	—0,4227	—0,4232	—0,4237	—0,4239	—0,4244
B_3	0,2104	0,2320	0,2394	0,2472	0,2502	0,2517	0,2526	0,2535	0,2539	0,2546

To evaluate the accuracy of Formula (4.26), Table 4.5 gives the errors which result from this formula in comparison with the exact Formula (4.22) with a constant initial temperature along the thickness of the plating.

It is apparent from Table 4.5 that the accuracy of Formula (4.26) is determined not only by the value of β, but also by the relative heating time τ/τ_s. At $\tau/\tau_s = 0$, Formula (4.26) produces the greatest error. However, these errors are substantially reduced when $\tau/\tau_s = 0.01$.

Formula (4.26) may also be used for β > 0.1, if in this case, τ/τ_s is sufficiently large. For example, in the case of β = 0.2 and $\tau/\tau_s = 0.1$, there are few errors.

It is apparent that the accuracy of Formula (4.25) will be approx-

imately the same as the accuracy of Formula (4.26).

TABLE 4.5

Accuracy of Formula (4.26) $\qquad$ $\theta = \dfrac{2\cos(\sqrt{\bar{\beta}\,\xi})}{1+\cos\sqrt{\bar{\beta}}}\, e^{-\tau/\tau_c},$

$\dfrac{\tau}{\tau_c}$	β	$\theta_{вн}$ ($\xi=0$)			$\theta_{ст}$ ($\xi=1$)		
		по (4.26)	по (4.22)	¹)ошибка в %	по (4.26)	по (4.22)	ошибка в %
0	0,05	1,012	1,000	+1,2	0,989	1,000	—1,1
0	0,10	1,023	1,000	+2,3	0,975	1,000	—2,5
0	0,20	1,050	1,000	+5,0	0,947	1,000	—5,3
0,01	0,05	1,002	0,997	+0,5	0,977	0,976	+0,1
0,01	0,10	1,013	0,999	+1,4	0,963	0,965	—0,2
0,01	0,20	1,040	1,000	+3,6	0,938	0,953	—1,6
0,10	0,05	0,918	0,917	+0,1	0,895	0,895	0
0,10	0,10	0,928	0,921	+0,8	0,883	0,879	+0,5
0,10	0,20	0,950	0,940	+1,1	0,860	0,854	+0,7

1) Error, in %.

In the case metal plating, β in many practical instances of aerodynamic heating will be less than 0.1 and consequently to reduce the amount of calculation while determining θ, we may use Formula (4.25) and (4.26) in these cases.

§4.3. THE CRITERION OF THIN PLATING

§4.1 gave a solution of the heat-conduction equation on the assumption that the plating was so thin that the temperature difference across its thickness was insubstantial. The question naturally arises, when can plating be considered thin; in other words, we must establish a criterion for thin plating.

Since the temperature difference across the thickness of the plating never equals zero, for all practical purposes it is necessary to establish the permissible difference at which the plating may be considered to be heating uniformly. We will characterize the heating equilibrium of the plating by the relation of the temperature increment of the inner plating surface to the temperature increment of the

of the outer surface, i.e.,

$$\Delta T_{вн}/\Delta T_{ст}.$$

Let us introduce the concept of a relative temperature difference across the thickness of the plate and designate it as ε_p, in which case

$$\varepsilon_n = \frac{\Delta T_{ст} - \Delta T_{вн}}{\Delta T_{ст}} = 1 - \frac{\Delta T_{вн}}{\Delta T_{ст}}. \tag{4.27}$$

Let us express the relative temperature of θ in terms of the temperature increment, using Formula (4.8):

$$\theta = \frac{T_r - T}{T_r - T_0} = 1 - \frac{\Delta T}{T_r - T_0},$$

where $\Delta T = T - T_0$,

hence

$$\Delta T = (1 - \theta)(T_r - T_0).$$

Consequently,

$$\varepsilon_n = 1 - \frac{(1 - \theta_{вн})}{(1 - \theta_{ст})} = \frac{(\theta_{вн} - \theta_{ст})}{(1 - \theta_{ст})}. \tag{4.28}$$

Assuming the values of the permissible relative temperature difference ε_p, from the latter equation we can find the plating thickness at which this temperature difference may be obtained. Evidently, thicknesses less or equal to that found will correspond to thin plating.

Since it is necessary to have an approximate solution for the criterion of thin plating, we can derive it from approximate functions. For thin shielding, the Fourier criterion, as can be seen from what follows, is $\varphi > 1$. Consequently, in the expression for the relative temperature (4.22) it is entirely possible to limit ourselves to one term of the expansion. For low values of β, as was shown in §4.2, we may assume that $k_1^2 = \beta$. In addition, the value of the coefficient B_1 according to Formula (4.20) may be assumed to be

$$B_1 \approx 4k_1/(2k_1 + 2k_1) = 1.$$

- 104 -

Then, with the assumption that $\zeta_1 = 1$, Formula (4.23) and (4.24) may be represented in the following form

$$\theta_{ct} = \cos \sqrt{\bar{\beta}}\, e^{-\beta\varphi}; \quad \theta_{su} = e^{-\beta\varphi}.$$

The relative temperature difference may now be represented in the form

$$\varepsilon_n = \frac{(1 - \cos \sqrt{\bar{\beta}})\, e^{-\beta\varphi}}{1 - \cos \sqrt{\bar{\beta}}\, e^{-\beta\varphi}}.$$

At low values of β we can expand the functions $\cos \sqrt{\beta}$ and $e^{-\beta\varphi}$ in series and limit ourselves to two term of the expansion, i.e., we may assume

$$\cos \sqrt{\bar{\beta}} = 1 - \frac{1}{2}\beta; \quad e^{-\beta\varphi} = 1 - \beta\varphi. \qquad (4.29)$$

Then

$$\varepsilon_n = \frac{1}{2} \frac{\beta(1 - \beta\varphi)}{1 - \left(1 - \frac{1}{2}\beta\right)(1 - \beta\varphi)} = \frac{1}{2} \frac{1 - \beta\varphi}{\frac{1}{2} + \varphi - \frac{1}{2}\beta\varphi}.$$

Hence

$$\varphi = \frac{1 - \varepsilon_n}{2\varepsilon_n + \beta - \varepsilon_n\beta} = \frac{1 - \varepsilon_n}{2\left[1 - (1 - \varepsilon_n)\left(1 - \frac{1}{2}\beta\right)\right]}.$$

At low values of β we may assume

$$1 - \frac{1}{2}\beta \approx 1;$$

then

$$\varphi = \frac{1}{2} \frac{(1 - \varepsilon_n)}{\varepsilon_n}. \qquad (4.30)$$

Taking into consideration β with respect to Formula (4.12), we obtain:

$$\delta_{o6} = \sqrt{2a\tau \frac{\varepsilon_n}{(1 - \varepsilon_n)}}.$$

Consequently, we may assume thin plating to be that plating at

- 105 -

which

$$\delta_{o6} \leqslant \sqrt{2a\tau \frac{\epsilon_n}{(1-\epsilon_n)}} \, . \qquad (4.31)$$

It should be borne in mind that this criterion of thin plating is applicable in cases in which the values of β are low, i.e., those values at which the above approximations for k_1, $\cos \sqrt{\beta}$ and $e^{-k_1^2 \varphi}$ are permissible, and this with a sufficient degree of accuracy.

With a view to comparing Formula (4.30) with the accurate solution, Fig. 4.3 gives the graph constructed from the results of exact calculation for φ with respect to β where ε_p = 0.1. It is appararent from this graph that for β < 0.1, the value of φ from Formula (4.30) is sufficiently close to the exact value. At high values of β, the value of φ drops, so that for β > 10 we can assume φ ≈ 1 for ε_p = 0.1. In this case:

$$\delta_{o6} \leqslant \sqrt{a\tau}. \qquad (4.32)$$

In the general case

$$\delta_{o6} \leqslant \sqrt{\frac{a\tau}{\varphi}}. \qquad (4.33)$$

This formula may be used together with the graph given in Fig. 4.3, from which we determine the value of φ at ε_p = 0.1.

When β > 10, φ may be determined from the following formula

$$\varphi = 0.933 \lg \left(\frac{1.273}{\epsilon_n} \right). \qquad (4.34)$$

The latter formula was found from the condition β = ∞.

For metals, β is generally of the order of 0.1 and less; consequently, we may use Formula (4.31) as a criterion of thin metal plating. For laminated plates, the thermal conductivity is less by a factor of a hundred than in the case of metals; consequently, β will be substantially lower in the case of metals, and so for laminated

- 106 -
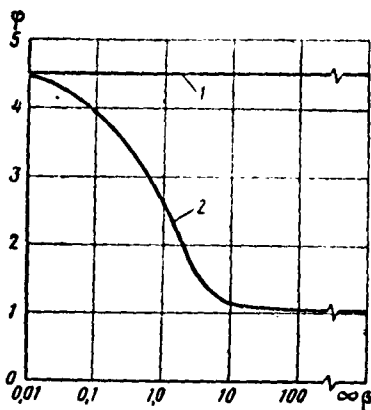
Fig. 4.3. Graph of the Fourier criterion for thin plating with a relative temperature difference of $\varepsilon_p = 0.1$. 1) From the following formula

$$\varphi = (1 - \varepsilon_p)/2\varepsilon_p;$$

2) from exact calculation.

plates and, in general, for plastic, we should use Formulas (4.33) and (4.34).

If the heat-transfer coefficient is small ($\alpha < 0.1$), then in the case of plastic the criterion of thin plating should be determined from Formula (4.31).

As far as ceramic materials are concerned, their thermal conductivity is lower by a factor of only ten than in the case of metals, and consequently the value of φ will be somewhere between the values for metals and laminated plates. These values of φ should be determined from graphs analogous to that given in Fig. 4.3, or, if we want to be especially cautious, we should calculate δ_{ob} from Formula (4.31).

Table 4.6 gives the maximum thickness values of a thin plating for various materials where $\varepsilon_p = 0.1$. Metal and aluminum-oxide calculations were carried out in accordance with Formula (4.31), while asbestos, glass, and laminated plastic calculations were carried out in accordance with Formula (4.32).

The thermal conductivity of metals in Table 4.6 was determined at 200° C.

§4.4. THE DETERMINATION OF THE THICKNESS FOR HEAT-INSULATION PLATING

A number of materials with low thermal conductivity are used for heat insulation. The required heat-insulation thickness in a steady-state thermal process is easy to find from Formula (3.4) in the presence of internal cooling;

$$\delta_{нэ} = \lambda_{нэ} \frac{\Delta T_{нэ}}{q_{ох}}.$$

(4.35)

- 107 -

TABLE 4.6.

Maximum Thickness Values of Thin Plating for Various Materials at
ε_p = 0.1.

Материал 1	Температуропроводность 2 $м^2/сек$ [25]	Предельная величина тонкой обшивки в мм 3	
		при $\tau=10$ сек. 4	при $\tau=100$ сек. 4
5 6 Алюминий	$8,7\cdot10^{-5}$	14	44
7 Магний	$7,2\cdot10^{-5}$	13.	41
Бериллий	$5,9\cdot10^{-5}$	11	36
8 Железо	$1,5\cdot10^{-5}$	5,8	18
9 Сталь 1Х18Н9Т	$0,42\cdot10^{-5}$	3	9,6
10 Титан	$0,6\cdot10^{-5}$	3,6	11
11 Молибден	$5,1\cdot10^{-5}$	11	34
12 Никель	$1,4\cdot10^{-5}$	5,6	18
13 Окись алюминия Al₂O₃ при 1000° С [51]	$6,2\cdot10^{-7}$	1,2	3,7
14 Текстолит при 20° С	$1,5\cdot10^{-7}$	1,2	3,8
15 Стекло при 200° С	$5,9\cdot10^{-7}$	2,4	7,6
16 Стеклотекстолит [6]	$2\cdot10^{-7}$	1,4	4,4
17 Асбест, $\gamma=100$ кг/м³	$7\cdot10^{-7}$	2,6	8,4

1) Material; 2) thermal diffusivity; 3) maximum size of thin plating,
in mm; 4) where; 5) aluminum; 6) magnesium; 7) beryllium; 8) iron;
9) steel 1Kh18N9T; 10) titanium; 11) molybdenum; 12) nickel; 13) alu-
minum oxide Al_2O_3 at 1000° C [51]; 14) textolite at 20° C; 15) glass
at 200° C; 16) glass-textolite [6]; 17) asbestos, γ = 100 kg/m^3.

The required insulation thickness is proportional to the thermal
conductivity and does not depend on its heat capacity.

Porous and loose fibrous materials exhibit the lowest thermal
conductivity. Moreover, as the porosity and brittleness increase and
the weight of the material correspondingly decreases, the thermal con-
ductivity of the material approaches the thermal conductivity of air.
The thermal conductivity of asbestos, depending on the degree of its
looseness, will be (see [25]):

1 при $\gamma=500$ кг/м³ . . . . $\lambda=2,5\cdot10^{-5}$ (1+0,0018 t)
. $\gamma=200$ . . . . $\lambda=1,8\cdot10^{-5}$ (1+0,0022 t)
. $\gamma=100$ . . . . $\lambda=1,5\cdot10^{-5}$ (1+0,0027 t)

1) Where.

The thermal conductivity of air

$$\lambda = 0{,}56 \cdot 10^{-5}(1 + 0{,}0030t).$$

The porous and loose fibrous materials have very low mechanical properties and consequently can be used only for the inner facing of the plating.

Among the heat-insulation materials of great strength are certain types of plastics and, in particular, laminated plastics. However, their thermal conductivity is greater than in the case of porous materials. For example, textolite has a thermal conductivity (see [25])

$$\lambda \approx 7 \cdot 10^{-5} \text{ kcal/m} \cdot \text{sec} \cdot \text{deg.}$$

The ceramic materials are heat resistant and sufficiently strong to be used for the outside coating; however, they have even greater thermal conductivity. For example, aluminum oxide Al_2O_3 has, at 1000° C, a thermal conductivity (see [51])

$$\lambda = 6 \cdot 10^{-4} \text{ kcal/m} \cdot \text{sec} \cdot \text{deg.}$$

In addition, ceramic insulation is very brittle and cracks easily under intense heating.

In a nonsteady-state thermal process, the required heat-insulation thickness should be determined from Eq. (4.24) in the general case; moreover, it is necessary to give the permissible temperature values of the inner surface. However, the solution of this equation for φ, and later also for δ_{1z}, in the general case can be obtained only graphically or by interpolation, if the values of φ are given.

The temperature of the inner surface can be assumed on the basis of the relative temperature difference [see Formula (4.27)]. For example, for practical purposes in a number of cases the following would be entirely acceptable.

$$\frac{\Delta T_{вн}}{\Delta T_{ст}} = 0{,}1;$$

then

$$\epsilon_n = 0{,}9.$$

Given the value of ε_p and knowing the value of θ_{st}, we can determine the relative temperature of the inner surface from Formula (4.28):

$$\theta_{вн} = \varepsilon_п + \theta_{ст}(1 - \varepsilon_п).$$

For the given equation we can limit ourselves to one term of the series in Eq. (4.23) and (4.24).

Then at $\zeta_n = 1$ (the constant temperature along the thickness of the plating at the beginning of its heating)

$$\theta_{ст}/\theta_{вн} = \cos k_1.$$

The calculation of exact values of θ_{st}/θ_{vn} and subsequent determination of the corresponding values of φ by successive approximations indicates that in the case of the given $\theta_{st}/\theta_{vn} = \cos k_1$, the errors will be at high values of ε_p. In reality, when ε_p increases, φ decreases and where $\varepsilon_p = 1$, $\varphi = 0$. This is evident from the structure of Eqs. (4.23) and 4.24), and also from Table 4.7.

Assuming that for all practical purposes we scarcely need a value of ε_p greater than 0.95, we can calculate the errors for $\varepsilon_p = 0.95$ at various values of β. The relative errors in the determination of the insulation thickness, assuming $\theta_{st}/\theta_{vn} = \cos k_1$ are as follows:

1 Значения β	0,1	1,0	10	100
Ошибки в определении толщины изоляции в %	4	5	0,7	0,4

1) The value of β; 2) errors in the determination of the insulation thickness, in %.

Where $\varepsilon_p < 0.95$, there will be even fewer errors in the required insulation thickness.

Assuming $\theta_{st}/\theta_{vn} = \cos k_1$, from the above-given value for θ_{vn},

we find:

$$\theta_{vn} = \frac{\varepsilon_n}{[1-(1-\varepsilon_n)\cos k_1]} \, .$$

(4.36)

Giving the value of ε_p, we can determine θ_{vn} for the given value of β from this formula.

The insulation thickness required to ensure the given relative temperature difference can be determined, if we know the value of the Fourier criterion;

then

$$\delta_{us} = \sqrt{\frac{a\tau}{\varphi}} \, .$$

(4.37)

The value of φ can be calculated in the following way. Assuming certain values of φ, let us find the corresponding values of θ_{vn} from Eq. (4.24). Having determined the required value of θ_{vn} from Formula (4.36), we can find the sought value of φ graphically or by linear interpolation.

Table 4.7 gives the determination of values of φ for various values of ε_p and β. We were limited to two terms of the series in the first three rows when we determined the values of θ_{vn} from Eq. (4.24). In the subsequent rows, the values of θ_{vn} were determined from Formula (4.36).

The value of φ was determined by linear interpolation; for $\beta = 0.01$ and 0.1, the value of φ was determined graphically.

The results of the calculations are presented graphically in Fig. 4.4. By using this graph, we can determine rather rapidly the required insulation thickness.

It should be noted that the indicated method for the determination of the insulation thickness was used formally under those conditions in which Eq. (4.24) was found. If the values of T_r and a are variable

- 111 -

in flight, it is possible approximately to determine the insulation

thickness by averaging T_r and α with respect to time.

TABLE 4.7.

The Determination of the Fourier Criterion (φ) at Various Relative
Temperature Differences

β		0,01	0,1	1,0	10	100	∞
$\theta_{вн}$ at $\varphi=0,1$		0,99987	0,9989	0,9919	0,9690	0,9496	0,9495
$\theta_{вн}$ at $\varphi=0,2$		0,99935	0,9939	0,9523	0,8295	0,7795	0,7720
$\theta_{вн}$ at $\varphi=0,3$		0,99851	0,9850	0,8915	0,6745	0,6144	0,6065
$\cos k_1$		0,995	0,952	0,652	0,1413	0,0158	0
$\varepsilon_n=0,80$	$\theta_{вн}$	0,99880	0,9877	0,9199	0,8230	0,8030	0,8000
	φ	0,272	0,275	0,253	0,204	0,186	0,184.
$\varepsilon_n=0,85$	$\theta_{вн}$	0,99912	0,99125	0,9423	0,8685	0,8522	0,8500
	φ	0,225	0,237	0,216	0,172	0,157	0,156
$\varepsilon_n=0,90$	$\theta_{вн}$	0,99950	0,99470	0,9628	0,9130	0,9015	0,9000
	φ	0,175	0,184	0,174	0,140	0,1283	0,1280
$\varepsilon_n=0,95$	$\theta_{вн}$	0,99974	0,99748	0,9820	0,9567	0,9506	0,9500
	φ	0,130	0,135	0,125	0,109	0,099	0,097

To illustrate the method for determining the required insulation

thickness, as an example, let us determine the required glass-textolite

thickness for the plating of the instrument bay of a cone subject to

intense aerodynamic heating for sixty seconds. Let us determine this

thickness for the initial data corresponding to the example considered

in §4.1.

It is necessary to assure a temperature for the inner plating

surface that is not higher than 80° C.

Let us initially determine the temperature of the outer surface

which, due to the low thermal conductivity of glass-textolite, can

approximately be assumed to be equal to the instantaneous equilibrium

temperature, understanding by the latter the temperature at which

$$q_a = q_{аэ}.$$

Let us find this temperature by successive approximations, using

Table 4.2. For $\tau = 20$ sec.:

1 Задаемся $T_{ст}$	750	780	779	778
2 Находим q_a	6,71	4,37	4,45	4,52
3 Находим $q_{из}$	3,85	4,50	4,48	4,46

1) Given T_{st}; 2) let us find q_a; 3) let us find q_{iz}.

Hence, it is apparent that at $\tau = 20$ sec., $T_{st} = 779°$ K. Similarly, let us find: for $\tau = 60$ sec., $T_{st} = 490°$ K.

Let us average the wall temperature with respect to time, assuming that the linear change of T_{st} is in the time intervals from 0 to 20 sec. and from 20 to 60 sec.:

$$(T_{ст})_{ср} = \frac{302+779}{2} \cdot \frac{20}{60} + \frac{779+490}{2} \cdot \frac{40}{60} = 604° K.$$

Consequently, the temperature increase for the outer surface

$$\Delta T_{ст} = 604° - 302° = 302°;$$

the temperature increase for the inner surface according to the condition

$$\Delta t_{вк} = 353° - 302° = 51°.$$

The relative temperature gradient

$$\varepsilon_n = 1 - \frac{51}{302} = 0,831.$$

Averaging α with respect to the temperature:

$$\alpha_{ср} = \frac{0,0323 + 0,0780}{2} \cdot \frac{20}{60} + \frac{0,0780 + 0,0465}{2} \cdot \frac{40}{60} = 0,0598.$$

To determine the value of β, a rough estimate of the plating thickness $\delta_{ob} = 5$ mm is assumed; then

$$\beta = \frac{\alpha \delta_{об}}{\lambda} = \frac{0,0598 \cdot 0,005}{7,10^{-5}} = 4,27.$$

From Fig. 4.4 we will find that $\varphi = 0.202$

Consequently, according to Formula (4.37)

$$\delta_{o\delta} = \sqrt{\frac{a\tau}{\phi}} = \sqrt{2 \cdot 10^{-7} \cdot \frac{60}{0,202}} = 0,0077 \text{ м.}$$

Let us make the second approximation, making the value of β more precise:

$$\beta = \frac{0,0598 \cdot 0,0077}{7 \cdot 10^{-6}} = 6,57.$$

From Fig. 4.4 we find that $\phi = 0.192$, and consequently,

$$\delta_{o\delta} = \sqrt{2 \cdot 10^{-7} \cdot \frac{60}{0,192}} = 0,0079.$$

It is apparent from the calculation that the effect of β on the result is insignificant. It should be noted that the scale of the axis of abscisses in Fig. 4.4 is logarithmic and encompasses a range of change in β from 0.01 to 1.00 (by factor of 10,000). Because β has little influence on the result of the calculation, we need not determine the value of a in the value of β with great accuracy.

The heat-insulation calculation given is based on the assumption that the temperature of the outer surface is equal to the instantaneous equilibrium temperature.

In fact, the temperature of the outer surface and, consequently, the obtained insulation thickness is somewhat increased. On the basis of the obtained data, we can determine the temperature of the outer surface and make more precise the required insulation thickness.

For $\beta = 6.57$, from Tables 4.3 and 4.4 we find: $k_1 = 1.36$, $k_2 = 4.14$, $B_1 = 1.25$, and $B_2 = -0.366$; consequently where $\phi = 0.192$ from Eq. (4.23) we find:

$$\theta_{st} = 1.25 \cdot 0.2108 \ e^{-0.355} + 0.366 \cdot 0.5446 \ e^{-3.28} = 0.1850 + 0.0075 = 0.1925.$$

To calculate the radiation we assume that the temperature of the adiabatic wall is equal to the equilibrium temperature; then we obtain:

$$\theta_{ст} = \frac{T_f - T_{ст}}{T_f - T_0} = \frac{604 - T_{ст}}{604 - 302} = 0,1925;$$

hence $T_{st} = 546°$ K. Consequently, $\Delta T_{st} = 546 - 302 = 244$ and

$$\varepsilon_n = 1 - \frac{\Delta T_{вм}}{\Delta T_{ст}} = 1 - \frac{51}{248} = 0,799.$$

From Fig. 4.4 we find $\varphi = 213$; consequently

$$\delta_{об} = \sqrt{2 \cdot 10^{-7} \cdot \frac{60}{0,213}} = 0,0075 \ м = 7,5 \ мм.$$

Consequently, the temperature taken equal to the equilibrium temperature produced an error of +5% in the determination of the heat-insulation thickness.
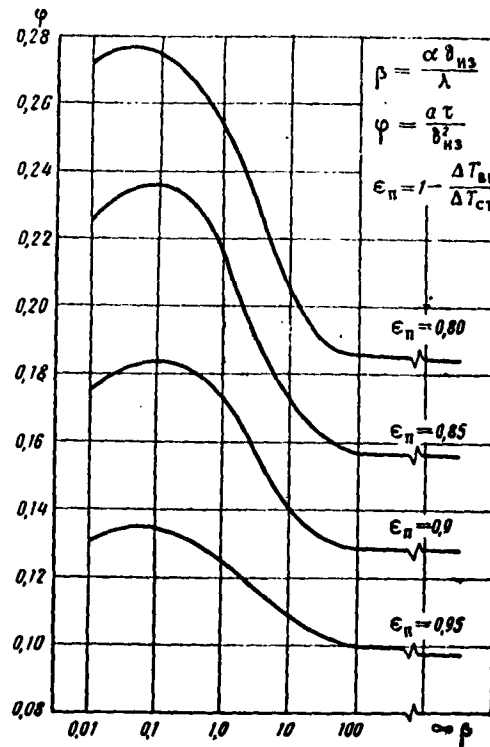

Fig. 4.4. Graph of the Fourier criterion at various relative temperature differences.

We can approximately estimate the value of the Fourier criterion from the following formula

$$\varphi = 1,7 \lg \frac{1,1}{\varepsilon_n}. \tag{4.38}$$

According to this formula, the error in the determination of the

thickness for $\varepsilon_p > 0.8$, will be less than 12%.

According to this formula, for the above-considered example

$$\varphi = 1.7 \lg \frac{1.1}{0.798} = 0.238.$$

Consequently

$$\delta_{o6} = 0.0071 \ \text{м},$$

i.e., the error is 5%.

When selecting the heat-insulation material, given satisfactory mechanical strength properties and physical (adhesion, breakdown temperature) properties assuring the possibility of its use under the given conditions, it is necessary to evaluate the feasibility of using a given material with respect to weight.

Formula (4.37) makes it easy for us to compare the various materials with respect to weight in a nonsteady-state thermal process. In reality, the weight of 1 m^2 of the sheet material for the required heat-insulation thickness will be:

$$\delta_{\text{из}\gamma} = \sqrt{\frac{\lambda \tau \gamma^2}{c \tau \varphi}} = \sqrt{\frac{\lambda \gamma}{c}} \sqrt{\frac{\tau}{\varphi}}.$$

The value of τ/φ is in the main determined by external conditions, and this is apparent from Formula (4.38). Consequently, the weight criterion, depending on the physical properties of the material and proportional to the weight of the required insulation, will be

$$\sqrt{\frac{\lambda \gamma}{c}}.$$

Table 4.8 gives the value of this criterion for certain heat-insulation materials.

Table 4.8 gives three groups of material: ceramic insulation, laminated plastics, and porous insulation (including loose fibrous insulation). Within each group, the heat-insulation materials have

weight criteria which are comparatively close. However, the weight criteria of materials from various groups differ greatly.

Porous materials possess the lowest weight criteria, but because of the low mechanical properties, they can be used only for internal insulation.

It should be noted that the thermal conductivity of porous materials increases substantially as the temperature increases; consequently the insulation should be calculated at an average temperature. Table 4.8 gives the thermal conductivity of porous materials at 200° C.

TABLE 4.8.

Ideal-Weight Criterion for Certain Heat-insulation Materials

1 Материал	$\dfrac{\lambda}{ккал}{м \cdot сек \cdot град}$	γ кг/м³	$\dfrac{c}{ккал}{кг \cdot град}$	$\sqrt{\dfrac{\lambda\gamma}{c}}$	Предельная температура применения 2 °C	Литературный источник 3
4 Окись алюминия	6·10⁻⁴	3200	0,30	2,5	2000	[51]
5 Окись циркония	2,1·10⁻⁴	4400	0,18	2,3	2600	[51]
6 Текстолит	0,7·10⁻⁴	1350	0,35	0,52	250	[25]
7 Стеклотекстолит	0,7·10⁻⁴	1600	0,24	0,69	300	[6]
8 Асбестовый картон	0,44·10⁻⁴	1000	0,20	0,47	450	[25]
9 Фторопласт	0,59·10⁻⁴	2200	0,25	0,72	400	[32]
10 Асбест распушенный	0,22·10⁻⁴	100	0,20	0,105	600	[25]
11 Минеральная вата	0,18·10⁻⁴	150	0,22	0,110	600	[25]
12 Стекловолокно (маты)	0,26·10⁻⁴	120	0,20	0,125	450	[25]
13 Пеностекло	0,26·10⁻⁴	200	0,20	0,160	500	[25]

1) Material; 2) temperature limit of application, in °C; 3) literature source; 4) aluminum oxide; 5) zirconium oxide; 6) textolite; 7) glass-textolite; 8) asbestos cardboard; 9) fluorine sheet; 10) loose asbestos; 11) mineral cotton; 12) fiberglas (mat finish); 13) foam glass.

Ceramic insulation possesses a weight criterion several times greater than the criterion for laminated plastics, but it has a higher breakdown temperature (melting). It is true that the temperature ad-

vantages of ceramic insulation cannot always be used, since the ceramic insulation may crack during intensive heating (thermal shock).

Like outer heat insulation, laminated plastics possess good weight qualities and have a comparatively low breakdown temperature. It should be noted that in Table 4.8, the practical temperature limits of laminated plastics correspond to the long-term effect (many hours) of high temperature. In the case of a short-term effect (seconds and single minutes), the permissible operating temperatures for laminated plastics may be substantially increased.

In the case of a single short-term effect, the laminated plastics may even be used at air temperatures of several thousand degrees; it is true, of course, that in this case the upper layer will be subject to erosion and sublimation, so that with time the thickness of the plate will decrease. In addition, it should be borne in mind that after this removal of metal the remaining thickness of the plate will have a carbonized upper layer, while the layer beneath will be broken down (cracks, folliation).

For example, in tests of glass-textolite in a plasmatron stream formed at normal atmospheric pressure, the loss rate depended on the temperature of the stream and ranged from 0.033 to 0.8 mm/sec.; in this case the temperature range was from 2000 to 13000° K [45]. For the temperature range 2000° K < T < 6000° K, the loss rate was almost linearly dependent on the temperature and consequently the thickness of the loss can be represented in the form

$$\delta_{yr} = (1.175 \cdot 10^{-4} T - 0.205) \tau \ \text{мм.}$$

(4.39)

The thickness of the carbonized layer and damage to the glass-textolite structure depend on the loss rate (see [45]) and for 3300° K < T < 6000° K may be expressed by the formula

$$\delta_{пв} = \frac{1.1}{\frac{\delta_{уг}}{\tau}} \ мм.$$

<div style="text-align:right">(4.40)</div>

For T < 3300° K, the value of δ_{pv} begins to drop.

Manu-script Page No.	[List of Transliterated Symbols]
86	$T_{ст} = T_{st} = T_{stena} = T_{wall}$
86	$q_{л} = q_{\underline{1}} = q_{luchistaya} = q_{radiant}$
87	$T_{об} = T_{ob} = T_{obshivka} = T_{plating}$
87	$q_{наг} = q_{nag} = q_{nagrevaniye} = q_{heating}$
92	вн = vn = vnutrennyy = inner
100	равн = ravn = ravnovesiye = equilibrium
100	еф = ef = effecktivnyy = effective
107	из = iz = izluchayemyy = radiated
107	ox = okh = okhlazhdeniye = cooling
113	cp = sr = srednyy = average
118	уг = ug = ugar = loss

REFERENCES

1. Arzhanikov N.S. and Mal'tsev V.N. Aerodinamika. Oborongiz [Aero-
    dynamics, State Defense Industry Press], 1956.

2. Bachinskiy A.I. Putilov V.V. and Suvorov N.P. Spravochnik po
    fizike. Upchpedgiz [Physics Handbook. Science Pedagogical Press],
    1951.

3. Bond D. Fizika plazmy i giperzvukovyye polety, VRT ("Voprosy rake-
    tnoy tekhniki", IL) [Physics of Plasma and Hypersonic Flight,
    VRT ("Problems in Rocket Engineering," Foreign Literature
    Press)], 1958, No. 6.

4. Bosvort R.Ch.L. Protsessy teplovogo perenosa. GITTL [Processes of
    Heat Transfer. State Publishing House of Technical and Theore-
    tical Literature], 1957.

5. Van-Drayst Ye.R. Problema aerodinamicheskogo nagreva [The Problem
    of Aerodynamic Heating] VRT, 1957, No. 5.

6. Vardenburg A.K. Plasticheskiye massy v elektrotekhnicheskoy pro-
    myshlennosti. Gosenergoizdat [Plastics in the Electrical-
    Engineering Industry. State Power Engineering Press], 1957.

7. Griffit V. Noveyshiye dostizheniya v izuchenii techeniy real'nogo
    gaza s giperzvukovymi skorostyami [Latest Achievements in the
    Study of the Flow of a Real Gas at Hypersonic Velocities], VRT,
    1958, No. 6.

8. Gulyar R. O vliyanii skorostey katalicheskoy rekombinatsii na
    teplootdachu pri tormozhenii giperzvukovogo potoka [The Influ-
    ence of the Rates of Catalytic Recombination on Heat Transfer
    in the Deceleration of Hypersonic Flow], VRT, 1959, No. 5.

9. Kondrat'yev G.M. Teplovyye izmereniya. Mashgiz [Thermal Measure-
    ments. State Scientific and Technical Publishing House for
    Literature on Machinery], 1957.

10. Krasnov N.F. Aerodinamika tel vrashcheniya [The Aerodynamics of
    Solids of Revolution] Oborongiz, 1958.

11. Kutateladze S.S., Borishanskiy V.M. Spravochnik po teploperedache
    [Heat Transfer Handbook], Gosenergoizdat, 1959.

12. Lin' Tsya-tsyao, Teoriya gidrodinamicheskoy ustoychivosti [The
    Theory of Hydrodynamic Stability] IL, 1958.

13. Logan D., Posledniye dostizheniya v izuchenii izlucheniy gazov
    pri vysokikh temperaturakh [The Latest Achievements in the
    Study of Gas Radiation at High Temperatures], VRT, 1959, No. 7.

14. Lykov A.V., Teoriya teploprovodnosti [The Theory of Thermal Con-
    ductivity (Heat Conduction)], GITTL, 1952.

15. Margolin I.A. and Rumyantsev N.P., Osnovy infrakrasnoy tekhniki,
    Voyenizdat [Fundamentals of Infrared Engineering, Military
    Press], 1957, Page 48.

16. Meyyerott R., Radiatsionnyy perenos tepla k giperzvukovym
    raketam [Radiative Heat Exchange to Hypersonic Rockets], VRT,
    1959, No. 11.

17. Mikheyev M.A., Osnovy teploperedachi [Fundamentals of Heat Trans-
    fer], Gosenergoizdat, 1956.

18. Namagatsu G., Posledniye issledovaniya v sverkhzvukovoy aerodina-
    micheskoy ustanovke GALSIT [Latest Research with the Supersonic
    Aerodynamic GALCIT Installation], VRT, 1955, No. 6.

19. Rozner D., Issledovaniya konvektivnogo teploobmena pri nalichii
    dissotsiatsii i rekombinatsii atomov [Investigation of Convec-
    tion Heat Transfer in the Presence of Dissociation and Recom-
    bination of Atoms], VRT, 1959, No. 2.

20. Romig M., Teploobmen v tochke tormozheniya v giperzvukovykh poto-
    kakh [Heat Transfer at the Point of Deceleration in Hypersonic
    Flows], VRT, 1957, No. 6.

21. Sibulkin M., Otsenka turbulentnoy teplootdachi v zvukovoy tochke
    tela s zatuplennym nosom [Evaluation of Turbulent Heat Trans-
    fer at the Sonic Point of a Body with a Blunt Nose], VRT,
    1959, No. 3.

22. Snodrass, Poletnyye ispytaniya po opredeliniyu aerodinamicheskogo
    nagreva i tochki perekhoda laminarnogo pogranichnogo sloya v
    turbulentnyy na nosovoy konicheskoy chasti rakety "Viking 10"
    [Flight Tests for Determination of Aerodynamic Heating and
    Point of Transition from Laminar Boundary Layer to Turbulent
    Boundary Layer at the Conic Nose Part of the "Viking 10"
    Rocket], VRT, 1957, No. 1.

23. Stolder D., Gudvin G. and Kriger M., Koeffitsient teplootdachi v
    potoke razrezhennogo gaza vysokoy skorosti [Heat Transfer Co-
    efficient in a Stream of Rarefied High-Velocity Gas], VRT,
    1954, No. 1.

24. Stolder D., Problemy teplootdachi pri giperzvukovykh skorostyakh
    [Problems in Heat Transfer at Hypersonic Velocities], VRT,
    1958, No. 6.

25. Teplofizicheskiye svoystva veshchestv, Spravochnik pod redakt-
    siyey prof. N.B. Vargaftika [Thermophysical Properties of
    Matter, Handbook edited by Professor N.B. Vargaftik],
    Gosenergoizdat, 1956.

26. Ferri A., Aerodinamika sverkhzvukovykh techeniy [Aerodynamics
    of Supersonic Flows], GITTL, 1952.

27. Frankl' F.I. and Karpovich Ye A., Gazodinamika tonkikh tel,
    Gostekhizdat [The Gasdynamics of Thin Bodies, State Publishing
    House of Theoretical and Technical Literature], 1948.

28. Fey Dzh., Riddell F. and Kemp N., Teploobmen v peredney kritiches-
    koy tochke v dissotsiirovannom potoke vozdukha [Heat Transfer

at the Forward Critical Point in a Dissociated Air Stream],
VRT, 1958, No. 2.

29. Khilton U.F., Aerodinamika bol'shikh skorostey [The Aerodynamics of
High Velocities], IL, 1955.

30. Khouart L., et al. Sovremennoye sostoyaniye aerodinamiki bol'shikh
skorostey [Contemporary State of Aerodynamics of Great Veloci-
ties], Vol. 1, IL, 1955.

31. Khouart L., et al. Sovremennoye sostoyaniye aerodinamiki bol'shikh
skorostey, Vol. 2, IL, 1956.

32. Chegodayev D.D., Ftoroplasty, Goskhimizdat [Fluorine-Based Plastics,
State Scientific and Technical Publishing House for Chemical
Literature], 1956.

33. Shlikhting G., Teoriya pogranichnogo sloya [Boundary-Layer Theory],
IL, 1956.

34. Shmidt K. and Khanaval't A., Temperatura poverkhnosti sputnika
[The Temperature of the Surface of a Satellite],VRT,1958,No. 3.

35. Ekkert E., Inzhenernyye metody rascheta laminarnogo i turbulent-
nogo teploobmena i treniya pri obtekanii poverkhnostey s pos-
toyannym davleniyem i temperaturoy potokom gaza bol'shoy
skorosti [Engineering Methods of Calculating Laminar Turbulent
Heat Transfer and Friction in the case of Flow past Surfaces
of a Gas Stream at High Velocity with Constant Pressure and
Temperature], VRT, 1957, No. 4.

36. Ekkert E.R., Vvedeniye v teoriyu teplo- i massoobmena [Introduc-
tion into the Theory of Heat- and Mass-Transfer], Gosenergoiz-
dat, 1957.

37. Erike K., Aerotermodinamika snizhayushchegosya iskustvennogo sput-
nika. Nauchnyye problemy iskustvennykh sputnikov [Aerothermo-
dynamics of a Descending Artificial Satellite. Scientific

Problems of Artificial Satellites], IL, 1959.

38. Bertman M., Exploratory Investigation of Boundary Layer Transition on a Hollow Cylinder at a Mach Number of 6,9, NACA Report, 1957, No. 1313.

39. Canadian Aeronautical Journal, 1958, No. 1-3, pp. 3-10, 39-46, 79-85.

40. De Corso S.M. and Coit R.L., Measurement of Total Emissivities of Gas-Turbine Combustor Materials, Transactions of the ASME, 1955, Nov., vol. 77, No. 8.

41. Detra R.W., Kemp W.H., and Riddele F.R., Addendum to "Heat Transfer to Satellite Vehicles Re-entering the Atmosphere", "Jet Propulsion", 1957, No. 12.

42. Dickinson T.A., Laminates for Space Flight, "Plastics", 1958, March, vol. XXIII, No. 246.

43. Eckert E.R., Hartnett J.P. and Irvine T.F., Measurement of Total Emissivity of Porous Materials in Use for Transpiration Cooling, "Jet Propulsion", 1956, vol. 26, No. 4.

44. Gazley C., Boundary-Layer Stability and Transition in Subsonic and Supersonic Flow, "Journal of the Aeronautical Sciences", 1953, vol. 20, No. 1.

45. Gruntfest I.J., Shenker L.H., and Saffire V.N., Behaviour of Reinforced Plastics at Very High Temperatures, "Modern Plastics", 1959, vol. 36, No. 8.

46. "Journal of the Astronautics", 1956, Spring, vol. 3, No. 1, p. 6.

47. Lees L., The Stability of the Laminar Boundary Layer in a Compressible Fluid, NACA Technical Report, 1947, No. 8761.

48. Monaghan R.J., On the Behaviour of Boundary Layers at Supersonic Speeds, International Aeronautical Conference, Los Angeles, 1955, 20-23 June.

FTD-TT-62-697/1+2

49. Rose P.H. and Stark W.I., Stagnation Point Heat-Transfer Measurements in Dissociated Air, "Journal of the Aeronautical Sciences", 1958, vol. 25, No. 2.

50. Schaaf S.A., Aerodynamics at Very High Altitudes, "Jet Propulsion", 1956, vol. 26, No. 4.

51. Sutton G.P., Heat Transfer in Rockets, "Journal of the British Interplanetary Society", 1956, vol. 15, No. 4.

52. Van Dreist E.R., Calculation of the Stability of the Laminar Boundary Layer in a Compressible Fluid on a Flat Plate with Heat Transfer, "Journal of the Aeronautical Sciences", 1952, vol. 19, No. 12.

53. Van Dreist E.R. and Boison J.C., Experiments on Boundary-Layer Transition at Supersonic Speeds, "Journal of the Aeronautical Sciences", 1957, vol. 24, No. 12.

DISTRIBUTION LIST

DEPARTMENT OF DEFENSE	Nr. Copies	MAJOR AIR COMMANDS	Nr. Copies
		AFSC	
		SCFTR	1
HEADQUARTERS USAF		ASTIA	25
		TD-Bla	5
AFCIN-3D2	1	TD-Blb	3
ARL (ARB)	1	BSD (BSF)	1
		AFFTC (FTY)	1
		SSD (SSF)	2
OTHER AGENCIES		APGC (PGF)	1
CIA	1		
NSA	6		
AID	2		
OTS	2		
AEC	2		
PWS	1		
NASA	1		
SPECTRUM	1		